

# **Near-surface Sediment Structures at Cold Seeps and their Physical Control on Seepage: A Geophysical and Geological Study in the Southern Gulf of Mexico and at the frontal Makran Accretionary Prism/Pakistan**

A Dissertation for Applying Doctoral Title



Feng Ding

Zentrum für Marine Umweltwissenschaften (Marum)  
Bremen International Graduate School for Marine Sciences (Glomar)  
Universität Bremen

**Near-surface Sediment Structures at Cold Seeps  
and their Physical Control on Seepage: A  
Geophysical and Geological Study in the  
Southern Gulf of Mexico and at the frontal  
Makran Accretionary Prism/Pakistan**

**Dissertation**

Zur Erlangung des  
Doktorgrades der Naturwissenschaften  
(Dr. rer. Nat.)

Im Fachbereich der Geowissenschaften  
der Universität Bremen

Vorgelegt von  
**Feng Ding**

Bremen, Oktober 2008

Date of the dissertation defense: **09. Feb. 2009**

Place of the defense: **Geo-Building, University of Bremen**

Reviewers: **Prof. Dr. Volkhard Spiess**  
**Prof. Dr. Gerhard Bohrmann**

Examiners: **Prof. Dr. Tilo von Dobeneck**  
**Prof. Dr. Wolfgang Bach**

## **Abstract of the Dissertation**

The major objective of the study is to investigate how near-surface sediment structures and other geological aspects control the nature and occurrence of cold fluid seepage. Mainly high resolution multichannel seismic data and swath bathymetry data were used to study near-surface seismostratigraphy, structure and seismic fluid-indicating features in two different fluid seepage provinces: Campeche Knolls, southern Gulf of Mexico and the frontal Makran, offshore Pakistan. The two areas have fundamentally different tectonic settings: The Campeche Knolls, southern Gulf of Mexico represents a passive margin influenced by salt tectonism, while the frontal Makran is the most basinward part of the Makran accretionary prism, characterized by plate subduction, sediment accretion, thrust faulting and development of sediment imbricate slices. However, they share quite a few similarities in shallow sediment structures and fluid seepage patterns.

Both study areas are characterized by high sedimentation rate, together with syn-sedimentary deformation that was initiated as near-surface folding at recent time: the Late Tertiary for Campeche Knolls and the Pliocene to Pleistocene for the frontal Makran. At Campeche Knolls, the initially folded structures are then modified by salt activity up to the present-day. This has resulted in various types of shallow structural traps, with very shallow salt or a few hundred meters of covering sediments as the seals. For the frontal Makran, the development of thrust faulting has segmented accreted sediments into imbricate slices and has folded the upper ends of these imbricate slices. The resultant anticlines form the core of the spectacular sediment ridges on the seafloor. These continuously uplifting anticlines may further incorporate newly deposited slope sediments and become shallow structural traps.

As a petroleum-prolific province, the shallow structural traps in Campeche Knolls have collected large amounts of ascending hydrocarbons. Ultra-shallow reservoirs in deep water and expected ample hydrocarbon supply may be responsible for an unusual phenomenon: large extents of massive asphalt deposition on the seafloor. Beside solid asphalts, the fluid phase hydrocarbon seeps predominantly cluster around these shallow traps. Furthermore, some seismic anomalies in the traps suggest free gas accumulations within the gas hydrate stability zone (GHSZ). Ample gas supply to these traps could have facilitated existence of free gas in the GHSZ, which is also a phenomenon observed in the frontal Makran. At the frontal Makran, overpressure in the accreted sediments is not indicated and dewatering flow rates are probably rather low, because the accreted sediments appear to be largely dewatered directly at the deformation front. This disfavours overpressured mud generation, mud volcanoes, or vigorous water flow along thrust faults as the major mode of fluid seepage. Instead, hydrocarbons, especially methane gas, may be guided by the tilted imbricate slices into structural traps, anticlines made of imbricate slides and slope sediments, where they exist as free gas or gas hydrates. Bottom simulating reflectors at the bottom of GHSZ indicate a pronounced gas hydrate layer across the frontal Makran. As a

possible cap rock, this layer may also have helped focusing fluids into the structural traps. Free gas seepage is widely found above the traps and the gas chemical characters indicate their thermogenic origin.

In all, despite of the fundamentally different tectonic settings, the seepage in both areas is caused by hydrocarbon fluids, generated by deep processes and ascending by their own buoyancy. These fluids are focused by near-surface sediment structures and accumulated in shallow structural traps. Fluid seeps are in turn clustered around these shallow traps, as the result of trap fluid leakage. Thus, in both areas, the near-surface geological processes, which have shaped the shallow structural patterns, have a significant influence on the occurrence and distribution of hydrocarbon seepage.

## Outline of the Dissertation

The dissertation is comprised of seven chapters. Chapter 1 introduces the category of cold seeps and their significance in natural environment, climate and industry. Chapter 2 provides an overview of geophysical survey methods for cold seep detection and the geological processes that contributed to the cold seep occurrence. Chapter 3 then details the scientific goal, dataset, study areas and methodological working flow of this PhD study, attached by an outlook of future methodologies. These three chapters combine to form an extensive introduction of the dissertation. They are followed by three manuscripts summarizing the outcomes of the PhD study. Chapter 4 presents the seismic interpretation on Chapopote and our inference on its seafloor asphalt occurrence. Chapter 5 describes the shallow subsurface structure style in north-western Campeche Knolls and their control on the seepage distribution. Chapter 6 proposes a scenario for the deformation style of accreted sediment at the frontal Makran, and how the resultant structures control the subsurface fluid distribution and seepage. The conclusion of the entire dissertation and an outlook are presented in Chapter 7.

### **Chapter 4. A conceptual model for hydrocarbon accumulation and seepage processes around Chapopote asphalt site, southern Gulf of Mexico: from high resolution seismic point of view**

*Feng Ding, Volkhard Spiess, Markus Brüning, Noemi Fekete, Hanno Keil, Gerhard Bohrmann*

*Published in Journal of Geophysical (vol.113, G08404 doi:10.1029/2007JB005484, 2008)*

A set of 2D high resolution seismic profiles was acquired across the Chapopote knoll to study sea floor asphalt occurrences. A more highly reflective, coarse grained sediment unit of late Miocene age is identified as a potential shallow hydrocarbon reservoir. At Chapopote, local salt tectonism has highly elevated the structure since the late Miocene, and the Miocene reservoir is locally above present-day regional datum. The elevation resulted in a thin (100-200 m), fine grained sediment cover on the crest of the knoll above the reservoir. The presence of high-amplitude reflector packages within the reservoir unit is interpreted as an evidence of hydrocarbons. The thin seal above the reservoir unit facilitates leakage of trapped hydrocarbons. Hydrocarbons apparently invaded into the seal sediments in the wider vicinity around the crest of the knoll, even extending beyond the area where seafloor asphalt is known. We propose that a shallow, large reservoir with deeply sourced, relatively heavy petroleum is principally responsible for the formation of asphalts on the seafloor.

### **Chapter 5. Shallow sediment deformation styles in north-western Campeche Knolls, Gulf of Mexico and their controls on the occurrence of hydrocarbon seepage**

*Feng Ding, Volkhard Spiess, Ian R. MacDonald, Markus Brüning, Noemi Fekete, Gerhard Bohrmann*

*Submitted to Marine and Petroleum Geology*

Chapter 5 studies the near-surface sediment structure and its relationship with hydrocarbon seepages in this salt province. The comprehensive seismic survey covered 18 individual bathymetric highs or ridges and identified three principle structural types: Passive Type, Chaopote Type, and Asymmetric Flap Type. The first type is the result of passive diapirism, while the latter two would be both initialized by a regional compressional event in the late Tertiary, but are differently modified by salt tectonism. Both Chapopote and Asymmetric Flap Type can focus and accumulate hydrocarbons. Hydrocarbon leakage from the thinly sealed reservoirs in these two structural types is the major mechanism for seepage occurrence in the study area, while their different structures results in different aerial distributions of seep sites.

The seep locations suggested by analysis of sea surface oil slick images of SAR satellite data are also examined in this study. These independently derived seep locations confirm that seepage occurs at sites predicted by our seismic interpretation and structural analysis.

**Chapter 6. Interaction between accretionary thrust faulting and slope sedimentation at frontal Makran Accretionary Prism, their resultant shallow sediment structures and some implications for hydrocarbon fluid seepage**

*Feng Ding, Volkhard Spiess, Noemi Fekete, Bramley Murton, Markus Brüning and Gerhard Bohrmann*

*To be submitted*

Chapter 6 presents a set of high resolution seismic data collected during the Meteor Cruise M74/2 to the Makran Accretionary Prism. Similar to the study in Campeche Knolls, the study inspects the shallow sediment structures in the area, suggesting their evolution history, and discussing their influences on cold fluid seepage occurrence. The study areas are divided into the deformation front, where shallow sediments structures are initiated, and the lower slope where they further deform, incorporating new slope basin sediments. At the deformation front, sediment ridges cored by anticlines are formed due to upward-propagating thrust faulting. These anticlines remain active at the lower slope, folding the newly deposited slope basin sediments. The geometry of the folds is strongly influenced by the presence of large volume of slope sediments. These folded imbricate slices and slope sediments in the lower slope form near-surface structural traps for fluids escaping from the greater depth. The accumulations of hydrocarbon fluids in these traps, especially free gas, are suggested by various seismic anomalies. When these traps are sufficiently charged they can induce diatremes and gas chimneys above them, and seeps on the surface. This is the major mode of seepage in the lower slope.

## Content

<b>Abstract of the Dissertation .....</b>	<b><i>i</i></b>
<b>Outline of the Dissertation.....</b>	<b><i>iii</i></b>
<b>Chapter 1. Occurrence and Significance of Cold Seepage</b>	
<b>1.1 Importance and Significance of Cold Fluid Seepage .....</b>	<b>1</b>
1.1.1 Climate and environment .....	1
1.1.2 Support of food matrix in deep water biomass and others .....	1
1.1.3 Other chemical flux to seafloor and ocean .....	2
1.1.4 Geological processes .....	2
1.1.5 Energy industry .....	3
<b>1.2 Category and Distribution of Submerged Cold Seeps .....</b>	<b>3</b>
1.2.1 Pockmarks .....	3
1.2.2 Mud volcanoes and diapirs .....	5
1.2.3 Focused seeps with other morphological features .....	5
1.2.4 Pervasive flow .....	5
<b>Chapter 2. Geophysical Detection and Geological Characteristics of Cold Seeps</b>	
<b>2.1 Current Geophysical Seepage Detection/Research Technologies .....</b>	<b>6</b>
2.1.1 Sea surface .....	6
2.1.2 Water column.....	7
2.1.3 Seabed.....	7
2.1.4 Subsurface.....	8
2.1.5 General comments .....	9
<b>2.2 Critical Control of Geological Processes on Seepage .....</b>	<b>10</b>
2.2.1 Fluid generation .....	10
2.2.2 Major drives for upward migration .....	14
2.2.3 Migration and retention .....	16
2.2.4 Chemical and physical alternation .....	17
2.2.5 Trapping, accumulation and seepage.....	18
<b>Chapter 3. The nature and objective of the PhD study</b>	

<b>3.1 Scientific Goals and Approach</b> .....	<b>22</b>
<b>3.2 Dataset</b> .....	<b>23</b>
3.2.1 High resolution multichannel seismic .....	23
3.2.2 Swath bathymetry .....	25
<b>3.3 Study Areas</b> .....	<b>25</b>
3.3.1 Campeche Knolls, Gulf of Mexico .....	25
3.3.2 Makran Accretionary Prism.....	27
<b>3.4 Methodology and Study Working Flow</b> .....	<b>28</b>
3.4.1 Seismic feature identification, interpretation, and mapping .....	28
3.4.2 Structure interpretation and evolutionary sequences .....	29
3.4.3 Use of structures interpretations and seismic features for seepage study..	30
.....	30
3.4.4 Limitations of the studies and future outlook.....	31
<b>References of Chapter 1 to 3</b> .....	<b>34</b>

## **Chapter 4. A Conceptual Model for Hydrocarbon Accumulation and Seepage Processes Around Chapopote Asphalt Site, Southern Gulf of Mexico: from High Resolution Seismic Point of View**

*Feng Ding, Volkhard Spiess, Markus Brüning, Noemi Fekete, Hanno Keil, Gerhard Bohrmann*

*Published in Journal of Geophysical (vol.113, G08404 doi:10.1029/2007JB005484, 2008)*

<b>4.1 Abstract</b> .....	<b>39</b>
<b>4.2 Introduction</b> .....	<b>39</b>
<b>4.3 Geological Setting and the Study Area</b> .....	<b>40</b>
<b>4.4 Data Acquisition and Processing</b> .....	<b>41</b>
<b>4.5 Observations and Descriptions</b> .....	<b>42</b>
4.5.1 Bathymetric features of Chapopote and the location of the asphalt site..	42
4.5.2 Seismic reflector units and their general characteristics .....	43
4.5.3 Observations on the Chapopote Ridge profiles .....	44
4.5.4 Comparison of the Chapopote Knoll profiles with those in Chapopote Ridge	45
.....	45
4.5.5 Age of the seismic units.....	49
<b>4.6 Interpretation and Discussion</b> .....	<b>51</b>
4.6.1 Evolution of the knoll uplift and the ridge faulting .....	51
4.6.2 A hydrocarbon trap-leakage model.....	52

4.6.3 Hydrocarbon leakage and seepage at Chapopote.....	54
4.6.4 Inference for deep sediment and salt structure under Chapopote.....	56
4.6.5 Occurrence of the asphalt seepage on the seafloor .....	57
4.7 Conclusion .....	58
4.8 Acknowledgements .....	59
References .....	59

## **Chapter 5. Shallow Sediment Deformation Styles in North-western Campeche Knolls, Gulf of Mexico and Their Controls on the Occurrence of Hydrocarbon Seepage**

*Feng Ding, Volkhard Spiess, Ian R. MacDonald, Markus Brüning, Noemi Fekete, Gerhard Bohrmann*

*Submitted to Marine and Petroleum Geology*

5.1 Abstract .....	63
5.2 Introduction .....	63
5.3 Regional Geology .....	64
5.4 Data Set and Processing.....	66
5.4.1 Seismic and bathymetry data .....	66
5.4.2 Locations of seep sites from satellite image interpretation .....	66
5.5 Results and Observations .....	67
5.5.1 Positive bathymetry features .....	67
5.5.2 Shallow subsurface features of the bathymetric highs .....	68
5.5.3 Occurrence of seep sites at different types of bathymetric highs.....	74
5.6 Discussion.....	75
5.6.1 The nature of HAPs .....	75
5.6.2 Shallow subsurface structures for different types of bathymetric highs .	75
5.6.3 Implications for the occurrence of seeps .....	80
5.7 Conclusion .....	82
5.8 Acknowledgments .....	83
References .....	84

## **Chapter 6. Interaction between accretionary thrust faulting and slope sedimentation at frontal Makran Accretionary Prism, their resultant**

## **shallow sediment structures and some implications for hydrocarbon fluid seepage**

*Feng Ding, Volkhard Spiess, Noemi Fekete, Bramley Murton, Markus Brüning and Gerhard Bohrmann*

*To be submitted*

<b>6.1 Abstract .....</b>	<b>88</b>
<b>6.2 Introduction .....</b>	<b>88</b>
<b>6.3 Data .....</b>	<b>89</b>
<b>6.4 Geological Setting .....</b>	<b>90</b>
<b>6.5 Study Area and Its Bathymetric Features.....</b>	<b>91</b>
<b>6.6. Seismic Observation and Primary Interpretation .....</b>	<b>92</b>
6.6.1 Nascent Ridge, First Ridge and their surroundings .....	92
6.6.2. Fifth Ridge area .....	93
<b>6.7 Discussion.....</b>	<b>98</b>
6.7.1 Imbricate folding and faulting at the deformation front.....	98
6.7.2 Fate of imbricate and secondary thrust faulting in Fifth Ridge area .....	100
6.7.3 Fluid accumulation and seepage.....	102
<b>6.8 Conclusion .....</b>	<b>103</b>
<b>6.9 Acknowledge.....</b>	<b>103</b>
<b>References .....</b>	<b>104</b>
<b>Chapter 7. Summary, Conclusion and Outlook</b>	
<b>7.1 Summary and Conclusion .....</b>	<b>107</b>
7.1.1 Sediment Composition .....	107
7.1.2 Structure evolutions, deformation mechanisms, tectonics and general sediment structures .....	107
7.1.3 Formation of fluid focusing mechanisms and traps .....	110
7.1.4 Fluid accumulation and seepage.....	111
<b>7.2 Outlook .....</b>	<b>113</b>
<b>General Acknowledgements .....</b>	<b>114</b>

## Chapter 1. Occurrence and Significance of Cold Seepage

### 1.1 Importance and significance of cold fluid seepage

Seepage, emission of fluids from the subsurface, can occur in many geological settings. The major types of fluids are water and hydrocarbons, but they can further dissolve and carry a variety of chemical species. Cold seeps refer to those whose emitting fluids have similar temperature to that of the seeps' ambient environment. They are distinguished from hydrothermal seeps, which emit typically chemically reduced water, heated by magma activities and having seeping temperature of ~100°C to ~400°C. While hydrothermal seeps occur mainly in magma active areas, e.g., mid-ocean ridges and volcanic arcs, cold seeps can virtually occur in all sedimentary settings. Beside focused, vigorous seepage, they can also occur as dispersive flow with low flow-rates but extending over larger areas. Cold seeps, and related subsurface fluid activities are involved in many geological processes. They also have been increasingly recognized to be an important means to exchange mass, heat, nutrients and other chemical species between geological and environmental systems (Kopf et al., 2001; Tryon et al., 2001; Judd and Hovland, 2007). Their importance can be categorized as follows:

#### 1.1.1 Climate and Environment

The masses emitted from cold seeps are mainly water and hydrocarbons. The latter ones do not only include higher hydrocarbons, which later decompose to CO<sub>2</sub>, but also methane (schematically illustrated in Fig. 1.1). The global emission of methane through cold seeps is not at all negligible. The present-day emission rate of offshore seepage is 8 – 65x10<sup>6</sup> T/yr (Hovland et al. 1993; Hornafius et al. 1999; Etiope and Klusman, 2002), 0.1% of the total methane inventory in the atmosphere, which is of the same magnitude as the current annual increase of atmospheric methane. The methane emission from onshore seepage such as from mud volcanoes, micro-seepage, focused natural seepage from hydrocarbon reservoirs may also have a similar magnitude. Judd (2004) suggested an annual atmospheric input of 27x10<sup>6</sup> T/yr, taking in account all sinks and buffers, which might occur after methane was emitted from seeps. Furthermore, large amounts of emitted methane may be dissolved in ocean water, locally increase its concentration in water, increasing the diffusion rate of methane from ocean to atmosphere. Thereby challenge the common view that the ocean is a minor methane contributor to the atmosphere (Judd and Hovland, 2007). All estimates are very crude, though, due the limitation of the available datasets. Nevertheless, it in turn motivates further investigations of cold seepage.

Moreover, cold seep and methane emission are geological phenomena, and have significant impact on paleoenvironments as well. Kopf (2003) stated that methane from mud volcanoes alone can incur profound effects on the climate since the Paleozoic. Massive methane emission is thought to be responsible for paleo-warming events (Luyendyk et al. 2005; Kennett et al. 2003; Nisbet, 2002), or even mass extinctions (Ryskin, 2003). Hydrocarbon discharge mediated by sea level and temperature change may play an important role in shaping the Quaternary glacial-interglacial cycles.

#### 1.1.2 Support of food matrix in deep water biomass and others

Cold fluid seeps carrying hydrocarbon and reduced chemical species support a variety of methanotrophic and chemosynthetic communities, both micro- and macro-fauna, in deep water (MacDonald, 1998). These communities have now been discovered in most of the deepwater hydrocarbon seeps worldwide (MacDonald et al., 2004; von Rad et al. 2000; Bohrmann et al.

2008a, b; Sahling et al., 2008). Hydrocarbon seeps also support the growth of corals and attract many fauna for various reasons, many of which have not been identified yet. The chemical flux from the seeps, the more abundant food around the sites and physical protection by pockmarks, authigenic carbonates, coral reefs are all contributing explanations (Judd and Hovland, 2007).

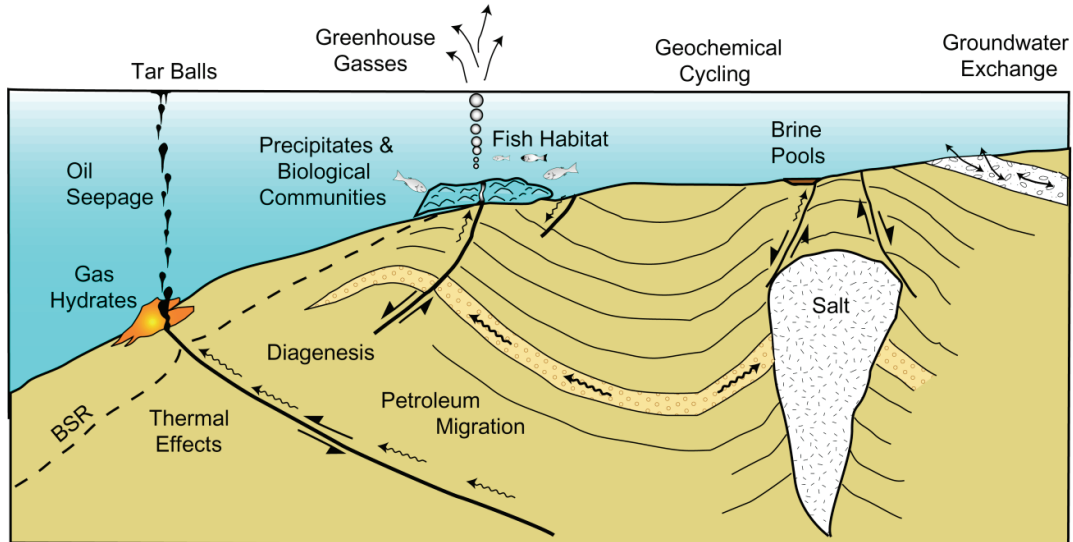


**Figure 1.1** Schematic illustrations of cold seepage category and occurrence in marine environments (after Marum E project proposal, 2006 - 2011).

### 1.1.3 Other chemical flux to seafloor and ocean

Most of seep-related mineral precipitation is driven by hydrothermal fluids. However, mineral-laden cold-seeping waters can result in similar precipitation, e.g., precipitation of iron minerals by submarine ground water discharge at Florida Escarpment (Judd and Hovland, 2007). When hydrocarbons are oxidized by microbial activities, the generated  $\text{CO}_2$  often precipitates at or near the seafloor as carbonate (Naehr et al., 2007; Bahr et al., in press). Furthermore, when pore water residing in deep sediments eventually seeps from mud volcanoes it can carry many volatile elements (You et al., 1996). The types of chemical species and their amount delivered to the ocean by cold seeps are not yet constrained.

### 1.1.4 Geological processes

Fluids that eventually seep at convergent margins may have a fundamental control on the ambient stress field, on fault dynamics and thermal evolution (Platt, 1990; Hyndman et al., 1993; Moore and Vrolijk, 1992). Together with convergence rate and sediment thickness (Clift, 2004), they may also influence if a convergent margin becomes erosive or accretionary (Le Pichon et al., 1993;). The principal mechanism behind all these phenomena is geopressure (overpressure) that the fluids, especially water, induce. High geopressure can significantly reduce the effective stress and shear strength of host formations, or even fluidize them to become the materials for mud diapirs and volcanism. These overpressured formations of low mechanical strength are ideal lubricants, mobile units or incompetent detachments, which render some fundamental features to deformation.

Similar lubricants can also influence the slope stability of passive margins (Dugan and Flemings, 2000; Mienert et al., 2005). For example, when methane that is either dissolved or trapped in gas hydrates is released as free gas within a sediment formation, it can similarly reduce its

mechanical strength, inducing slope failure (Fig. 1.2). During such events, the methane may be released into the ocean and even to the atmosphere in large quantities, and thereby affect the climate system.

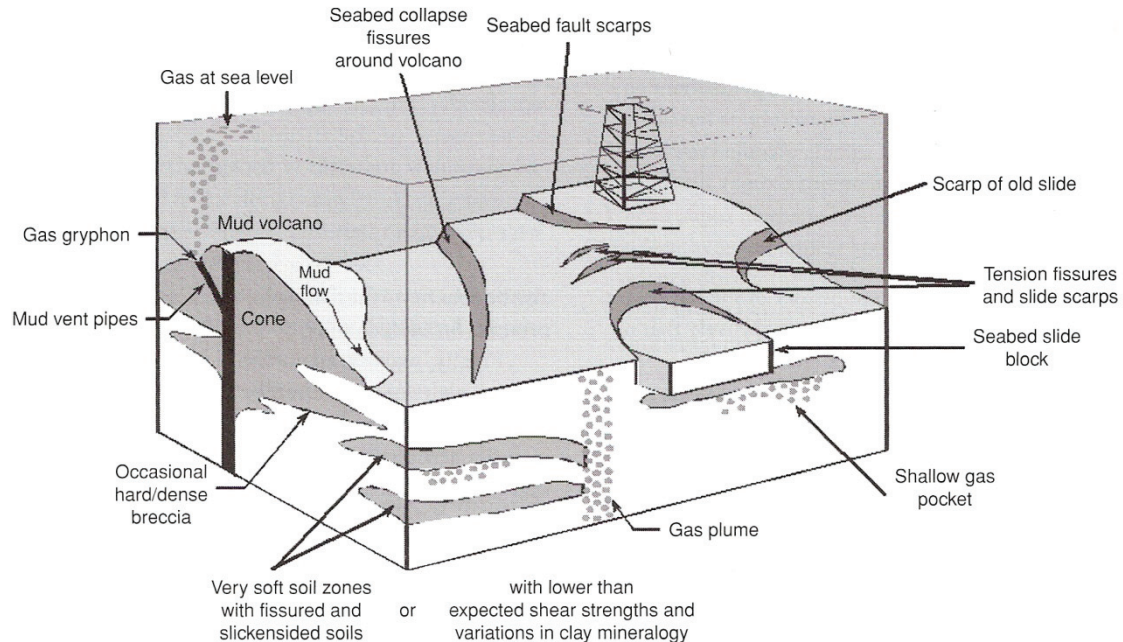


*Figure 1.2 Types of slope instability factors in Caspian Sea (after Judd and Hovland, 2007)*

### 1.1.5 Energy industry

Petroleum seepage gives the first indications of presence of petroleum in most of the regions where hydrocarbons are produced (Link, 1952). The seepage can occur both as focused petroleum seep and as dispersive hydrocarbon emission. There is virtually no petroleum-prolific region without seepage signature (Abrams, 2002). Furthermore, the methods to detect and characterize the seeps and its fluids (satellite imaging, acoustic survey, gravity coring, water column chemical sniffers) are low in cost compared to conventional exploration methods. Thus, they provide an economical means to indicate the presence of deep petroleum reservoirs and maturity of source rocks, reducing the risk of exploration.

## 1.2 Category and Distribution of Submerged Cold Seeps

Cold seeps occur globally. Virtually every regime with sediment deposition, active tectonic activity, or ground water movement can induce cold seeps. In marine and lacustrine settings, cold seeps may also occur in abyssal plains, but the overwhelming portion of identified submerged cold seeps is found along continental margins. An example is shown in Figure 1.3.

Cold seeps can be categorized by many criteria. When distinguished by seeping material, there can be water seeps, fluidized mud (typically mud volcanoes), hydrocarbon seeps. However, there is a broad spectrum of mixtures between different fluids, making the categorization rather difficult. We present a morphology- and seep rate-based criterion to introduce the variety of cold seeps.

### 1.2.1 Pockmarks

Pockmarks are negative morphological features and are related to fluid seepage. They are typically tens of meters across and a few meters deep on soft, fine-grained sediments (Judd and Hovland, 2007), but a huge variety of size exists, ranging from a few meters to hundreds of meters. The exact mechanism shaping pockmarks is still under debate. Mostly, pockmarks may be caused by erosion of surface sediments and the eroding agents are from beneath the seafloor. It can form by seep fluid washing away sediments, or explosive events when pressured shallow fluids are released, which however, can also be categorized as collapse depressions. Beside pure erosional processes, pockmarks could even be depositional, when ascending fluids in the water column prevent deposition of sediments at their surroundings.

Note that many processes other than fluid seepage can create features that appear very much like pockmarks, such as iceberg drop stones, meteoritic impacts, or even bombing pits, etc. They are distinguished from pockmarks in our context because they are not formed by fluid activities that are from beneath the depressions. Thus, a pockmark is not only a morphologic feature but also a fingerprint of geofluid activities, which may not necessarily be active at the present-day. The type of fluids that are related to pockmark formation may vary. In the North Sea, where the pockmarks were first discovered, gas seepage may play an essential role (King and MacLean, 1970). Focused water seeps may also generate similar features, such as meteoric water discharge (Whiticar, 2002) or surface expression of diatremes (Kopf, 2002).

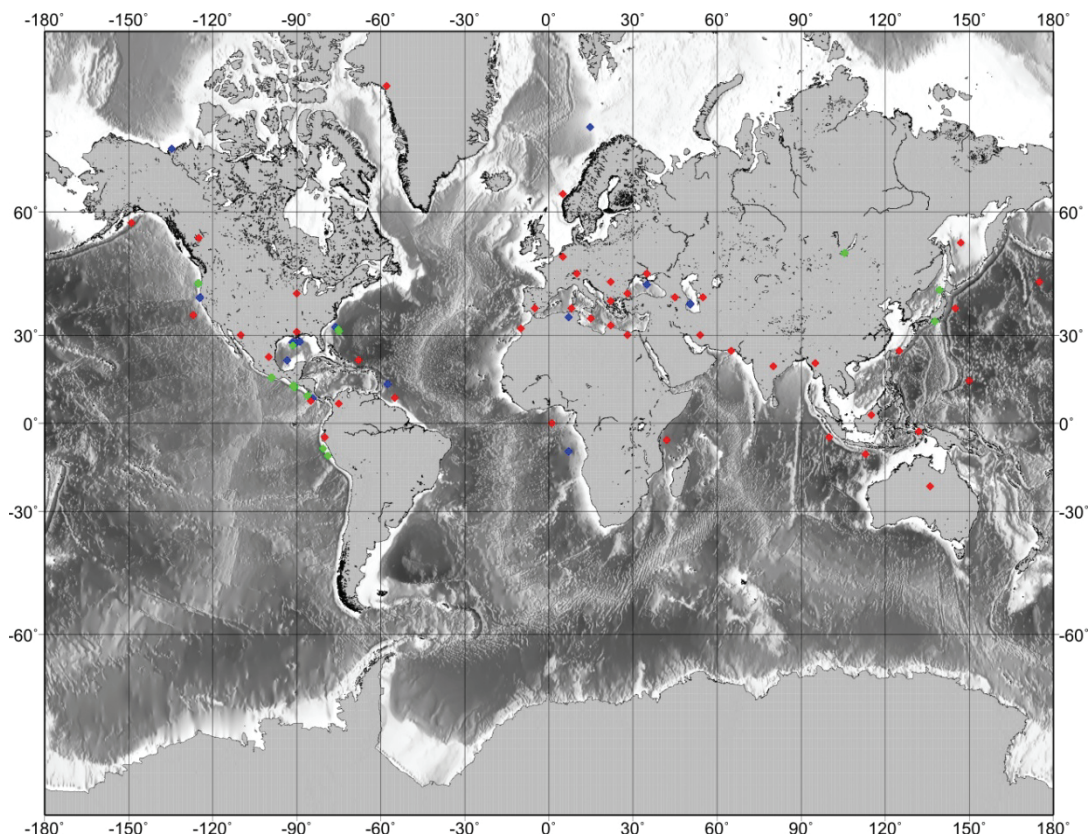


**Figure 1.3** Global occurrence of mud volcano and detected gas hydrate sites. Red dots for mud volcanoes (data source Kopf, 2002), blue dots for gas hydrates sites with fast gas flow, and green dots for gas hydrates sites with low gas flow (data source Milkov, 2005)

### 1.2.2 Mud Volcanoes and diapirs

In contrast to pockmarks, mud volcanoes are positive in morphology. It also differs from pockmarks in that the seeping mass includes fluidized mud and other rock clast inclusions, which are emitted and stacked on surfaces, forming volcano like mounds. Similar to igneous volcanoes, the viscosity of the emitted solid materials dictates the shape and slope angle of these volcanoes. Low porosity, high cohesive materials forming mud domes, while high water content, low cohesive ones forming mud pies (Kopf, 2002). More than a pure surface feature, mud volcanoes can repeatedly stacked upon each other and extend into great depth. This gives rise to the inference that the mud may have intruded laterally into the sediments, but alternatively, those subsurface patches can simply be buried surface features (Van Rensbergen et al., 1999). If all mud patches are buried or intrude only in subsurface, they are called mud diapirs. The conduits needed to transport the uprising mud may be typically very narrow (several meters to submeter scale), much narrower than the diameters of these volcanoes (Kopf, 2002).

The fact that mud volcanoes are deposited from fluidized mud from greater depth suggests availability of mud and fluid overpressure at greater depth. Any mechanism that can induce overpressure (discussed in **Section 2.2.1** and **2.2.2**) in muddy sediments can thus trigger mud volcanism. It in turn means the nature of seeping fluids through mud volcanoes can vary, ranging from water, water-gas mixture (Sassen et al. 2003) to water higher order hydrocarbon mixture (Whiticar et al., 1995; Kholodov, 2002). Furthermore, the waters from greater depth may carry a range of chemical species, which may reveal the processes for overpressure generation (Carson and Screaton, 1998; Kopf, 2002).

### 1.2.3 Focused seeps with other morphological features

The two types of seeps introduced above may have been associated with spectacular morphological features as a direct result of seepage. However, cold seeps are not necessarily associated with a distinct morphology, and many high flow rate seeps reveal only minor morphologic expressions. One example is the seepage at Hydrate Ridge, Cascadia Margin (Tryon et al., 2002), where the seeping fluids migrate through a fracture network beneath the crest of the ridge. Around the seep, there is no distinct morphology that is related to seepage, except for some carbonate mounds and features resulting from colonization of chemo-synthetic communities. These features are often quite limited both in elevation and extent, and thus can be difficult to image in bathymetry, but they can show strong backscatter anomalies in sidescan/multibeam surveys.

### 1.2.4 Pervasive Flow

It has been implied that the above mentioned three seep types are all focused, fast flow rate seeps, which is indeed mostly the case, although seepage can be episodic. They have relative fast fluid rates in limited areas, while the surrounding may be totally quiescent or with much reduced seepage rates. In contrast, pervasive seepage has low fluid emission rates, which are evenly distributed over large areas. Because focused seeps are usually rather spectacular in morphology and in the amount of seeping masses at focused spots, they also have received the most attention from researchers. However, dispersive seeps, with much lower flow rates spreading over large areas, can emit as much fluid volume into the environment as those focused seeps (Tryon et al., 2001). Extensive occurrence of carbonates and gas hydrates are indirect indications of the existence dispersive flow.

## Chapter 2. Geophysical Detection and Geological Characteristics of Cold Seeps

### 2.1 Current Geophysical Seepage Detection/Research Technologies

#### 2.1.1 Sea surface

Oil drops and bubbles from active hydrocarbon seeps can uprise through the water column to the sea surface and subsequently drift down-wind and down-current, forming linear “slicks” (MacDonald et al., 1993; MacDonald et al., 2002). These slicks are readily detected in satellite synthetic aperture radar images (SAR) (Espedal and Wahl, 1999) (Fig 2.1), and airborne visual or remote-sensing surveys (Thrasher et al., 1996). Since it is so straightforward to survey large areas with satellites or aircrafts in short periods of time, tracing the sea surface slicks gives an economical means to detect petroleum seeps.

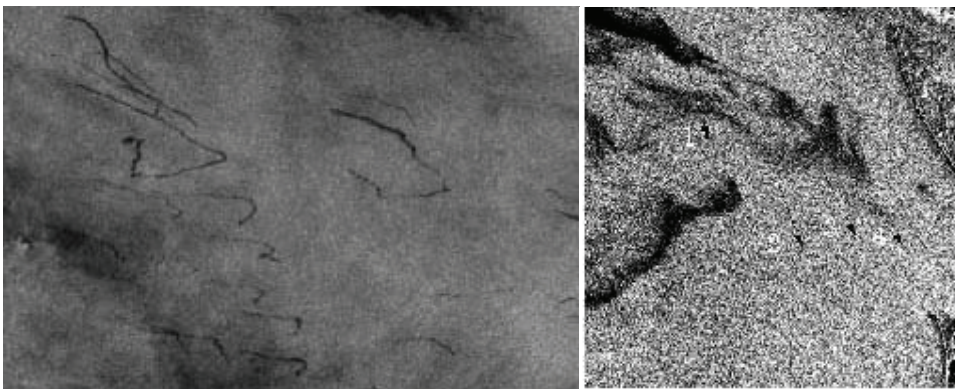


**Figure 2.1.** a) Oil Slicks on the Atlantic (Source NPA); b) MSSM velocity vectors output for the elongated oil slick pattern on Carmarthen Bay superimposed on ERS-1 SAR sub-image. (Clemente-Colón et al. 2007)

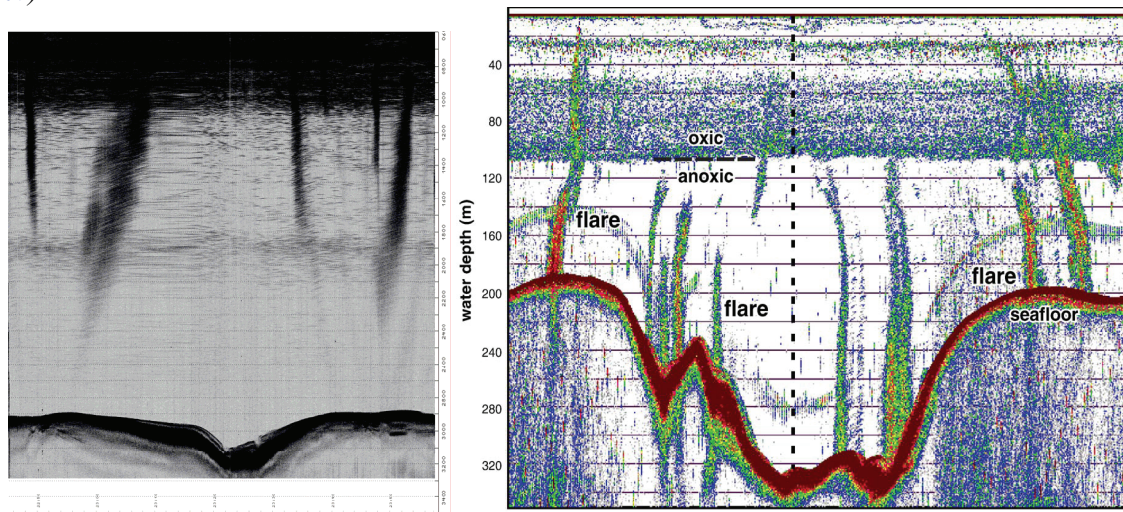


**Fig. 2.2** a) Parasound imagery of gas bubbles creating flares through 2000 m of the water column until their image is smeared by the plankton backscatter in shallowest depth. The profile is acquired during Cruise M67/2a at Campeche Knolls. b) Single-beam echogram showing a typical hydroacoustic manifestation of rising methane bubbles in flare-like shape in the Black Sea. The image shows several flares rising from different depths between 190 and 325m (x-axis span  $\approx$ 22min), with shallower flares almost reaching the seasurface and crossing the oxic/anoxic boundary at about 110m. (After Greinert et al., 2006)

### 2.1.2 Water column

High frequency echosounders (20 – 180 kHz) transmit signals with wavelengths smaller than or equivalent to typical sizes of free gas bubbles in the water column (0.5 – 50 mm, Judd and Hovland, 2007). The free gas bubble streams from active seep sites are thus capable of backscattering the acoustic signal, and appear as gas flares in the echosounder profiles (Fig 2.2). This also offers a convenient way to detect the bubble streams and thus active gas seeps, since the echosounder systems can operate concurrently with other surveys. The echosounders do not only include high frequency profilers (e.g., high frequencies of 18 and 40 kHz of the Parasound echosounder), but also multibeam, side scan systems, and any other high frequency acoustic system that is designed to record water column returns.

### 2.1.3 Seabed

Section 1.2 has already described that many seep sites have surface features, especially mud volcanoes and pockmarks. Those with >10 m scale (both lateral and vertical) can be readily detected with current multibeam bathymetric systems. Ultra high resolution bathymetry achieving sub-meter scale resolution (Monahan et al. 2008), e.g., by various AUV mounted swath sonars, is also available for academic purposes, and can resolve more subtle morphologic features such as carbonate mounds, or detailed topographic variations of mud volcanoes (Fig 2.3).

Another means to detect seep sites by seabed survey technologies is to explore their backscatter characteristics. Many hydrocarbon seeps are associated

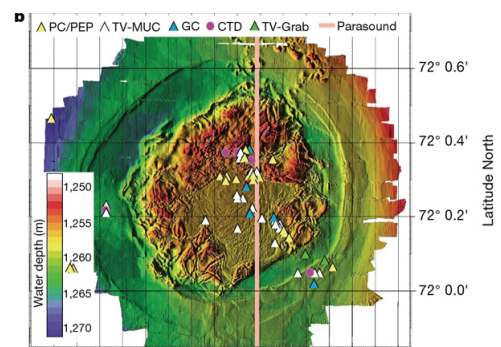
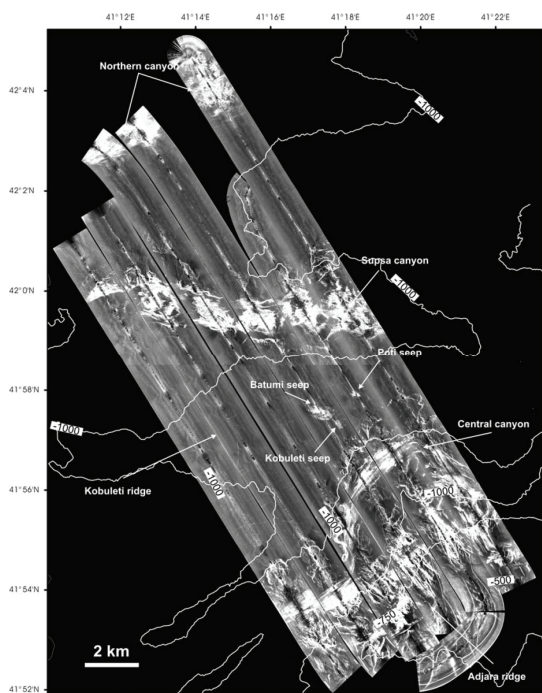


**Figure 2.3** High resolution bathymetry resolves a newly found mud volcano: Hakon Mosby. (After Niemann et al. 2006)



with carbonate precipitation or colonized by chemo-synthetic communities, such as tubeworms, mussels and even corals. Their occupation results in very rough seabed, and can strongly scatter acoustic signals. Thus, these colonies present nice targets for side-scan sonar survey. Furthermore, similar to bathymetry, side-scan is also capable of detecting larger morphological features, e.g., mud volcanoes and pockmarks. Mud volcanoes, as mud patches, flows and clastes often reveal different backscatter properties, are typically appear highlighted in side-scan surveys due to their morphologic and backscatter characteristics (Fig 2.4)

**Figure 2.4** 75 kHz DTS-1 side-scan sonar mosaic showing the canyon-ridge system offshore Batumi and several seep locations. White represents high back scatter intensity. (after Klauke et al., 2006).

### 2.1.4 Subsurface

For subsurface imaging, only lower frequency systems (<4 kHz) can be used, because only such an acoustic signal is capable of penetrating sediments. High frequency echosounders or sediment profilers (Chirp, boomer, Parasound etc.) have typical frequencies in the range of 2 – 10 kHz, for the purpose of imaging the shallow sub-seafloor (~10 m to max. ~200 m, depending mainly on sediment lithology). The penetration of conventional echosounder signals is further limited in deep water because of their wide beam angle, spreading energy in large areas. In comparison, systems using the parametric effect for beam forming produce a much narrower beam, as e.g., a beam angle of 2° for the Parasound system, corresponding to a footprint of ~7% of the water depth (3dB points). This in turn increases penetration, lateral resolution and may enhance the signal-to-noise ratio (Fig 2.5).

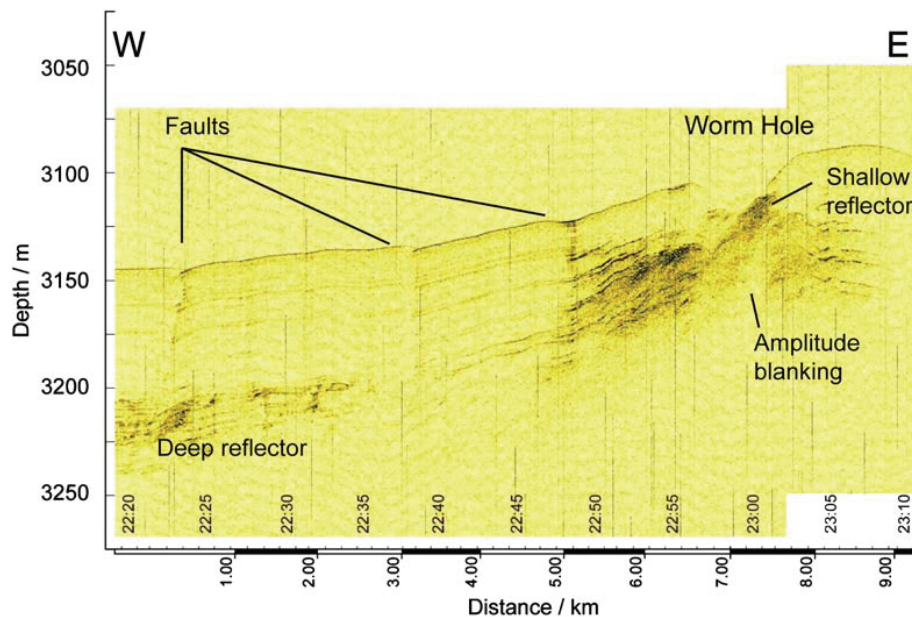


**Figure 2.5** Parasound profile of Worm Hole, offshore Angola. High amplitude reflections along stratigraphic units form a deep reflector about 50 m below the seafloor. Towards Worm Hole the reflector shallows. A shallow chaotic reflector reaches the surface at the base of the pockmark. (After Sahling et al. 2008)

For imaging the deeper subsurface, seismic sources such as air guns, GI guns, water guns have to be used, which generates seismic signals in the range of 20 Hz to 1.6 kHz. Large gun arrays can even produce signals penetrating down to the upper crust, although at the cost of resolution. These seismic sources coupled with multichannel streamers as recording units, and multichannel seismic processing methods, can image most of the sediment basins in the world. Multichannel seismic systems with long streamers (up to 12 km) and thus large gun-receiver offsets, not only acquire only deep subsurface structure, but also make rock physical properties analysis possible, including seismic velocity and others, grossly named as seismic attributes (e.g., Chopra and Marfurt, 2005). These advantages of multichannel seismic systems make them the most important tools for petroleum exploration.

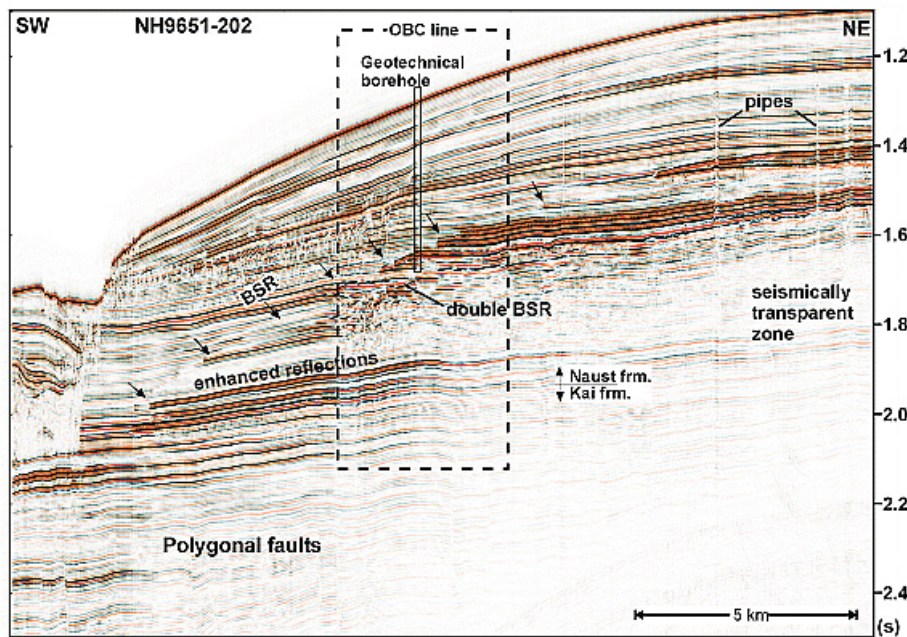


**Figure 2.6** Time-migrated seismic section from the northern flank of the Storegga Slide. The BSR on the mid-Norwegian margin is mainly identified as the termination of enhanced reflections. The base of the Naust formation is characterized by high reflection amplitudes. Pipes can be identified on the upper part of the slope between the Vøring and the Møre basins. Underneath them is a seismically transparent zone. (After Büinz and Mienert., 2004)

Subsurface imaging tools can also be used for seepage detection because seepage is a geological process, with fluids often sourced from greater depth. This process and the presence of fluids in sediments can both show up as anomalies in acoustic or seismic profiles (Fig 2.6). The appearances of these anomalies vary greatly. Features such as acoustic turbidity or acoustic blanking are main signatures of shallow gas in fine-grained sediments (Judd and Hovland, 2007). Seismic chimneys are often interpreted to be pathways of fluid migration, which can either still be filled with fluids or simply represent relict, fractured sediments. Seismic bright spots and high amplitude anomalies are, on the other hand, typical indications for gas-filled, coarse sediments. When gas hydrates and free gas underneath forms a laterally continuous zone, it can appear seismically as bottom simulating reflectors (BSRs, Shipley et al. 1979). Multichannel seismic data can also be used to generate various seismic attributes: instantaneous frequency, acoustic velocity, AVO etc. for easier numerical representation of rock physical properties and indications for fluids.

### 2.1.5 General comments

These introduced technologies have been increasingly refined in recent years, because survey studies benefit from the interest of energy industry and environmental research. When these technologies are effectively combined, the chances for discovering existing seeps are significantly increased. Most of them are also used in recent cruises related to my PhD study, and proved to be rather useful seep hunters (Bohrmann et al., 2004; Bohrmann et al. 2008a; Bohrmann et al. 2008b; Spiess' Makran cruise report).

However, these tools can be most effective only in detecting focused fluid seepage, while it is much more difficult to detect pervasive flows which show more subtle physical anomalies. Water chemical sniffers may fill in this gap. Furthermore, it must be noted that these

technologies are after all survey tools. They detect the presence and distribution of seeps and even the types of fluids at a seep site, setting the stage for further research. They rarely directly hint to the mechanisms which are driving fluid seepage, and hardly reveal the lifetime of discovered seeps. However, without this understanding, the significance of seepage on environments and all other aspects cannot be addressed. After all, seepage is a surface expression of many geological processes that often occur at some or greater depth. These processes are involved in the full range of activities related to seeping fluids, from generation through migration to seepage at the seafloor. Fluid seepage is a net result of these geological processes at greater depth, sometimes involving the entire sediment column or even deeper levels. **Section 2.2** briefly summarizes the mechanisms for generation, migration, accumulation and eventual seepage of fluids, in order to reveal that geological processes are heavily involved in all these aspects. This should in turn suggest that surface seeps are windows into these deep processes. By the same token, seepage may be better understood only with a better knowledge of the deep processes, our major motivation to study these geological processes as part of seepage research in **Chapter 3**.

## 2.2 Critical Controls of Geological Processes on Seepage

### 2.2.1 Fluid generation

#### Water

##### 2.2.1.1. Sediment Compaction

The term sediment compaction is dedicated to reductions of sediment pore volume by external mechanical stress or chemical processes, including depositional compaction, tectonic compaction and chemical compaction. Loading of new sediments upon compressible rock volume tends to reduce sediment porosity and thus generates excess fluid in sediment column (Osborne and Swarbrick, 1997; Waples and Couples, 1998). Sediments can also be laterally shortened under tectonic stress, e.g., at convergent margins, causing similar effects of porosity reduction. Alternatively, when sediments are laterally shortened, the units also become thicker, known as tectonic thickening (Hyndman et al., 1993; Wang, 1994; Carson and Screaton, 1998). This thickened sediment column exerts higher pressure on sediment in the greater depth, tending to further reduce the porosity of deeper sediments. Cementation of sediments by mineral precipitation, such as re-crystallization of quartz, can also reduce pore volume, tending to expel extra water (Wangen, 2000). This would usually happen in greater depth, when temperature, pressure and other physical conditions deviates from surface conditions and thus diagenesis occurs.

Note that all these mechanisms have the tendency to reduce pore volume and to create excess water, but the water may not be immediately expelled from the rock formations. If they cannot be expelled easily, the incompressible water shall maintain void volume, and will become overpressured: higher than hydrostatic. The mechanism and consequence of overpressure will be discussed in 2.2.2.1. Alternatively, the excessive water is readily expelled and forms water flow. Nevertheless, this does not mean that it would directly reach the seafloor. In a depositional basin, the seafloor is growing by sedimentation. Hence, the upward water flow must be faster than sedimentation rate to form a net upward flow. This is not always the case, as in some slow sedimentation basins, the net pore water flow is downward, despite of compression at greater depth (Haacke et al., 2007).

##### 2.2.1.2. Aquathermal Expansion of Water

When being deeper buried, rock formations find ever increasing temperature, with typical global temperature gradients ranging from 20 – 80 °C/km. The volume of water expands distinctly with higher temperatures (Fig 2.7). Expanded water volume in fixed or reducing sediment pore spaces tends to expel its excessive volume from the formation, causing either water flow or overpressure.

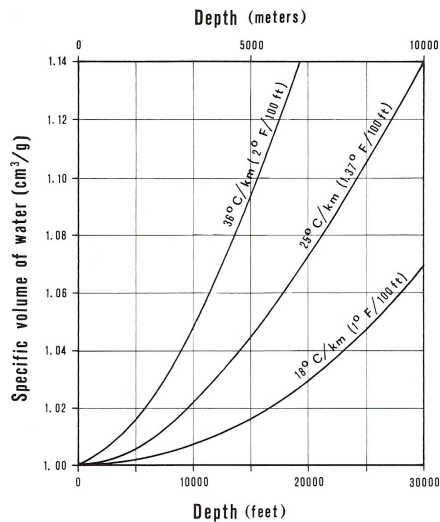


**Figure 2.7** Relationship between specific volume of water and increasing depth of burial for different geothermal gradients. (After Magara, 1974)

### 2.2.1.3. Water-generating Diagenesis

As mechanisms of generating water flow, the above-mentioned two processes do not generate new water, but in contrast, some diagenesis processes do so. Diagenesis refers to changes of sediment physical and chemical properties and compositions in greater depth, including the chemical compaction mentioned above. This section is dedicated specially to those processes that generate new water volume. Some examples include:

Decomposition of organic matter is a well known process in shallow sediments, and reduces pore water salinity in the very upper part of the sediment column (Boetius and Suess, 2004). However, this process is limited to the very shallow sediment column. In greater depth, in the first place most of the organic matter is transformed into kerogen, which has little potential to generate new water, and second, the increasing temperature becomes hostile to microorganisms that decompose organic matter, and thus their activity is largely limited.

Decomposition of gas hydrates is an additional water-releasing mechanism in shallow sediment. The decomposition can be triggered by any mechanism that changes pressure and temperature conditions of host sediments, ranging from a change of the bottom water temperature, sea level change, tectonic uplift etc. Strictly speaking, the water is not newly formed, but is simply pore waters trapped in gas hydrate crystals. However, since gas hydrate formation have concentrated both water and gas, their decomposition also causes concentrated release of water volume.

Clay dehydration, compared to the processes above, is located considerably deeper in sub-bottom depth. Dehydration occurs when clay minerals loose their interlayer water, or when they are transformed into other minerals: smectite-illite transformation and gypsum-anhydrite transformation. Interlayer water loss and transformation typically require high temperatures (smectite-illite 70 – 150°C, gypsum-anhydrite 40 – 60°C), thus greater burial depth. The net

volume expansion of water, after subtracting the loss of mineral volume in these transformations, is, however, limited. In addition, when the generated water causes overpressure, it prohibits further dehydration to occur, because high pressure hinders volume expansion reactions to continue, according to thermodynamic considerations. These two limiting factors underscore clay dehydration as effective overpressure generation mechanism (Osborne and Swarbrick, 1997), even though many investigators speculate about its role in observed overpressured systems (e.g., Kopf et al., 2001; Alnes and Lilburn, 1998).

#### 2.2.1.4 Ground water invasion and discharge

During this process, the water mass is increased not through chemical processes but by the migration of ground water from land, and most of the waters are meteoric. In marine settings, migration of ground water into a submerged, growing basin requires connectivity of permeable basin sediments forming ground water aquifers. More importantly, meteoric water can inflow into marine rock formations only when its pressure is greater than the formations' pore water pressure, otherwise, the reverse would happen (Fig 2.8). If a basin is hydrostatic or only slightly overpressured, then ground water, with its water-level readily higher than sea level, can invade into marine rock formations. However, when the marine sediments' overpressure exceeds ground water's pressure head, water in marine rock formations would intrude into land (Einsle, 2001). This leads to the classification of sedimentary basins into juvenile basins, intermediate basins, and senile basins (Coustau et al., 1975)

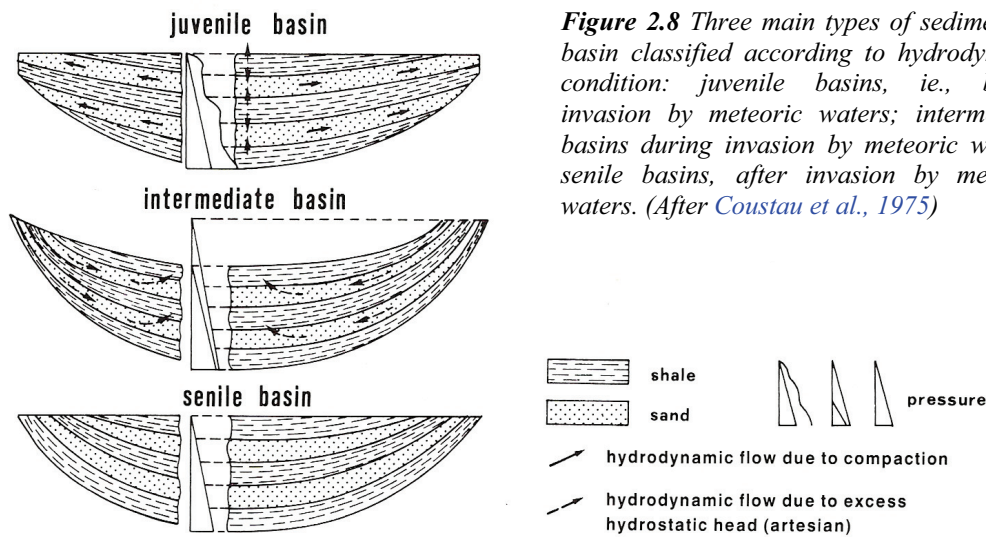


**Figure 2.8** Three main types of sedimentary basin classified according to hydrodynamic condition: juvenile basins, ie., before invasion by meteoric waters; intermediate basins during invasion by meteoric waters; senile basins, after invasion by meteoric waters. (After Coustau et al., 1975)

**Hydrocarbon:**

2.2.1.5. Thermal maturation of kerogen

As mentioned, during burial and early diagenesis most organic matter is transformed into kerogen. With different ancestor organic matter, kerogen also has different compositions and can be subdivided into Types I to III (Tissot and Welte, 1984). To state simply, Types I to III indicate increasing amounts of marine organism components and decreasing terrestrially originated portions (Fig 2.9). When they are further buried and exposed to higher temperature, kerogen decomposes by thermal cracking to generate oil. This is called primary cracking and is the prime mechanism for producing hydrocarbons exploited by industry. The generated hydrocarbons are fairly complicated mixtures, ranging from alkanes, aromatics, resins and asphaltenes. In addition, different thermal stages of kerogen, different regions, and later alteration all contribute to a great variety of composition mixtures.

Petroleum generation turning solid kerogen into liquid petroleum can result in a significant total fluid volume expansion of up to 25% (Meissner, 1978). As a new fluid in the

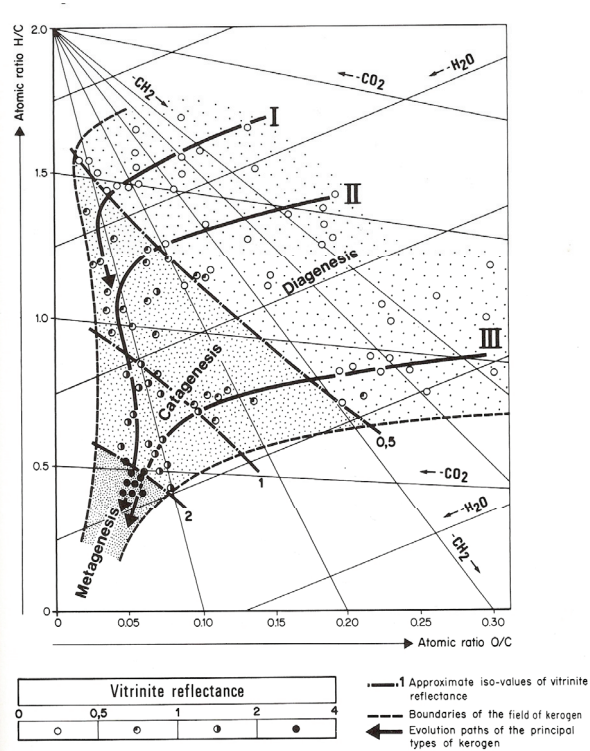


**Figure 2.9** General scheme of kerogen evolution from diagenesis to metagenesis in the van Krevelen diagram. Approximate values of vitrinite are shown for comparison. (After Tissot and Welte, 1984)

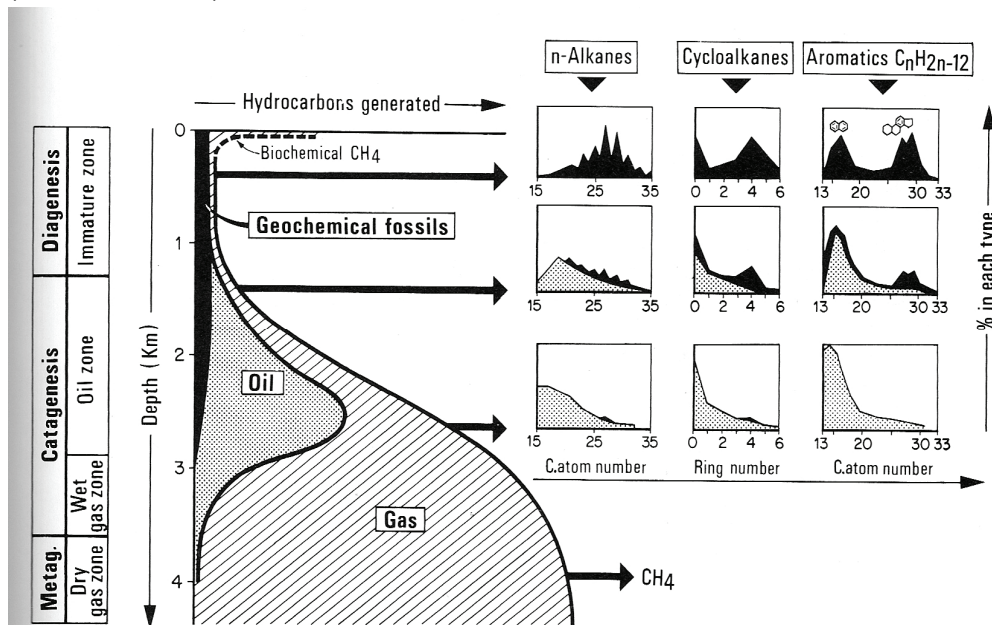


**Figure 2.10** General scheme of hydrocarbon formation as a function of burial of the source rock. The evolution of the hydrocarbon composition is shown in insets for these structural types. Depth is only indicative and correspond to an average on Mesozoic and Paleozoic source rocks. Actual depths vary according to the particular geological conditions: type of kerogen, burial history, geothermal gradient. (After Tissot and Welte, 1984)

system, the petroleum also reduces the pore space available for water. Thus, both petroleum and water become excessive for the host sediments. When generated hydrocarbons are later exposed to even higher temperature conditions, they would further decompose, with lighter hydrocarbon components with the potential of mobilization and heavier components as residuals. This is named as secondary cracking and over-maturation. When such process continues, petroleum will disproportionate into methane and asphalten.

#### 2.2.1.6. Biogenic gas

Biogenic gas production refers to the generation of hydrocarbons through activity of micro-organisms. Since the predominant product of this process is methane, with trace amounts of heavier n-Alkanes (Tissot and Welte, 1984; Colwell et al., 2008), this hydrocarbon-generation process is simply called biogenic gas production. A typical example is the decomposition of freshly deposited organic matter by methanogenic microbial organisms, as part of the hydrocarbon production series (Fig. 2.10). Furthermore, a spectrum of organisms is capable of degrade thermogenic petroleum, with end-products of methane and heavy petroleum residues (reducing API, increasing asphalten; Bence et al., 1996; Miller et al., 1987).

#### Others

##### 2.2.1.7. Inorganic Components:

During the diagenesis of organic matter, biogenic gas production and petroleum generation, a collection of inorganic components is also generated as by-products, such as CO<sub>2</sub>, H<sub>2</sub>S, SO<sub>4</sub>, He, N<sub>2</sub>, P<sub>2</sub>O<sub>4</sub>, NH<sub>4</sub>, noble gases etc. (Tissot and Welte, 1984). These components can either form separate phases or be dissolved in water and hydrocarbons. They are usually not considered to be voluminous to form significant fluid flow or overpressure. However, some of them, when seeping together with carrier fluids, are fingerprints for certain chemical processes in the subsurface. Furthermore, the concentrations of H<sub>2</sub>S or SO<sub>4</sub> are also an indicator for the quality of petroleum.

##### 2.2.1.8. Chemical Elements

Similar to inorganic components, chemical elements (B, I, metallic elements, rare earth elements, as well as different isotope members of these elements) in pore water and minerals also exchange during diagenesis and methanogenesis. Obviously, these are not fluids and can become mobile only when they are dissolved in carrier fluids, mostly water. However, since a certain combination of elements represent certain equilibrium PT conditions, they are, if found in seep water or extruded sediment pore waters, fingerprints for the depth origin of the water volume.

### 2.2.2 Major driving forces for upward migration

Fluids expelled and generated in the deep formations, must migrate upwards to become hydrocarbon accumulations or seeps. The upward migration requires a driving force to overcome gravity. Notably, in sedimentary basins the seafloor is shifting upwards due to sediment accumulation. Thus, the flow rate must be faster than the sedimentation rate, to form a net upward flow.

#### 2.2.2.1. Pressure Gradient

For water, an upward decreasing pressure, steeper than hydrostatic pressure gradient is the lone drive for upward water flow. All porosity-reducing or water-generating mechanisms

immediately increase pore pressure, and potentially force water to flow, since water is incompressible. When pressurized water cannot be readily evacuated because of limited permeability of the rock media, porosity would not reduce, but stress is taken up by pore water and thus overpressure occurs.

How large overpressure can be built up depends on three factors. 1) the total pore volume loss or amount of new water, 2) how fast these processes are accomplished, and 3) lithology and thus permeability of compacted and carrier beds (2.2.3.1). Thus, besides water-generating and pore-space reduction, lithology is critical to either allow fluids to flow or to build up overpressure (Roberts and Nunn, 1995; Osborne and Swarbrick, 1998; Luo and Vasseur, 2002). This becomes a major limiting factor for some of the water-generating mechanisms to be efficient overpressure contributors. Nevertheless, most publications identify types of overpressure exclusively by the mechanism of water-generation or pore-space reduction. For instance, the disequilibrium compaction of Osborne and Swarbrick (1997) refers to overpressure induced by sediment depositional compaction. All other fluid expelling or generating mechanisms would accordingly cause overpressure, when lithological conditions are favorable.

#### 2.2.2.2. Buoyancy

Overpressure can also help hydrocarbons to migrate especially in source rocks (primary migration), but for these fluids, another force plays a dominant role for their migration in carrier beds (secondary migration): buoyancy. Hydrocarbons are lighter than water, and this provides them buoyancy in water saturated rock media. Indeed, the buoyancy is so efficient that taking this factor alone, the time for hydrocarbons to move through kilometres of sediments is instantaneous on geological time scales. Furthermore, buoyancy does not only drive hydrocarbons through available porous paths or any other pathways (faults, joints and cracks etc.), but also may make their own way through rather impermeable sediment intervals. When hydrocarbons form continuous stringers, they would also pressurize barrier layers to squeeze themselves through or crack the sediments (Berg, 1975; Nunn, 1996). The pressure is determined by the vertical height of the stringer and the density difference between the stringer and water, so it is called column height pressure. Note that this pressure is totally independent of the water pressure, and can be present under hydrostatic conditions.

#### 2.2.2.3. Concentration Gradient – Diffusion

When a dissolved component has different concentrations at different locations, the component will move from highly concentrated locations to lower concentrated ones through diffusion. In this case, there is no mass movement of media: sediments, water or other fluids as dissolvent. Thus, it is called diffusive flow in contrast with various advective flows discussed above. If there is no source and sink of this material in the media, its concentration will be eventually unified everywhere. However, when the material is continuously consumed at one location and generated elsewhere, a continuous chemical flux will be established. How fast the components can be so transported depends on the concentration gradient and the diffusion coefficient of the media. A particular limiting factor is that materials must be first dissolved in media (mostly pore water) for this process. Overall, such flow is generally regarded a slow process for migration and accumulation of hydrocarbons to industrial level reserves. Furthermore, since diffusion tends to unify concentration at different locations, it tends to prevent concentrated accumulation of hydrocarbons (Krooss et al., 1992). However, exceptions such as that diffusion may help form gas reservoirs are suggested by some studies (Leythaeuser et al., 1982). In near-surface

sediments, this is regarded as a critical means transporting oxidants for microbial alternations of hydrocarbons.

### 2.2.3 Migration and Retention

#### 2.2.3.1 Migration and Permeability

The fluids under discussion include water, hydrocarbons and many inorganic materials. The non-water fluids appear in usually water-saturated media and can be present as colloidal or molecular solutions in water, or as separate phases. When in solution, the mobility of the non-water components depends on the mobility of the carrier water, or their chemical gradient and their diffusion coefficient. When non-water components form their own phases (e.g., gas bubbles and oil stringer), their migration also needs pathways in geological formations, although the driving forces derive more from buoyancy than from a pressure gradient.

Besides the character of the fluids, the mobility of fluids in sediments is media dependent. They can move through tortuous paths of connected pore space, micro-cracks or –joints, and macro-scale fractures and faults. For a flow through a porous medium, the flow velocity is controlled by the permeability of the medium (Darcy's law), or for diffusive flow by the diffusion coefficient (Fick's first law). If hydrocarbons flow as a separate phase, their permeability is always a fraction of water permeability due to their higher viscosity compared to water (Teige et al. 2006). While the diffusion coefficient is a function of many chemical aspects other than lithology, permeability is the function of the medium lithology and porosity. For siliciclastic sediments, coarser grained and lesser compacted sediments show higher permeability, but carbonate sediments may consolidate in an early stage of diagenesis, and become more or less impermeable.

However, breached carbonate rock reveals extremely high permeability, because the pathways are macro-scale fractures, so do fractures in igneous rocks etc. Faults, however, may not always be very permeable or not be permeable at all, namely it can be either permeable or infinitely impermeable (Aydin, 2000; Fisher and Knipe, 2001; Yielding et al., 1997). In petroleum industry, many faults are interpreted to be seals for the closure of hydrocarbon traps. Other discontinuities, such as a salt-sediment interface, and salt welds may also be permeable enough to be pathways. However, like faults, they may also vary from very permeable to infinitely impermeable. Micro-scale cracks can increase the permeability of fine-grained sediments, but can exist only when the medium is highly overpressured. When this overpressure is removed, these cracks close again and permeability drops. This may cause episodic pressure build-up and later release of fluids in some overpressure provinces (Robert and Nunn, 1995). Synthetic overpressure by gas or liquid injections into production well is a common practice to produce micro-cracks, increase permeability and productivity of petroleum reservoirs.

Permeability makes migration of fluids, and their focusing and seepage possible. However, low permeability is equally important for these to happen. In uniform highly permeable geological formations, excess water may seep as dispersive flow, and hydrocarbons would escape from sediments almost instantaneously by buoyancy alone, also as dispersive seeps. Hydrocarbon reservoirs, focused hydrocarbon and water seepage would not exist without low permeable intervals and focusing mechanisms.

#### 2.2.3.2 Retentions of Fluids

Retention here refers to physical stalling of advancing fluids, typically caused by barrier beds, e.g., lithological intervals of low permeability. Obviously, low permeability should have opposite lithological properties to that of high permeable beds and pathways just discussed. This can be fine-grained sediment intervals, consolidated carbonates, salt tongues, lava or sill intrusions etc.. The term 'low permeable' here does not only apply to permeability for water and liquid, but also to 'capillary pressure'. Since many such intervals have fine grain sizes, they represent a very high capillary pressure zone, inhibiting infiltration of high molecular fluids, particularly hydrocarbons (Berg, 1975; Vavra et al., 1992). Aside from lithological intervals, many other mechanisms can physically hinder fluid migration. The precipitation of solid materials from fluids, as discussed in 2.2.2.1, can also lower media permeability. Yet, fluids can be trapped completely without a low permeable interval, e.g., when a highly overpressured interval is situated above fluids, downward dewatering flows can prevent ascent of deeper fluids: dynamic sealing. Such high pressure would develop due to either fluid injection from elsewhere or overpressure in shallower sediments.

#### 2.2.4 Chemical and Physical Alteration

When fluids migrate, the physical and chemical environment of the medium changes. Accordingly, their physical phase and chemical composition may also be altered. For the fluids under discussion, this alteration applies to hydrocarbons and elements or compositions dissolved in water. Note that items listed in the following are just examples. As long as the change of physical and chemical conditions can cause a component to become unstable, alteration can occur.

##### 2.2.4.1. Biodegradation and Microbial Oxidation of Hydrocarbons

Biodegradation is microbial alteration of hydrocarbons. It preferentially consumes and removes lighter components of petroleum (Bence et al., 1996; Miiller et al., 1987). For petroleum in greater depth, this may require substantial water flow through the petroleum to provide oxidants, e.g., oxygen, sulphate etc., for microbial activities. For petroleum near the seafloor, beside by advective flow, the oxidants may derive from sea water through diffusion. A special case of biodegradation is microbial oxidation of methane in shallowest sediment column, which removes methane ascending from greater depth, mostly dissolved in pore water, and transforms into CO<sub>2</sub> at the consumption of sulphate (Boetuis et al., 2000). This process virtually occurs in all aerobic ocean basins: SMT (Sulphate Methane Transition), which prevents substantial amounts of methane from entering ocean circulation and climate system.

##### 2.2.4.2. Thermal Alternation (secondary cracking)

When petroleum is trapped in sediments (discussed in **Section 2.2.5**), it may be subjected either to higher temperature when being buried deeper, or exposed to a high temperature for substantial time. The heavier components of petroleum may break down, and disproportionate into lighter petroleum and heavy residues. At extreme, all components would be altered into methane in anaerobic conditions (Tissot and Welte, 1984), but the completeness of this process is certainly a function of time and temperature.

##### 2.2.4.3. Gas Hydrate Precipitation and Other Phase Alterations

As mentioned, the essential cause of the alteration of fluids is the change of physical and chemical conditions during their migration. Besides all the chemical alteration discussed above, fluids also change their physical phase (dissolved, gaseous, liquid or solid) as a result of changing temperature and pressure. Decreasing pressure for ascending petroleum releases

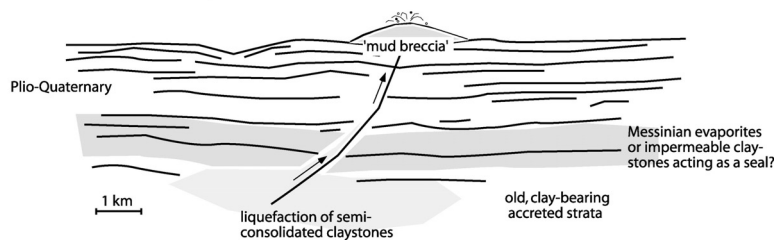
increasing amounts of the gaseous phase (wet gas), which then can follow a separate migration path than their mother petroleum liquid. Ascending methane of thermogenic or deep biogenic origin may contribute a large portion of gas hydrate accumulation in global scale (Milkov, 2005), with the other one being in-situ microbial methane generation. Such methane can be dissolved in water. With upward-decreasing water solubility, it would become oversaturated near or inside the gas hydrate stability zone (GHSZ), and exsolve as free gas or gas hydrates. When methane is already oversaturated and moves also as free gas, similar gas hydrate precipitation also occurs from such methane.

Note that gas hydrate precipitation, among many chemical and physical processes which turn fluid into a solid phase (chill of heavy petroleum at low temperature and mineral precipitation), may occupy fluid pathways, hindering migration of additional fluids (Kleinberg et al., 2003; Zühlsdorff et al., 2000). This is one means of restraining fluid migration, but retention of fluids is more often accomplished by low permeable intervals in the fluid migration media (Section 2.2.3).

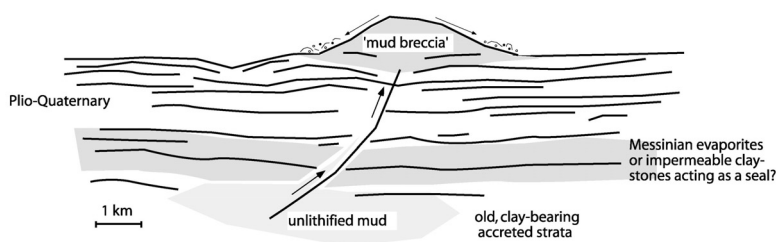
## 2.2.5 Trapping, Accumulation and Seepage

### 2.2.5.1 Water Seepage

#### Eruptive phase, early clastic cone



#### Turbidity currents, mud debris flows



#### Subsidence, continued mud flows

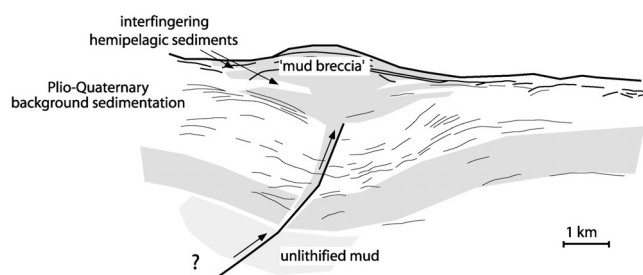


**Figure 2.11** Model for MV evolution proposed by Kopf et al. (1998) for a violent eruption with numerous debris-flow events in the Mediterranean.

Building up of overpressure through temporary traps water in the sediment, subsequently may facilitate more focused and vigorous water flow. Mud volcanism, for example, typically needs highly pressurized water to fluidize buried mud. The water in these muds can be original pore water from the deposition, or be later injected by dewatering of more permeable formations from elsewhere. The low permeability of mud makes dewatering from it, either as original pore water or later injected, much more difficult than from coarse-grained sediments, where overpressure is easier to dissipate by dewatering. Thus, upon fluidization, mud and water cannot be easily separated, and would move as a single phase to potential pathways. This is regarded to be the principle mechanism for mud volcanoes (Fig 2.11). Note that fluidized mud is not only mobilized by a pressure gradient, but also through buoyancy, since the mixture of mud and water has virtually always a much lower density than the surrounding formations. The pathways could be faults or any other weak zones in the geological formations (Carson and Screaton, 1998). Interestingly, the pathways for mud transport should be very narrow (submeter scale) by theoretical considerations of Poiseuille's law (Kopf, 2002). Those kilometre wide blanking zones under some mud volcanoes would imply astronomically fast mass flow, if the entire width of the blanking zones functions as pathways. Build-up of overpressure can also eventually enable trapped fluids to overcome the lithological barriers by fluidization, e.g. diatreme, or induce microfractures in sediments (Luo and Vasseur, 2002; Robert and Nunn, 1995).

Alternatively, the overpressure zone acts as a mechanically incompetent interval and causes failure of sediment slopes which in turn may release fluids. Fluidized muds, along with its low density, also have rather low shear strength (Jackson and Vendeville, 1994), and thus can serve as ductile detachment layer. This facilitates sliding or slumping of slopes or other thin-skinned deformation. By doing so, either the mud would be directly exposed to the seafloor or deformed surrounding formations provide new pathways for mud to escape. Or, an overpressured mud layer can serve as decollement in convergent margins (Le Pichon et al., 1993), facilitating imbricate faulting of accreted sediments. Consequently, fluidized mud can rise through these faults to the seafloor.

#### 2.2.5.2. Hydrocarbon

The cases for liquid and gaseous hydrocarbons to directly fluidize sediments are rare, although one notable exception is the role of hydrocarbon gas in mud volcanism and slope instability (Dickens et al., 1997; Dillon et al., 2001; Van Rensbergen et al., 2002). Hydrocarbon gas has upward decreasing solubility in water. Thus, if the dissolved gas is moved into shallower formations, it can become oversaturated. A gaseous phase can also be produced by decomposition of gas hydrates, due to increasing temperature and/or lowered sea level. Exsolution or gas hydrate decomposition does not always results in a net volume expansion, while highly depending the formation pressure (Xu and Germanovic, 2006). However, if net volume expansion does occur, it increases overpressure, and the gaseous phase would assist overpressured water to fluidize the muds. Alternatively, the gaseous phase alone can create a low shear zone, facilitate slope failure (Paull et al., 1996; Mienert et al., 2005), as for example for the interesting match between the gas hydrate dissociation area and the headwall at the Storegga slump, Norway (Fig 2.12).

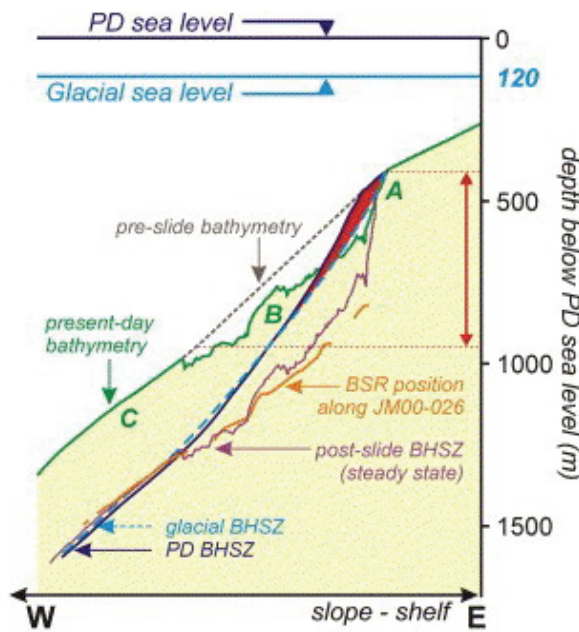


**Figure 2.12** A gas hydrate stability study at Storegga slump headwall area (Mienert *et al.*, 2005). The dotted brown line is the reconstructed pre-slide bathymetry in our model; the green curve is the present-day bathymetry picked along their seismic profile. The blue lines mark the estimated hydrate stability limit for the LGM (light dashed) and the present (dark), ignoring the effect of the slide process itself. The orange line represents the present-day BSR picked along their seismic profile and the purple line is the present-day steady-state location of the 3-phase boundary (methane, average salt water, hydrate). Remarkably, the critical area of hydrate dissociation (red zone and red arrow) matches the location of the Storegga headwall. In addition, the present-day theoretical extent of the hydrate stability zone (purple line) lies close to the depths read from the seismic record (orange), illustrating the quick response of hydrate conditions to environmental changes of climate and slope failure.

Overpressure of hydrocarbon fluids may play a prime role in migration of fluids through their source rocks. Newly generated petroleum in TOC-rich but low permeable source rocks may not easily escape and become highly overpressured. The pressurized fluids would cause micro-cracks in the rocks, which are completely saturated with hydrocarbons. These fluid pathways are regarded as a predominant mechanism for petroleum to migrate through their source rocks and reach more permeable carrier beds: primary migration (Tissot and Welte, 1984).

The processes discussed above are, however, much less likely to occur in high permeable carrier beds. Although similarly overpressured, they would have much less influence on the mechanical strength of the formations, and even overpressured, the major driving force for migration is buoyancy. When stalled in straight vertical directions by low permeable or high capillary pressure beds, fluids would flow more laterally, as for example fluids in a tilted carrier bed buried by low permeable sediments. Alternatively, low permeable barriers would focus fluid in fault planes, fracture zones or other more permeable pathways, which have limited spatial extent. If such pathways end in the subsurface, fluids would accumulate. However, either case would focus hydrocarbons only if these pathways lead to a trap structure, a critical factor for oil industry and also for cold seepage.

Traps mainly refer to more permeable beds that are upward and laterally closed by low permeable beds, so that the permeable sediments can store and accumulate hydrocarbons. Permeable beds are defined as reservoirs, and they can range from coarse-grained sediments, fractured igneous rocks to carbonates (discussed in 2.2.3.1). Those low permeable beds act as seals. They can be fine-grained sediments, intact igneous rocks, carbonates or salt (discussed in 2.2.3.2). Interestingly, many fault surfaces that cut through reservoirs are regarded as important seals and laterally close the reservoirs.

Aside from the various lithologies of reservoirs and seals, the geometry of traps can also be originated from a variety of processes. Traps may be divided into these two process-based

categories: structural traps and stratigraphic traps. Structural traps are those formed through deformation, such as folding and faulting of sediments, active salt diapirism etc. Stratigraphic traps are defined as structures resulting exclusively from depositional processes, such as channel-levees structures, sediment waves, interfingering between fine-grained and coarse-grained sediments etc. Obviously, stratigraphic traps can also be subject to deformation after their formation and become a mixture between the two end members.

In order that the accumulated hydrocarbons eventually break through the seals of traps and escape, seals must be breached. High water overpressure should be one possibility to fracture the seals. Another very common mechanism breaching sealing beds are column height pressure exerted through thick and continuous hydrocarbon phases (discussed in **2.2.2.2.**). Alternatively, since the traps are only closed upward and laterally, when sufficient amount of hydrocarbons are charged into the trap, they would totally fill the closure and spill at the traps' outer rings. The escaping fluids would move either into shallower traps or onto the seafloor and become seeps. Because the fluid volume has been first concentrated in traps, the seep sites are also focused in discrete locations, through which large volumes of hydrocarbon fluids outflow, as opposed to dispersive seeps resulted from lack of any focusing mechanism.

## Chapter 3. The Nature of the PhD Study

### 3.1 Scientific Goals and Approach

The general scientific goal guiding the PhD study is to understand cold fluid seeps from various geological perspectives. In **Chapter 2** we have outlined that geological processes are heavily involved in the occurrence of seeps. Virtually all aspects ranging from sedimentation history (and resultant lithology), sediment deformation history, sediment physical and chemical properties, sedimentary structures and geothermal history can all influence the occurrence and nature of seepage. Strictly speaking, all these aspects would have to be well understood to predict the seeps' occurrence, characterize their nature, and reconstruct their evolution. In the end, if seepage is understood as a geological phenomenon and over geological time scales, their contribution to global climate change, marine environments and marine water chemical inventories can be better judged.

Under this general guideline, the PhD study was focusing on near-surface (1 – 2 km below seafloor) sediments and structural imaging of features under targeted seepage sites to reveal the causal link between geological processes in upper sediment column and fluid seepage processes. More specifically, the approach aims to a better understanding of sedimentation and tectonic history of the near-surface sediments, and the resultant subsurface structures. It is complemented by the analysis of fluid-indicating seismic features: bright spots, blanking zones, BSRs etc. By applying these results, the ultimate goal is to discuss their controls on migration, focusing, accumulation of cold fluids, as well as the occurrence and evolution of fluid seepage. The methodology will be introduced in detail in **Section 3.4**. Such a study would also more directly assist other studies of the *Marum* Project Area “Seepage of fluid and gas”, which focuses mostly on seafloor or extremely shallow chemical and geological processes at seep sites.

Cold seep areas predominately cluster around continental margins ([Fig. 1.2](#)), and occur in a great variety of sedimentation and tectonic regimes on global scales. In order to cover a reasonable range of tectonic and sedimentological processes for discussion, two study areas were chosen for the study, which have distinctly different tectonic settings. They are namely the *Campeche Knolls Area* in the southern Gulf of Mexico, a passive margin under active salt tectonism, and the *Makran* accretionary prism, a convergent margin with thickest converging sediments in the world. The regional settings of both study areas are described in detail in **Section 3.3**. The selection of the two study areas enables us not only to investigate individual areas, but also to compare them for a general discussion of the relationship between shallow geological processes and cold seepage.

To serve this study goal, proper datasets that can reveal near-surface features of seepage area and further hint into the geological processes behind these features, are required. For the two deep water study areas, we chose high resolution multichannel seismics as the prime dataset, because it can both provide detailed subsurface structural information and allow moderate penetration. In principle, high frequency echosounder (e.g., Parasound) and swath bathymetric data can be supplementary for the study. Although using predominantly seismic and acoustic data, the research goal distinguishes the methodology from direct acoustic mapping of seepage (e.g. in the water column), as introduced in **Section 2.1**. In addition, because the study approach emphasizes on geological processes and general structural patterns, it does not always require seismic and acoustic data with ultra-high spatial density. Instead, we can fully utilize sparsely spaced 2D seismic data (in addition to some higher density seismic grids at

several sites), which were collected as part of reconnaissance surveys and due to limited acquisition time.

## 3.2 Dataset

### 3.2.1 High Resolution Multichannel Seismic

#### 3.2.1.1 The acquisition system

The seismic data used for the studies were collected during R/V Meteor Cruises M67/2a and M74/2 in 2006 and 2007, respectively (Bohrmann et al., 2004; Bohrmann and Spiess, 2008; Bohrmann et al. 2008; Spiess (M74/2 Makran cruise report; in prep)). Both cruises employed a high resolution multichannel seismic system, custom designed at the University of Bremen, to optimize all system components for high resolution. The complete system is outlined in Figure 3.1. For the seismic sources used in the two cruises, the 0.16L water gun is for ultra-high resolution surveys (600 Hz to 2 kHz). 1.7x1.7L GI (volume can be reduced by reducers) and 4.1x1.7L GI are for high resolution survey at deep water areas, and their source signal frequency is around 20 Hz to 400 Hz.

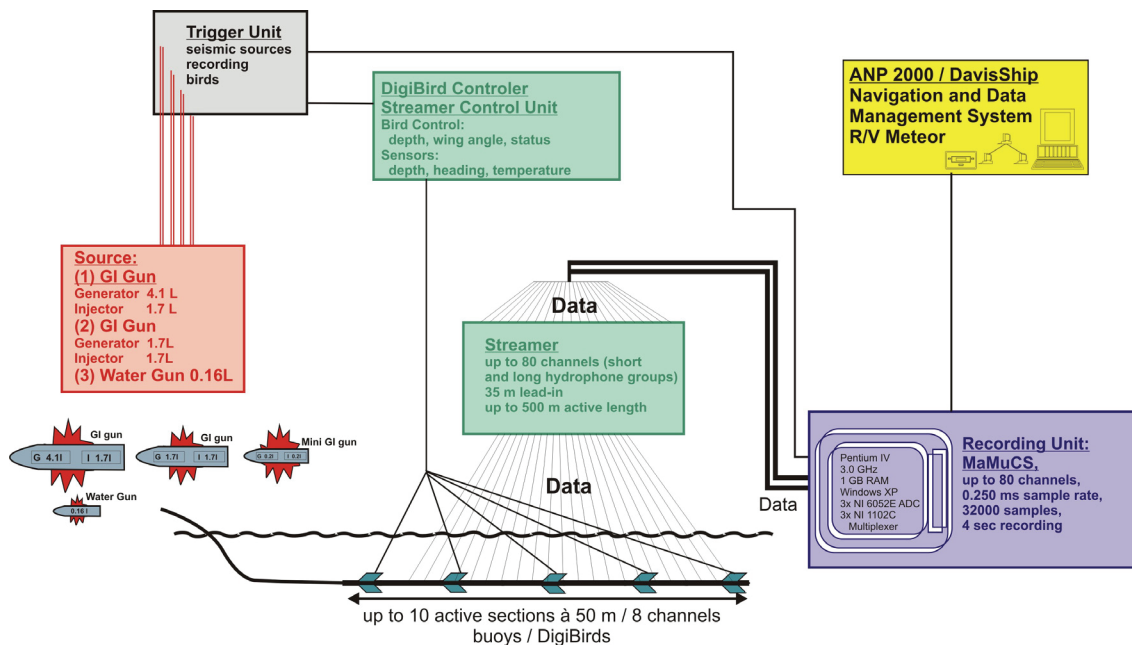


Figure 3.1. Outline of the Bremen high resolution reflection seismic system.

The return signals are recorded by Syntron<sup>TM</sup> streamer sections. Each section is 50 m long, containing 8 high resolution hydrophone groups. Consequently, the distance between every two groups is 6.25 m. These sections are stacked to form channels during acquisition. A total of 8 of such sections was available for both the M67/2a and M74/2 Cruises. During acquisition, birds (DigiCourse Inc.) were attached to the streamer to control its towing depth. Furthermore, the birds also recorded their actual depth and orientation during acquisition for the purpose of geometry calculation.

The data digitization and recording is performed by (Marine Multichannel System) MaMuCS, a custom designed software that can digitize and store simultaneously max. 96 channels. In addition, during recording, MaMuCS can also display not only the latest acquired return shot gather but also the entire on-line stacked seismic profile set since the start of recording. Cruise

M67/2a saw the first time the MaMuCS system being used for a research cruise. During the M74/2 cruise, the MaMuCS system has been capable of receiving and recording ship navigation differential GPS data.

### 3.2.1.2 Acquisition configuration for the datasets used in this study

During the seismic acquisition of both Cruises M67/2a and M74/2, up to 8 active Syntron™ streamer sections were deployed for recording. During M67/2a, a stretch and a lead-in section towed the streamer, so the maximum gun-receiver offset was 480 m. During M74/2, the stretch section could not be used, resulting in a maximum offset of 430 m. During both surveys, the streamer depth was controlled and recorded by 5 – 6 Digicourse birds attached to the streamer. The target towing depth was 3 m, although the real depth varies typically from ~1 to ~5 m depending on weather and sea state (+/- 0.5 for good weather conditions). During M67/2a, two profile sections were acquired concurrently with the DTS-10 deep tow sidescan sonar, and at that time, total deployed streamer length was shortened to 150 m. Ten regional profiles during M74/2 were acquired in parallel with the TOBI deep tow sidescan sonar acquisition, and the streamer was towed at the starboard side of the vessel, instead of conventionally at center of the vessel. The total streamer length was not reduced, but the streamer depth was controlled by some 20 buoys attached at equal distance to the streamer, resulting in a towing depth of 1 – 2 m.

During M67/2a, two seismic sources were in action, a 0.16L water gun and a 4.1L+1.7L GI gun. Typically, in a recording period, the water gun was shooting first, and the GI gun was triggered 1.5 seconds later. The return signals of both sources were recorded in the same single trace. In ultra-deep water (> 3000 m), two water gun shots and one GI gun shot were possible for a recording period. Such a shooting configuration enabled faster shot rates for both guns than the alternating mode, ensuring high lateral resolution of recorded data as well as sufficient coverage. More detailed trigger schemes and other configurations are given in the M67/2 cruise report (Bohrmann and Spiess, 2008). During M74/2, only the 4.1L+1.7L GI was used for acquisition, requiring a simple trigger scheme that varies only according to water depth (Spiess et al.; M74/2 Cruise report; in prep).

During the M67/2a acquisition, the water gun was towed ~1 m deep, while the 4.1L+1.7L GI was deliberately towed as deep as 7 m. Although a source ghost may occur in records, this towing depth has generated stronger seismic signals than for shallower towing depth. The acquisition of M74/2 maintained the same towing depth of 7 m for the GI gun.

### 3.2.1.3 Data processing

The seismic datasets from both M67/2a and M74/2 were processed with a multichannel seismic processing method, using the Vista™ seismic processing software package. In addition, the custom developed GeoApp program has been used for geometry and CMP binning calculations. For the M67/2a dataset, the CMP binning distance was first chosen to be 10 m, but was further reduced to 5 m or 3 m to better resolve the steeply dipping and laterally varying features in the study area. For the M74/2 dataset, a uniform binning distance of 5 m was applied, while some profiles were tested for 3 m bin distance.

Dead and extremely noisy channels were removed from both datasets. Traces with random spike noise were also marked as dead traces. Velocity was picked for all profiles, and was used together with the CMP binning calculated by GeoApp for the normal move-out (NMO) correction and CMP stacking. The stacked datasets were filtered with a broad band-pass filter of 30/60-

600/800 Hz to preserve both the high resolution and the deeper penetration signals, while still filtering out the greater part of the frequency dependent noise. The stacked profiles were then time migrated with a finite difference method. Both stacked and migrated profiles are exported from the Vista software as SEG Y data and imported into the Kingdom<sup>TM</sup> Suite software for further interpretation work.

### 3.2.2 Swath Bathymetry

#### 3.2.2.1 Acquisition System and Parameters

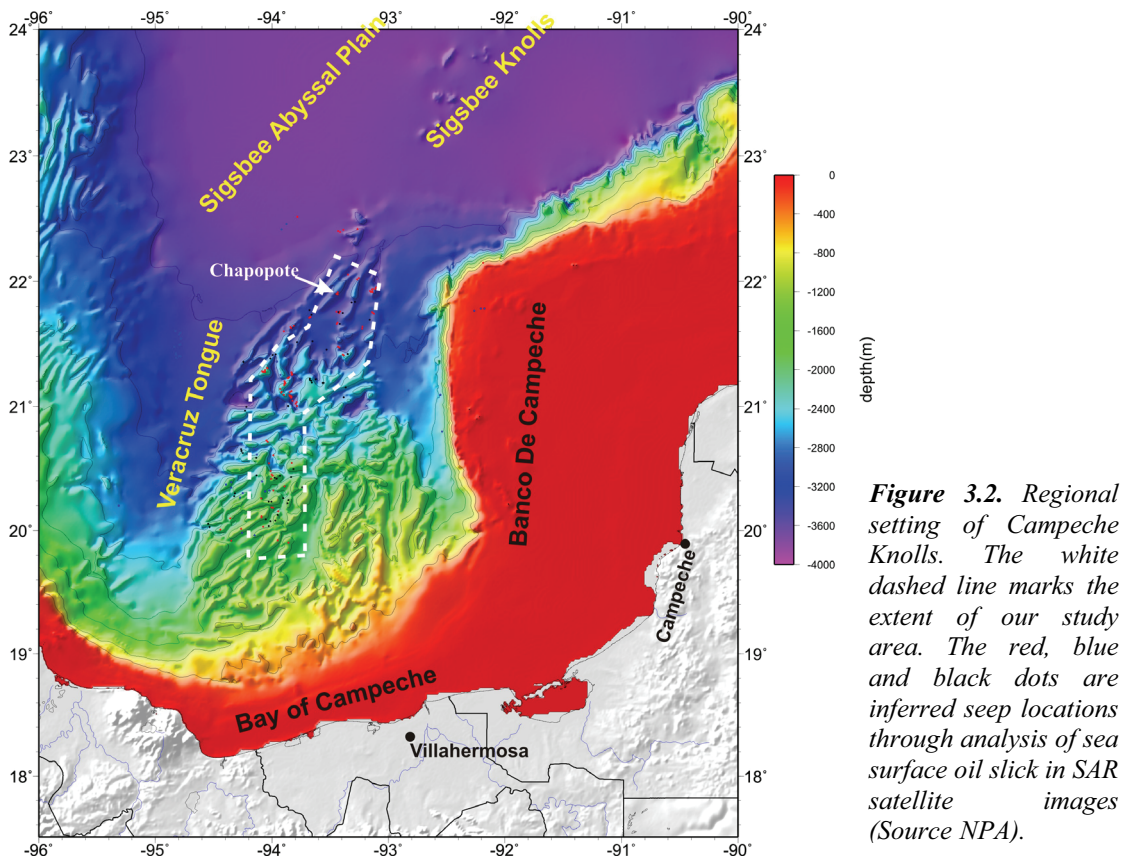
Both Cruises M67/2a and M74/2 were carried out on R/V Meteor, and the same ship-mounted multibeam system Simrad<sup>TM</sup> EM120 (Kongsberg) was used for the acquisition equipment of bathymetric data, which can cover virtually the entire ocean depth range. The system has a signal frequency of 12 kHz and 191 beams. The outermost beam angle was set between 50° to 70° (single side), changing with varying weather conditions and ship velocity (Bohrmann et al., 2008). Many other settings such as ping rate, yaw correction can be automatically adjusted by the recording software.

The processing was carried out with the Caribes<sup>TM</sup> software. Procedures include sound-velocity modelling, motion correction, trace editing and gridding. Previously available bathymetry data from an R/V Sonne cruise in the study areas were also incorporated in the newly acquired data. For Campeche Knolls (M67/2a), a 100-m grid spacing was applied for the entire region, while 40-m to 25-m grid spacing was applied for detailed bathymetric displays of individual knolls, particularly Chapopote. For Makran (M74/2), a 50-m grid was used for further investigations. Markus Brüning has performed most of the data processing during both cruises. To display the bathymetric grid and seismic line locations, the GMT software (Wessel and Smith, 1991) was used.

### 3.3 Study Areas

#### 3.3.1 Campeche Knolls, Gulf of Mexico

Campeche Knolls is one of the two active salt provinces in the southern Gulf of Mexico. Together with the Sigsbee Knolls, it makes up the salt regime in southern GoM, which is separated from Mississippi-Texas-Louisiana salt province by the Sigsbee Abyssal Plain (Bryant et al., 1991; Buffler, 1991). The two regions are described as knolls because previous seismic surveys had indicated a widespread occurrence of uplifted domes. The Sigsbee Knolls are located to the northeast of the Campeche Knolls, and are bounded by the carbonaceous Banco de Campeche (Campeche Bank) and the Sigsbee Abyssal Plain. The Campeche Knolls are bounded by the Banco de Campeche to the east, and the Bay of Campeche to the south (Fig 3.2). A salt-free abyssal plain called Veracruz Tongue (Bertagne, 1984; Bryant et al., 1991) is located between the Campeche Knolls and the Mexican Ridges further west. Northwards, the Campeche Knolls are connected to the Sigsbee Knolls. The salt activity in the southern deep GoM basin is believed to be an analog to that of the Texas-Louisiana shelf in the northern GoM (Garrison and Martin 1973). Most of the salt is inferred to have deposited in the Late Jurassic (Challenger Unit of Watkin et al. 1978), during the rifting stage of the gulf (Salvador, 1991), equivalent to the Louisiana salt of the northern gulf.



As typical for basins in Gulf of Mexico, the Campeche Knolls had been covered by a thick column of sediments, most of it above the salt unit. The total sediment thickness reaches 5 – 10 km, varying with water depth and distance from the southern coast. The sediments are even thicker in the near-shore Bay of Campeche and onshore areas (e.g., [Ambrose et al., 2003](#); [Viniestra, 1981](#)). The thick sediments provided prolific petroleum source rocks with the most productive one being of latest Jurassic and Cretaceous age. (e.g., [Magoon et al., 2001](#); [Santamaria-Orozco et al., 1998](#)). However, most of the sediments are deposited during Cenozoic times, controlled by both orogenic events in Mexico and sea level changes.

Hydrocarbon generation makes the Campeche Knolls a high-ranked, prolific petroleum region ([Magoon et al. 2001](#)) and studies have long shown that salt activity supports leakage of gas and oil. During DSDP Leg 10, at Site 88, drilling into the crest of one of the knolls had to be abandoned because of indications of highly pressurized gas ([Worzel et al., 1973a and b](#)). Oil seepages can also be indicated by widespread natural oil slicks on the sea surface of the region, quite similar to the oil slicks in northern Gulf of Mexico ([MacDonald et al., 1996](#); [De Beukelaer et al., 2003](#)). These oil slicks can be imaged by SAR satellite imagery, which are then used to track back the location of its source, which is likely very close to seep sites. More recently, such remote sensing results in Campeche Knolls guided R/V Sonne Cruise SO174 ([Bohrmann and Schenck, 2004](#)) to the discovery of gas, oil and asphalt seepage on the top of one knoll in the northern tip of the province: Chapopote ([MacDonald et al., 2004](#)).

Although it is not the first time that natural asphalt was found in the deep GoM basin ([Pequegnat et al., 1971](#)), the Chapopote asphalt site is particularly notable for its large spatial distribution, with many individual patches over hundreds of square meters. On the other hand, we note that the asphalt deposition does not cover the entire surface of Chapopote, instead it

only occurs in an area of about 1 km<sup>2</sup> located on the southern part of the knoll. A most recent survey on board of the Mexican research vessel *Justo Sierra* has further discovered natural surface asphalt pavement on several other knolls, distributed across the entire Campeche Knolls area (MacDonald et al., 2007).

### 3.3.2 Makran Accretionary Prism

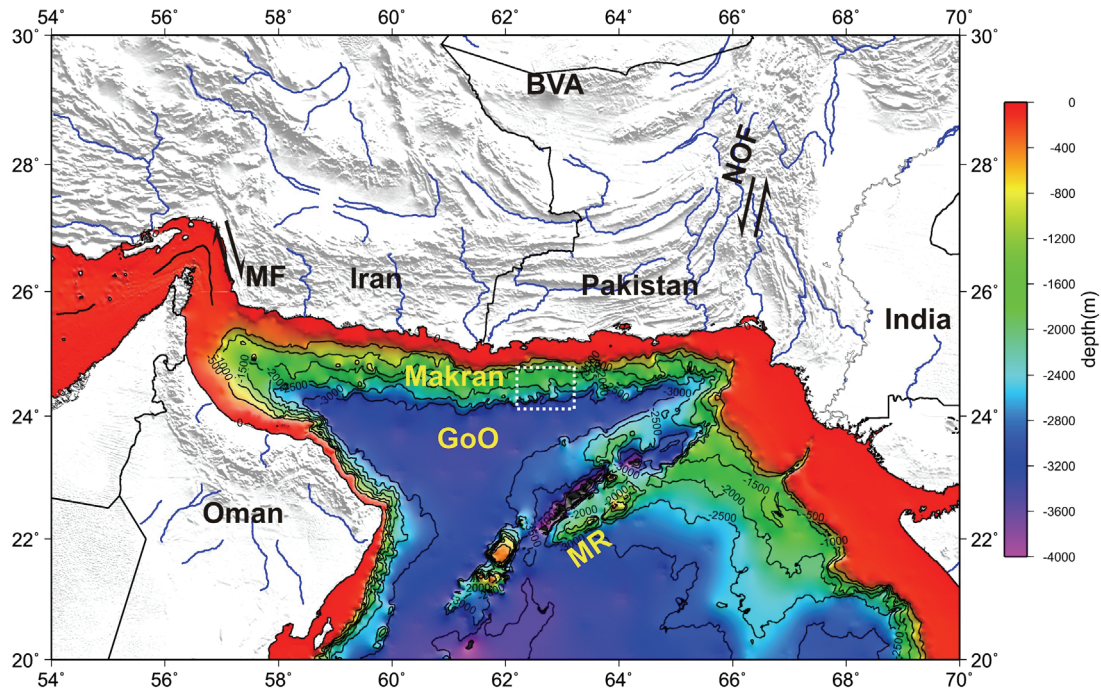


**Figure 3.3.** Regional setting of Makran Accretionary Prism. The dashed block outlines the extent of our study area. MF = Minab Fault System, MR = Murry Ridge, BVA = Baluchistan volcanic arc, ONF = Ornach-Nai Fault System, GoO = Gulf of Oman.

The Makran Accretionary Prism marks an accretionary convergent margin, where oceanic crust in the Gulf of Oman is subducting under the continental Asian Plate. To its west and east, the prism is separated from Zagros Range and Himalaya, respectively by two strike-slip faults, namely the Mainb Fault and the Ornach-Nai Fault. The prism trends largely west-east and slightly curved at both ends (Fig. 3.3). Currently, the convergence rate is 3 - 5 cm/yr (Quittmeyer and Kafka, 1984; DeMets et al., 1990), approximately normal to the strike of the prism. The Makran Prism is an extraordinarily wide accretionary prism, extending 150 km offshore and 200-300 km onshore (White and Klitgord, 1976). Even at present-day, it grows 11 km/Ma into the Gulf of Oman (Platt et al., 1985). The accretion history of the prism dates back to the late Cretaceous (Arthurton et al., 1982; Harms et al., 1984), and thus it is a convergent margin since the time of the Tethys Ocean. Substantial underplating since no later than the late Miocene (Platt et al., 1985) uplifted large part of the prism above sealevel. Turbiditic sediments in the Gulf of Oman and Makran were first sourced from the Himalayas and the Indus River. Recently (~10 Ma, under debate), the uplift of Murray Ridge has dammed Indus fan sediment from entering Makran. Instead, the predominant sediment supply shifted to the hinterland of Makran from the north (Gaedicke et al., 2002). Both deposition episodes have consecutively kept the Gulf of Oman being a fast sedimentation regime since the Oligocene. Presently, the total sediment thickness immediately seaward of the Makran Prism amounts to 5 - 7 km (Fruehn et al., 1997; Schlüter et al., 2002).

Around our study area (E62°45' to E63°8', Fig. 3.3), the décollement of the prism is about 4 km below seafloor at the deformation front (Fruehn et al., 1997; Kopp et al., 2000; Kukowski et al., 2001), and is made from a ductile layer. Sediments above the décollement are being accreted by imbricate thrusting (Fruehn et al. 1997). The frontal Makran is designated as the portion of the prism immediately inboard of the deformation front. It is comprised of lower slope ridges and a mid slope terrace defined by Kukowski et al. (2001). The lower slope is featured by many steep-sided sediment ridges, marking the surface expression of imbricate slices. These ridges can stand several hundred meters above the surrounding floor, but vary in elevation along-strike. The mid slope terrace is a relatively flat area, apparently as the result of ridges being buried by sediments from the north (Kukowski et al., 2001). Further landward, the frontal Makran is bounded by a steep upper slope and the shelf break.

The Makran Prism is segmented by a plate boundary fault, the Sonne Fault, which separates the underlying oceanic crust into two plates: an oceanic part of the Arabian Plate and the Ormara Plate (Kukowski et al., 2000). The fault causes a left-lateral offset to the sediment ridges in the lower slope. Natural earthquake solution also indicates faster movement of Ormara Plate, where the majority of seismic activities occurred. The surface trace of the Sonne Fault is taken by a canyon, running from the upper slope down to the abyssal plain. Several canyons also run down-slope across the frontal Makran, mostly zigzag cutting through the ridges (Kukowski et al. 2001).

### 3.4 Methodology and Study Working Flow

#### 3.4.1 Seismic Feature Identification, Interpretation, and Mapping

##### 3.4.1.1 Reflection feature identification and mapping

When the processed seismic data are loaded into the Kingdom software, the interpretation first focuses on individual 2D seismic profiles. (1) It first inspects seismic reflectors and their reflectivity, distinguishing between continuous seismic units, intermittent reflectors, and chaotic reflections. (2) It then identifies every structural features (folds, faults, monoclines, etc.) and reflection termination features (onlap, toplap, downlap, etc.). (3) It also identifies seismic anomalies such as blanking zones and high reflection amplitudes. While the first two kinds of features are usually indicators for geological phenomena (sedimentation, salt movement, interaction of the two and other postdepositional and deformation features), the third kind of features are usually seismic indicator of fluid activities (Fig. 3.4). Thus, they are not spatially exclusive to each other, and may overlap.

The identified features in some individual profiles are then mapped through the entire dataset. Mapping involves to a certain extent interpretation, in which it judges if two similar observations in different profiles belong to the same feature. Since the features in high resolution seismic data are from the near-surface and resulted from the most recent activities, they may often display seafloor expressions, such as bathymetric ridges are related to folds in subsurface, or domes to salt diapirs. Thus, high resolution bathymetry (10 to 100 m) presents a useful reference for the mapping of features in the subsurface, reducing the uncertainties of interpretation.

##### 3.4.1.2 Lithologic interpretations

Lithologic interpretation is to identify the lithology of defined and mapped seismic units. This includes the nature and origin of siliciclastic sediments, in terms of grain size, debris flows,

turbiditic or hemipelagic origin, etc. In addition, the distinction between salt units and other chaotic seismic features is also required. Besides, the nature of the seismic data, e.g. reflectivity and geometry of seismic units, regional sedimentation history, can also be used to aid such interpretation, if the seismic units are dated clear enough. The purpose of lithologic interpretation is mainly to infer the permeability of different units, to identify aquifer and seal intervals for the discussion of seepage occurrence (Fig. 3.4).

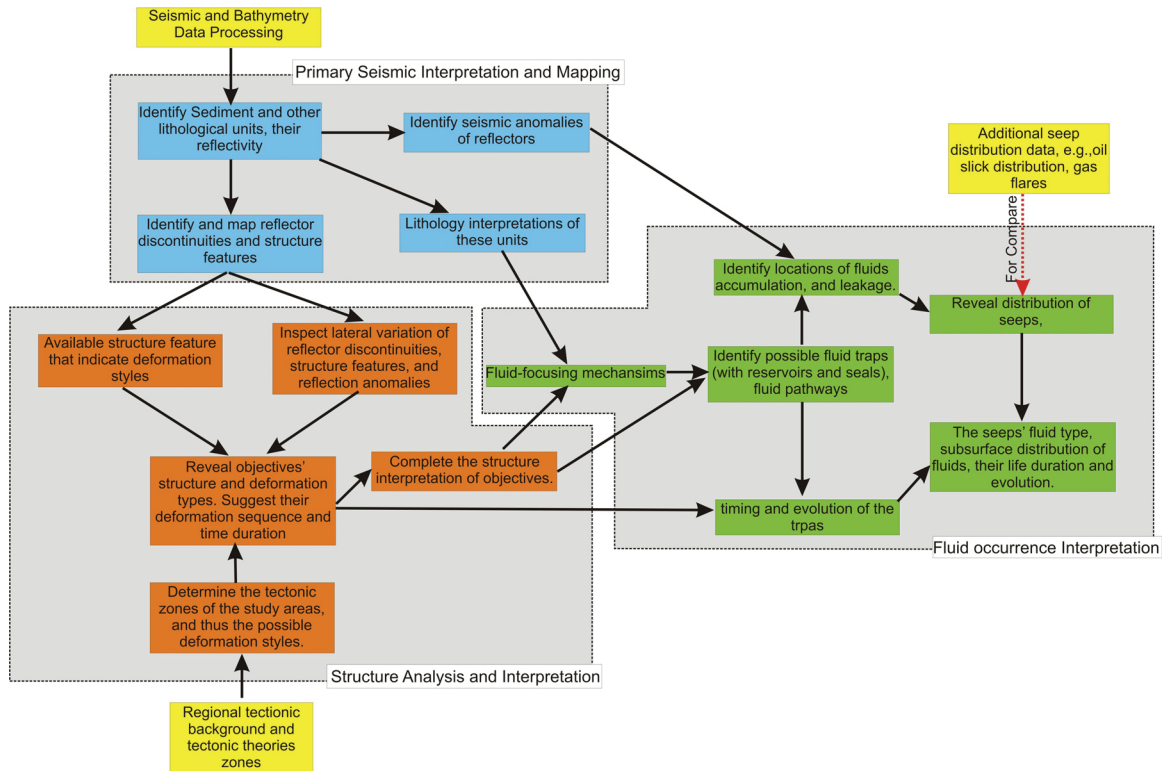


**Figure 3.4.** The working flow of our seismic interpretation and fluid seepage study. See text Section 3.4.

### 3.4.2 Structural Interpretation and Evolutionary Sequences

The features identified in the previous step should be distinguished from targets of the investigation. A target is a lithologic body, either distinctive in morphology, e.g., Chapopote, Nascent Ridge, or an arbitrarily ascribed area. A target may comprise a combination of the features discussed above. The geological features mapped in the profiles may not always reveal complete structures of targets due to limited signal penetration, reflector discontinuity or disturbance by high amplitude/blanking features. Ambiguous observations in seismic profiles can commonly leave different possibilities for the interpretation of complete subsurface structures of targets. However, narrowing down alternatives for complete and even detailed structural reconstruction is needed, because it can be very critical for interpreting seep occurrence (Section 3.4.3).

The lateral gaps and sometimes vertical gaps left by feature mapping should be filled. Beside experience (shows up as hunts) and simple interpolation, this could also be accomplished on a theoretical basis. A certain style or pattern of deformation, e.g., active diapirism, salt withdraw basin, thrust faulting, can only deform targets in certain ways. So, if the deformation style of a target can be understood, there would be better constraints on the geometry of resultant

structures that could be produced. This could narrow down different possible interpretations in filling the gaps, and also fulfil our goal of tectonic reconstruction. However, this means that the interpretation sequence would be reversed: a historical and kinematic perspective of a target should be established before their complete structure could be outlined, and this historical perspective shall help to completely depict the structure of a target (Fig. 3.4).

We regard such reversed interpretation could be possible with three approaches (Fig. 3.4). The first of them is to examine the lateral variation of study targets. In many cases, the seismic profiles running through the most deformed parts of a study target fail to image a clear structure, simply because too much deformation and too many fluid-related features are overlapping in the profiles. So, profiles that are located at an increasing distance from the center of deformation may more clearly indicate individual deformation processes, e.g., faulting, folding. Waning and waxing these processes at lateral directions, either along-strike or across-strike, may also further reveal the linkage between them.

Secondly, we investigate available deformation features from our profiles from a tectonic point of view. Even when profiles cannot provide a complete structure of study targets, the many mapped deformation features can offer indications for the deformational style for the targets under investigation. For example, repeated reflector onlaps and steeper deeper reflectors suggest continuous on-going uplifting and deformation. Very small wavelength folding of near-surface sediments suggests these sediments are detached from deeper sediments, and thus salt is present in shallow depth to enforce as the detachments. These combined indicators may not suggest a concrete deformation style of the study targets, but may significantly boil down possibilities.

The last but not the least is to view the study area from a regional perspective. It is meant to understand the regional tectonic and sedimentation framework and history of study areas. Both the previous studies of salt tectonics and sediment accretion can provide general and regional models for these two modes of sediment deformation. Regional tectonic zones could then be divided using these models coupling with complicating factors of a specific region, e.g., sedimentation and plate tectonic history. Some of these tectonic framework studies may be already presented in the literature. Otherwise, accessible regional datasets may also provide such hints. These tectonic frameworks can then suggest the deformation zones where our specific study areas are situated, where only a specific set of deformational styles could possibly occur. We notify that this approach can be totally independent of our study dataset (Fig. 3.4), while makes better use not only of available, additional datasets, but also of previous studies and the general understanding of regional tectonics. It requires stronger tectonic background to carry out this approach, and significantly expands the scope of our own studies, although caution must be paid because these general framework models can be very ambiguous and need to be refined.

### 3.4.3 Use of Structural Interpretation and Seismic Features for Seepage study

The knowledge acquired from **Sections 3.4.1 and 3.4.2** on target structures' and their evolution, their lithologic composition, and on seismic anomalies can then be used to suggest seepage prone areas (Fig. 3.4). An ideal working procedure includes: (1) To identify fluid-focusing mechanisms, through tilted aquifers, fracture zones, faults, salt-sediment boundaries etc.; (2) To identify reservoirs that can store fluids guided by focusing mechanisms. If these reservoirs are to a certain extent sealed, then they form traps; (3) To identify the timing for the initiation and evolution of the traps (e.g., to test if they are before the main deep fluid generation window); (4)

To infer the sealing capability of the traps. Those weakly sealed but fluid filled traps are candidates for seepage areas; (5) To compare the mapped seismic anomalies (fluid-indicating features) with seep-prone areas indicated from the structure knowledge.

As obvious, the study of fluid seepage occurrence critically relies on the results of structural and lithological studies. Especially the discussion of sealing capacity is always not directly based on seismic data, because in seepage areas, the seal and reservoirs often lie within seismically chaotic zones. For step 3, the time line for trap evolution might be outlined in our studies, but the understanding of the regional fluid generation window may not be developed yet, if there is a shortage of regional studies. The study can still carry on if the seismic anomalies allow to clearly indicate the presence of fluids. Furthermore, additional data for seepage distribution can also be incorporated into the study for independent comparisons. For example, the seep locations inferred from sea surface oil slick distribution imaged by SAR satellite data or gas flares, identified through detailed Parasound or other echosounder surveys (Fig. 3.4), support those direct seepage detection techniques.

Seepage locations indicated from these data may not be always consistent with the seep-prone areas indicated from our working flow. Note that our working flow mostly provides seep-prone areas, instead of exact locations of seep sites. This is because our emphasis lies on the geological aspects of seepage, rather than on discovering specific positions of seep sites (discussed in **Section 3.1**). Furthermore, the predicted seep-prone areas may be suggested to be seepage absent by those direct seepage detection techniques, but uncertainties remain. After all, our approach only accounts for the control of near-surface structures and lithologies on the occurrence of seepage. The generation and initial migration of deep fluids are not addressed, but based solely on previous studies. Thus, instead of disproving either results, the inconsistencies may be used to hint to the influence of deep geological processes on the fluid seepage.

### **3.4.4 Limitations of the studies and future outlook**

#### **3.4.4.1 Limitations**

Our study method focuses on the near-surface structure for their influence on fluid focusing and seepage occurrence. Thus, it accounts only for migration of fluids at shallowest sediment intervals (sub-bottom depths down to 1-2 km). However, we have already discussed in **Section 2.2** that the source of fluids is usually at much greater depth. These fluid generation processes can be totally independent of shallow sediment structures. Deeper structures can also focus fluids into areas different from, where the shallow sediment structures would do. All these topics cannot be addressed by our approach and by the nature of our data. Published data and studies on such topics are usually very rare, either because the studies are few or the results are often industrially confidential. This shortage of fluid generation knowledge also hinders us to quantify the total mass seeped during the life time of the seep sites under study.

The lithologic interpretation employed in the studies is solely based on the seismic features: reflectivity for grain size, geometry for turbiditic or hemipelagic origin, etc. The conductivity of faults is mainly inferred by observing if there is any seismic anomaly along the faults. Based on such interpretation, the discussion of conductivity of carrier beds, reservoirs, and capability of seals has to be qualitative. There is for example no borehole data to ground-truth the lithologic and hydraulic character of our defined seismic units. The lack of borehole data and age-dating of seismic data in our study further limits the age definition of these seismic units.

The fluid-indicating seismic features that can best be imaged in our data are mostly signatures of free gas, gas hydrates and carbonates. Because of the difficulty may limited time to try out seismic attribute studies on our data, physical properties that can indicate e.g., gas concentrations, existence of liquid phase petroleum, overpressures, etc. are missing. This fact, when together with the absence of knowledge for deep fluid generation processes, hinders our data to reveal the presence of liquid petroleum.

#### 3.4.4.2 Outlook

The perceivable limitations in our approach described above also prescribes how further improvements should be made. I regard to involve deep processes, down to the depth of fluid generation are needed to study seepage, although seepage is apparently a surface phenomenon. Studying deep processes does not only complete the coverage from source to seepage, but also enable us to reconstruct the evolutionary history of fluid discharge. It is also desired that the study can also laterally expand to basinal scales, to encompass fluid migration processes in entire basins. Basin modelling software can in this context be used in seepage studies. After all, the initial motivation for the seepage study is to estimate their impact on environmental systems: climate system, ocean chemical inventories etc. To finally achieve this, the history of seepage and its occurrence on regional scales, including both focused seeps and pervasive discharge, must be characterized.

These historical and basinal study approaches may also create even more links with the current hydrological and chemical studies on the seep sites, which are undertaken by various working groups e.g. in the *Marum* project area “Seepage of fluid and gas”. After all, investigation and characterization of seep sites can only take present-day snapshots on numerically limited, under-represented sites. These investigations and the understanding of modern seeps can be perfect calibration data for basin modelling, because they alone cannot be reasonably projected into basinal scale and into the geological history without a regional and historical understanding of the entire basin. Such projections and extrapolations are needed to reveal the impact of the seepage on marine and atmospheric environments.

If deep and basinal approaches become available to fully characterize the generation of seepage, an improvement on lithological interpretation by incorporation of borehole data will allow a better characterization of how fluids would migrate, accumulate and seep. Similarly, new seismic datasets with larger gun-receiver offsets or use our current data in a geophysical intensive way shall better characterize seismic anomalies and allow various seismic attribute studies. The envisaged seepage research resembles petroleum exploration in that it also studies migration of fluids through the deep sediments column, and pursuits the evolutionary history of basins and the distribution of fluids in basinal scales.

Nevertheless, the seepage study also differs from petroleum exploration studies in two important aspects. First, the seepage study concerns a quantitative estimation of how much fluids have been generated in a basin, and eventually seeped, so their impact on e.g., the climate system can be evaluated. Petroleum exploration cares solely about how much hydrocarbon fluids are still retained in sediments. Secondly, the seepage study shall pursuit seeping of all geological fluids, including hydrocarbons, water and their dissolved chemical elements and components, because all these masses can alter environmental systems in their own ways. The petroleum exploration is interested predominately in hydrocarbon fluids.

In the end, the limitations of the current study approach do not mean it cannot be applied to further seepage areas. The advantage of our current approach and the requirements for our scientific objectives in the seepage study are already presented in detail in **Section 3.1**. If similar datasets are and would become available in other seepage regions of similar geological nature, it can be further applied to understand the geological control of seepage in these areas. Notably, the University of Bremen has already collected a treasure of geophysical data in many other seepage occurrence areas. These data are extremely similar to those used in our study, and thus can be readily used to apply our current study approach.

## References for Chapter 1 to 3

- Abrams, M.A.**, 2002. Surface geochemical calibration research study: an example of research partnership between academia and industry. In: *New Insights Into Petroleum Geoscience Research Through Collaboration Between Industry and Academia*, Geological Society, London, UK, May 8–9, 2002
- Alnes, J. R.** and R. A. Lilburn, 1998. Mechanisms for Generating Overpressure in Sedimentary Basins: A Reevaluation: Discussion. *American Association of Petroleum Geologists, Bulletin*, 82(12), 2266 - 2269
- Bahr, A.**, T. Pape, G. Bohrmann, A. Mazzini, M. Haeckel, A. Reitz, and M. Ivanov, (in press). Authigenic carbonate precipitates from the NE Black Sea: implications from mineralogical, geochemical and microbiological analyses. *International Journal of Earth Sciences*
- Bence, A. E.**, K. A. Kvenvolden, and M. C. Kennicutt, 1996. Organic Geochemistry Applied to Environmental Assessments of Prince William Sound, Alaska, after the Exxon Valdez Oil Spill—a review. *Organic Geochemistry*, 24, 7 – 42
- Berg, R. R.**, 1975. Capillary pressure in stratigraphic traps. *American Association of Petroleum Geologists, Bulletin*, 59, 939 – 956
- Boetius, A.**, K. Ravensschlag, C. J. Schubert, D. Rickert, F. Widdel, A. Gieseke, R. Amann, B. B. Jorgensen, U. Witte, and O. Pfannkuche, 2000. A marine microbial consortium apparently mediating anaerobic oxidation of methane. *Nature*, 407, 623 – 626
- Boetius, A.**, and E. Suess, 2004. Hydrate Ridge: a natural laboratory for the study of microbial life fueled by methane from near-surface gas hydrates. *Chemical Geology*, 205, 291 – 310
- Bohrmann, G.** and S. Schenck, 2004. R/V Sonne Cruise Report SO 174. *GEOMAR Report*, 40 – 50, IFM-GEOMAR, Kiel
- Bohrmann, G.**, V. Spiess, and cruise participants, 2008a. Report and preliminary results of R/V Meteor Cruise M67/2a and 2b, Balboa – Tampico – Bridgetown, 15 March - 24 April, 2006. Fluid seepage in the Gulf of Mexico. *Berichte, No. 263*, Fachbereich Geowissenschaften, Universität Bremen, Bremen
- Bohrmann, G.**, A. Bahr, F. Brinkmann, M. Brüning, S. Buhmann, V. Diekamp, K. Enneking, D. Fischer, et al., 2008b. Report and preliminary results of R/V Meteor Cruise M74/3, Fujairah – Male, 30 October – 28 November, 2007. Cold seeps of the Makran subduction zone (continental margin of Pakistan). *Berichte, No.266*, Fachbereich Geowissenschaften, Universität Bremen, Bremen
- Carson, B.** and E. J. Screaton, 1998. Fluid flow in accretionary prisms: Evidence for focused, time-variable discharge. *Reviews of Geophysics*, 36(3), 329 – 351
- Clemente-Colón, P.**, W. Pichel, X. Yan, 2008. Evolution of oil slick pattern as observed by SAR off the coast of Wales. 3rd ERS SYMPOSIUM Florence 97 - Abstracts, <http://earth.esa.int/workshops/ers97/papers/>
- Clift, P.** and P. Vannucchi, 2004. Controls on tectonic accretion versus erosion in subduction zones: Implications for the origin and recycling of the continental crust. *Review of Geophysics*, 42, RG2001
- Colwell, F. S.**, S. Boyd, M. E. Delwiche, D. W. Reed, T. J. Phelps, and D. T. Newby, 2008. Estimates of Biogenic Methane Production Rates in Deep Marine Sediments at Hydrate Ridge, Cascadia Margin. *Applied Environmental Microbiology*, 74, 3444 – 3452
- Coustau, H.**, J. L. Rumeau, C. Sourisse, A. Chiarelli, and J. Tison, 1975. Classification hydrodynamique des bassins sédimentaires, utilisation combine avec d'autres methods pour rationaliser l'exploration dans des bassins non-productifs. Proceeding of 9<sup>th</sup> World Petroleum Congress. Tokyo. London: Applied Science Publication. Vol. II. 105 – 119
- Dickens, G. R.**, M. M. Castillo, and J. C. Wlaker, 1997, A blast of gas in the latest Paleocene: Simulating first order effect of massive dissociation of oceanic methane hydrate. *Geology*, 25, 259 – 262
- Dillon, W.**, J. Nealon, M. Taylor, M. Lee, R. Drury, and C. Anton, 2001. Seafloor collapse and methane venting associated with gas hydrate on the Blake Ridge: Causes and implications to seafloor stability and methane release, in *Natural Gas Hydrates, Occurrence, Distribution and Detection*. In: C. K. Paull and W. P. Dillon, eds., *Geophysical Monograph Series*, 124, 211 – 233, American Geophysical Union, Washington, D. C.

- Dugan, B.** and P. B. Flemings, 2000. Overpressure and fluid in the New Jersey continental slope: implications for slope failure and cold seeps. *Science*, 289(July), 288 – 291
- Einsele, G.**, 2001. Sedimentary Basins: Evolution, Facies, and Sediment Budget (Second Edition). Springer-Verlag, Berlin, Heidelberg, Germany
- Etioppe, G.**, and R. W. Klusman, 2002. Geologic emissions of methane to the atmosphere. *Chemosphere*, 49, 777 – 789
- Espedal, H.**, and T. Wahl, 1999. Satellite SAR oil spill detection using wind history information. *International Journal of Remote Sensing*, 20(1), 49 – 65
- Fisher, Q. J.**, and R. J. Knipe, 2001. The permeability of faults within siliciclastic petroleum reservoirs of the North Sea and Norwegian Continental Shelf. *Marine and Petroleum Geology*, 18(10), 1063 -1081
- Jackson, M. P. A.**, and B. C. Vendeville, 1994. Regional extension as a geologic trigger for diapirism. Geological Society of America, Bulletin, 106, 57 – 73
- Judd, A. G.**, 2004. Natural seabed gas seeps as sources of atmospheric methane. *Environmental Geology*, 46, 988 – 996
- Judd, A. G.**, and M. Hovland, 2007. Seabed fluid flow, the impact on geology, biology, and the marine environment. Cambridge University Press, Cambridge, UK
- Haacke, R. R.**, G. K. Westbrook, and R. D. Hyndman, 2007. Gas hydrate, fluid flow and free gas: Formation of the bottom-simulating reflector. *Earth and Planetary Science Letters*, 261, 407 – 420
- Hornafius, J. S.**, D. Quigley, and B. P. Luyendyk, 1999. The world's most spectacular marine hydrocarbons seeps (Coal oil point, Santa Barbara Channel, California): Quantification of emissions. *Journal of Geophysical Research*, 104(C9), 20,703 – 20,711
- Hovland, M.**, A. G. Judd, and R. A. Burke, 1993. The global flux of methane from shallow submarine sediments. *Chemosphere*, 26, 559 – 578
- Hyndman, R.D.**, K. Wang, T. Yuan, and G.D. Spence, 1993. Tectonic sediment thickening, fluid expulsion, and the thermal regime of subduction zone accretionary prisms: the Cascadia margin off Vancouver Island. *Journal of Geophysical Research*, 98, 21,865-21,876
- Kennett, J.**, K. G. Cannariato, I. L. Hendy, and R. J. Behl, 2003. Methane hydrates in Quaternary climate change: the Clathrate Gun Hypothesis. American Geophysical Union, Washington, DC,
- King, L. H.**, and B. MacLean, 1970. Pockmarks on the Scotian Shelf. *Geological Society of America, Bulletin*, 81, 3141 - 3148
- Kholodov, V. N.**, 2002. Mud Volcanoes, their distribution regularities and genesis: communication 1. Mud volcanic provinces and morphology of mud volcanoes. *Lithological and Mineral Resources*, 37(3), 197 – 209
- Kopf, A. J.**, D. Klaeschen, and J. Mascle, 2001. Extreme efficiency of mud volcanism in dewatering accretionary prisms. *Earth and Planetary Science Letters*, 189, 295 – 313
- Kopf, A. J.**, 2002. Significance of mud volcanism. *Review of Geophysics*, 40(2), 1005
- Kopf, A. J.**, 2003. Global methane emission through mud volcanoes and its past and present impact on the Earth's climate. *International Journal of Earth Sciences*, 92, 806 – 816
- Krooss, B. M.**, D. Leythaeuser, R. G. Schaefer, 1992. The quantification of diffusive hydrocarbon losses through cap rocks of natural-gas reservoirs - a reevaluation. *American Association of Petroleum Geologists, Bulletin*, 76(3), 403 – 406
- Kleinberg, R. L.**, C. Flaum, D. D. Griffin, P. G. Brewer, G. E. Malby, E. T. Peltzer, and J. P. Yesinowski., 2003. Deep sea NMR: Methane hydrate growth habit in porous media and its relationship to hydraulic permeability, deposit accumulation, and submarine slope stability. *Journal of Geophysical Research*, 108(B10), 2508
- Leythaeuser, D.**, R. G. Schaefer, and A. Yüklér, 1982. Role of diffusion in primary migration of hydrocarbons. *American Association of Petroleum Geologists, Bulletin*, 66, 408 – 429
- Link, W. K.**, 1952. Significance of oil and gas seeps in world oil exploration, *American Association of Petroleum Geologists, Bulletin*, 36, 1505 – 1540
- Luyendyk, B.**, J. Kennett, and J. F. Clark, 2005. Hypothesis for increased atmospheric methane input from hydrocarbon seeps on exposed continental shelves during glacial low sea level. *Marine and Petroleum Geology*, 22, 591 – 596

- MacDonald, I. R.**, N. L. Guinasso, Jr., S. G. Ackleson, J. F. Amos, R. Duckworth, R. Sassen, and J. M. Brooks, 1993. Natural oil slicks in the Gulf of Mexico visible from space. *Journal of Geophysical Research*, 98(C9), 1,6351 – 1,6364
- MacDonald, I. R.**, 1998. Natural oil spills. *Scientific American*, November, 30 – 35
- MacDonald, I. R.**, I. Leifer, R. Sassen, P. Stine, R. Mitchell, and N. L. Guinasso, Jr., 2002. Transfer of hydrocarbons from natural seeps to the water column and atmosphere. *Geofluids*, 5, 95 – 107
- MacDonald, I. R.**, G. Bohrmann, E. Escobar, F. Abegg, P. Blanchon, V. Blinova, W. Brückmann, M. Drews, A. Eisenhauer, X. Han, et al., 2004. Asphalt Volcanism and Chemosynthetic Life in the Campeche Knolls, Gulf of Mexico. *Science*, 304 (14 May), 999 – 1002
- MacDonald, I. R.**, E. Escobar, T. Naehr, S. Joye, V. Spiess, and Chapopote III cruise participants, 2007. The Asphalt Ecosystem of the Gulf of Mexico: Results from the Chapopote III Cruise. *EOS*, 88(52), AGU Fall Meeting Supplements, Abstract B43E-1660 INVITED
- Magara, K.**, 1974. Aquathermal fluid migration. *American Association of Petroleum Geologists, Bulletin*, 58, 2513 – 2526
- Meissner, F.F.**, 1978, Petroleum geology of the Bakken Formation, Williston Basin, North Dakota and Montana: Proceedings of 1978 Williston Basin Symposium, September 24–27, Montana Geological Society, Billings, 207 – 227
- Mienert, J.**, M. Vanneste, S. Bünz, K. Andreassen, H. Hafidason, and H. P. Sejrup, 2005. Ocean warming and gas hydrate stability on the mid-Norwegian margin at the Storegga Slide. *Marine and Petroleum Geology*, 22, 233 – 244
- Miiller, D. E.**, A. G. Holba, and W. B. Huges, 1987. Effects of biodegradation on crude oils, in R. F. Meyer, ed., *Exploration for Heavy Crude Oil and Natural Bitumen*. AAPG Studies in Geology No. 25, p. 233-241, Tulsa, Oklahoma, AAPG
- Milkov, A. V.**, 2005. Molecular and stable isotope compositions of natural gas hydrates: A revised global dataset and basic interpretations in the context of geological settings. *Organic Geochemistry*, 36, 681 – 702
- Monahan, D.**, K. Schwehr, R. Wigley, M. J. Uddin, N. Tinmouth, P. Jinadasa, K. Ito, and D. Goncalves, 2008. "GEBCO Visual Library, Proof of Concept", International Bathymetric Science Day, Tokyo, Japan, 27 May. Conference Presentation Only.
- Moore, J.C.** and P. Vrolijk, 1992. Fluids in accretionary prisms. *Review of Geophysics*, 30(2), 113 – 135
- Naehr, T.H.**, P. Eichhubl, V.J. Orphan, M. Hovland, C.K. Paull, W. Ussler III, T.D. Lorenson, and H.G. Greene, 2007. Authigenic carbonate formation at hydrocarbon seeps in continental margin sediments: A comparative study. *Deep Sea Research Part II: Topical Studies in Oceanography*, 54(11-13), 1268-1291
- Niemann, H.**, T. Lösekann, D. de Beer, M. Elvert, T. Nadalig, K. Knittel, R. Amann, E. J. Sauter, M. Schlüter, M. Klages, J. Foucher, and A. Boetius, 2006. Novel microbial communities of the Haakon Mosby mud volcano and their role as a methane sink. *Nature*, 443(October), 854 – 858
- Nisbet, E. G.**, 2002. Have sudden large release of methane from geological reservoirs occurred since the last glacial maximum, and could such releases occur again? *Philosophical Transactions of the Royal Society of London, A*, 360, 581 – 607
- Ryskin, G.** 2003. Methane-driven oceanic eruptions and mass extinctions. *Geology*, 31(9), 741 – 744
- Nunn, J. A.**, 1996. Bouyancy-driven propagation of isolated fluid-filled fractures: Implications for fluid transport in Gulf of Mexico geopressed sediments. *Journal of Geophysical Research*, 101(B2), 2963 – 2970
- Osborne, M. J.** and R. E. Swarbrick, 1998. Mechanisms for Generating Overpressure in Sedimentary Basins: A Reevaluation: Reply. *American Association of Petroleum Geologists, Bulletin*, 82(12), 2270 – 2271
- Paull, C.**, W. J. Buelow, W. Ussler, and W. S. Borowski, 1996. Increased continental-margin slumping frequency during sea-level lowstands above gas hydrate-bearing sediments. *Geology*, 24, 143– 146
- Platt, J. P.**, 1990. Thrust mechanics in highly overpressured accretionary wedges. *Journal of Geophysical Research*, 95(B6), 9025 – 9034

- Le Pichon, X.**, P. Henry, and S. Lallemand, 1993. Accretion and erosion in subduction zones: The role of fluids. *Annual Review of Earth Planetary Sciences*, 21, 307 – 331
- Ryskin, G.**, 2003. Methane-driven oceanic eruption and mass extinctions. *Geology*, 31(9), 741 – 744
- Sahling, H.**, G. Bohrmann, V. Spiess, J. Bialas, M. Breitzke, M. Ivanov, S. Kasten, and R. Schneider, 2008. Pockmarks on the northern Congo Fan, SW Africa: complex seafloor features shaped by fluid flow. *Marine Geology* 249(3-4), 206-225.
- Sassen, R.**, A. V. Milkov, H. H. Roberts, et al. 2003. Geochemical evidence of rapid hydrocarbon venting from a seafloor-piercing mud diapir, Gulf of Mexico continental shelf. *Marine Geology*, 198(3-4), 319-329
- Shiple, T. H.**, M. H. Houston, R. T. Buffler, F. J. Shaub, K. J. McMillen, J. W. Ladd, and J. L. Worzel, 1979. Seismic evidence for widespread possible gas hydrate horizons on continental slopes and rises. *American Association of Petroleum Geologists, Bulletin*, 63, 2204 – 2213
- Teige, G. M. G.**, W. L. H. Thomas, C. Hermanrud, P. E. Øren, L. Rennan, O. B. Wilson, and H. M. Nordgård Bolås, 2006. Relative permeability to wetting-phase water in oil reservoirs. *Journal of Geophysical Research*, 111, B12204
- Tissot, B. P.**, and D. H. Welt, 1984. Petroleum formation and occurrence. Springer-Verlag, Berlin Heidelberg, Germany.
- Thrasher, J.**, A.J. Fleet, S. Hay, M. Hovland, and S. Düppenbecker, 1996. Understanding geology as the key to using seepage in exploration: the spectrum of seepage styles. In: Schumacher, D. and M. A. Abrams, (eds.), Hydrocarbon Migration and its Near-Surface Expression. *AAPG Memoir*, 66, 223 - 241
- Tryon, M.**, K. Brown, L. Dorman, and A. Sauter, 2001. A new benthic aqueous flux meter for very low to moderate discharge rates. *Deep-Sea Research, Part I*, 48, 2121 – 2146
- Tryon, M.**, K. Brown, and M. E. Torres, 2002. Fluid and chemical flux in and out of sediments hosting methane hydrate deposits on Hydrate Ridge, OR, II: Hydrological processes. *Earth and Planetary Science Letters*, 201, 541 – 557
- Van Rensbergen, P.**, C. K. Morley, D. W. Ang, T. Q. Hoan, and N. T. Lam, 1999. Structural evolution of shale diapirs from reactive rise to mud volcanism: 3D seismic data from the Baram delta, offshore Brunei Darussalam. *Journal of Geological Society London*, 156, 633 – 650
- Van Rensbergen, P.**, M. De Batist, J. Klerkx, R. Hus, J. Poort, M. Vanneste, N. Granin, O. Khlystov, and P. Krinitsky, 2002. Sublacustrine mud volcanoes and methane seeps caused by dissociation of gas hydrates in Lake Baikal. *Geology*, 30, 631 – 634
- Vavra, C. L.**, J. G. Kaldi, R. M. Sneider, 1992. Geological applications of capillary-pressure – a review. *American Association of Petroleum Geologists, Bulletin*, 76(6), 840 – 850
- Wang, K.**, 1994. Kinematic models of dewatering accretionary prisms. *Journal of Geophysical Research*, 99(B3), 4429 – 4438
- Wangen, M.**, 2000. Generation of overpressure by cementation of pore space in sedimentary rocks. *Geophysical Journal International*, 143, 608 – 620
- Waples, D. W.**, and G. D. Couples, 1998. Some thoughts on porosity reduction-rock mechanics, overpressure and fluid flow. In: S. J. Düppenbecker and J. E. Iliffe (eds.), Basin modelling: practice and progress, *Geological Society Special Publication 141*, 73 – 81
- Whiticar, M. J.**, M. Hovland, M. Kastner, and J. C. Sample, 1995. Organic geochemistry of gases, fluids, and hydrates at the Cascadia accretionary margin. In: Carson, B., G. K. Westbrook, R. J. Musgrave, and E. Suess, (eds.), *Proceeding of Ocean Drilling Program, Scientific Results*, 146 Part 1, 385 – 397, College Station, University of Texas, Texas
- Whiticar, M. J.**, 2002. Diagenetic relationships of methaogenesis, nutrients, acoustic turbidity, pockmarks and freshwater seepages in Eckernförde Bay. *Marine Geology*, 182, 29 – 53
- Xu, W.** and L. N. Germanovich, 2006. Excess pore pressure resulting from methane hydrate dissociation in marine sediments: A theoretical approach. *Journal of Geophysical Research*, 111, B01104
- Yielding, G.**, B. Freeman, and D. T. Needham, 1997. Quantitative Fault Seal Prediction. *American Association of Petroleum Geologists, Bulletin*, 81(6), 897 – 917

**You, C. F.**, P. R. Castillo, J. M. Gieskes, L. H. Chan, and A. J. Spivack, 1996. Trace element behavior in hydrothermal experiments: Implications for fluid processes at shallow depths in subduction zones, *Earth Planetary Science Letters*, 140, 41 – 52

**Zühlsdorff, L.**, V. Spieß, C. Hübscher, H. Villinger, and A. Rosenberger, 2000. Implications for focused fluid transport at the northern Cascadia accretionary prism from a correlation between BSR occurrence and near-sea-floor reflectivity anomalies imaged in a multi-frequency seismic data set. *International Journal of Earth Sciences*, 88, 655 – 667

## **Chapter 4. A conceptual model for hydrocarbon accumulation and seepage processes around Chapopote asphalt site, southern Gulf of Mexico: from high resolution seismic point of view**

**Feng Ding, Volkhard Spiess, Markus Brüning, Noemi Fekete, Hanno Keil, Gerhard Bohrmann**

RCOM (Research Center Ocean Margins), Universität Bremen, Klagenfurter Strasse, Bremen 28359, Germany

*Published in Journal of Geophysical Research (Vol. 113, G08404 doi:10.1029/2007JB005484, 2008)*

### **4.1 Abstract**

As part of the German R/V Meteor M67/2 expedition in 2006 to the southern Gulf of Mexico, a set of 2D high resolution seismic profiles was acquired across the Chapopote knoll to study sea floor asphalt occurrences. Based on regional seismostratigraphic studies and DSDP drilling, a more highly reflective, coarse grained sediment unit of late Miocene age is identified as a potential shallow hydrocarbon reservoir. Although a unit of that age would typically be buried by Pliocene and Pleistocene sediment cover, at Chapopote, local salt tectonism has highly elevated the structure since the late Miocene, and the Miocene reservoir is locally above present-day regional datum. The elevation resulted in a thin (100-200 m), fine grained sediment cover on the crest of the knoll above the reservoir. Because oil and gas production can be expected at depth in Jurassic, Cretaceous and Tertiary source rocks, the presence of high-amplitude reflector packages within the reservoir unit is interpreted as an evidence of hydrocarbons. This is variously supported by observations of cross-cutting reflectors, polarity reversal, and drops in instantaneous frequency. The thin seal above the reservoir unit facilitates leakage of trapped hydrocarbons. Hydrocarbons apparently invaded into the seal sediments in the wider vicinity around the crest of the knoll, even extending beyond the area where seafloor asphalt is known. The asphalt site thus may be a currently active spot, while the rest of the crest may be temporarily sealed by solid phase hydrocarbons. We propose that a shallow, large reservoir with deeply sourced, relatively heavy petroleum is principally responsible for the formation of asphalts on the seafloor.

### **4.2. Introduction**

Chapopote is one of the knolls related to salt activity in the northern tip of Campeche Knolls, southern Gulf of Mexico (GoM). It is a relatively small member of Campeche Knolls, approximately 7 km in diameter, rising 400 m above the basin floor, and in a water depth exceeding 3000 m. It received attention recently because of spectacular lava-flow like, massive, natural asphalts discovered on the crest of the knoll [MacDonald et al., 2004]. Within an area several hundred meters in diameter, a large number of flow-like patches up to hundreds of square meters in extent were discovered with different degrees of weathering, indicating episodic deposition of the asphalts. Although asphaltenes are among the major components of petroleum [e.g. Tissot and Welte, 1984], deposition of massive asphalt on basin surfaces is a rare phenomenon (another example is in the Caspian Sea coast, Kholodov [2002]), and cannot be readily explained by conventional concepts of petroleum migration.

Thus, studying Chapopote may reveal important geological processes that have been overlooked so far, such as the supercritical water hypothesis of Hovland et al. [2005]. So far, the true understanding for the migration of such heavy hydrocarbon toward the seafloor at

Chapopote is still limited by a shortage of physical and chemical constraints. The direct purpose of this study is to constrain one of the most important boundary conditions: the internal structure and deformation history of Chapopote, in order to interpret its internal hydrocarbon accumulation and migration patterns. By doing so, we may already be able to test different hypotheses for asphalt surface deposition at Chapopote.

In addition, satellite images have revealed prevailing occurrences of natural oil slicks on the sea surface of the southern GoM, indicating that Chapopote is also a petroleum seep site [MacDonald et al., 2004], together with many other knolls with similar morphology in the region. A study of the internal structure and hydrodynamic processes inside Chapopote is also a prerequisite for understanding the occurrence and distribution of hydrocarbon seeps on the knoll. Processes revealed at Chapopote can provide hints for further investigating seepage processes in nearby knolls.

A high resolution 2D seismic dataset across Chapopote was analyzed in this study. Its meter scale vertical resolution enables the imaging of detailed subsurface seismic features directly beneath the knoll and a comprehensive documentation of these features, which allows reconstruction of its deformation history. This reconstruction further indicates the dominant hydrocarbon accumulation and seepage processes beneath Chapopote. Integration of the structure studies and the understanding of fluid-migration processes leads to a conceptual model, suggesting how hydrocarbons are accumulated in the knoll and why hydrocarbon seepage occurs at the asphalt site. In the end, constraints indicated by the model also enable us to speculate about a more concrete mechanism for asphalt deposition at Chapopote.

### 4.3. Geological Setting and the Study Area

The salt activities in southern GoM are concentrated in two provinces: Sigsbee Knolls and Campeche Knolls [Watkins et al., 1978; Bryant et al., 1991; Buffler, 1991] (Fig 4.1a). They are characterized as knolls because the seafloor is apparently dominated by domes indicated by previous seismic surveys. The Sigsbee Knolls area lies further to the northeast, and is bound by the carbonaceous Banco de Campeche (Campeche Bank) and the Sigsbee Abyssal Plain. Campeche Knolls are bound by Banco de Campeche to the east and the Bay of Campeche to the south. A salt-free abyssal plain called Veracruz Tongue [Bertagne, 1984; Bryant et al., 1991] is located between Campeche Knolls and Mexican Ridges further to the west. Northwards, Campeche Knolls are connected to Sigsbee Knolls (Fig 4.1a).

Most of the salt is inferred to have been deposited in the Late Jurassic, during the rifting stage of the gulf [Salvador, 1991]. Since then, approximately 5 – 7 km of sediments have been deposited upon the salt in the southern deep GoM basin [Shaub et al., 1984]. In the near-shore and onshore areas, the sediment thickness is even larger. The thick sediments provide very prolific petroleum source rocks in the region, mostly Jurassic and Cretaceous in age [e.g. Viniestra, 1981; Magoon et al., 2001]. Most of the loading sediments were deposited during the Cenozoic, controlled by orogenic activities in Mexico and sea level variation.

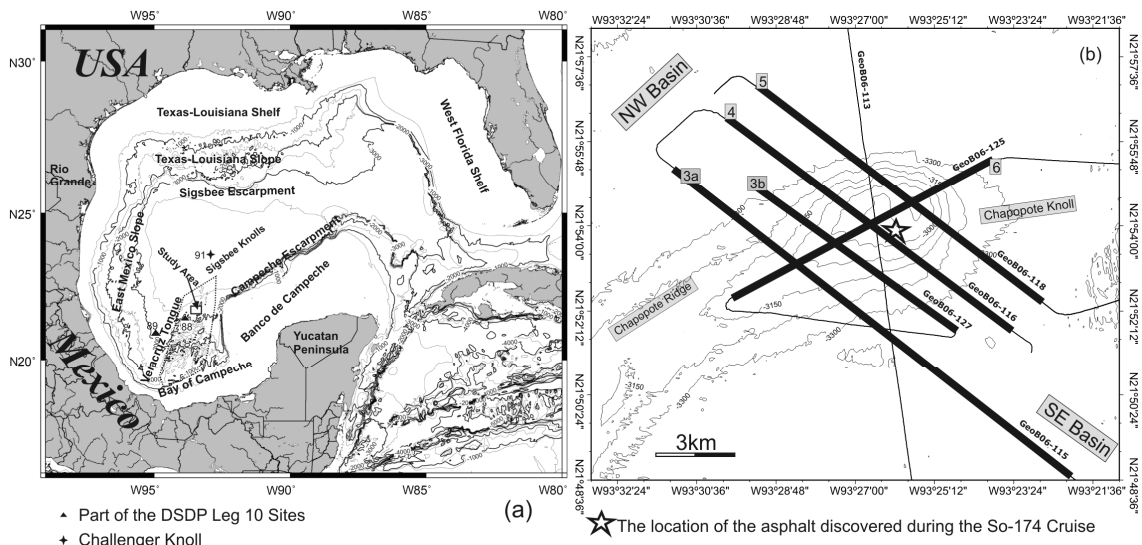


**Figure 4.1.** a) Gulf of Mexico and the location of the study area. The dashed box outlines the extent of Campeche Knolls. Names for geographic regions are taken from Bryant *et al.* [1991]. b) The seismic lines for this study and bathymetry contour in the Chapopote area. The locations of other figures are shown with thick lines and marked with their respective figure numbers. The star marks the location of the asphalt site discovered during the cruise SO-174.

The knolls in Campeche Knolls are generally believed to be related to salt diapirism [e.g. Garrison and Martin 1973; Watkins *et al.*, 1978; Salvador, 1991]. Further north of the study area, Challenger Knoll has been drilled to the salt cap rock [Ewing *et al.*, 1969]. Salt activity and hydrocarbon generation facilitate petroleum seepage, which is indicated by natural oil slicks occurring on the sea surface in the area. These slicks can also be inferred from satellites images of the sea surface, indicating that seeps concentrate mostly around the tops of the knolls [MacDonald *et al.*, 2004].

Chapopote is located in the northern tip of Campeche Knolls (Fig 4.1a). Natural asphalt pavement and chemosynthetic bio-communities were first discovered at Chapopote during the R/V Sonne Cruise SO-174 [Bohrmann and Schenck, 2004; MacDonald *et al.*, 2004]. Although it is not the first time that natural asphalt was found in the deep GoM basin [Pequegnat *et al.*, 1971], the Chapopote asphalt site is particularly notable for its large spatial distribution, with many individual patches over hundreds of square meters. On the other hand, we note that the asphalt deposition does not cover the entire surface of Chapopote, instead it only occurs in an area of about 1 km<sup>2</sup> located on the southern part of the knoll, more specifically, on the southern outer rim of a depression that is located at the knoll centre (Fig 4.1b). This area will be called the asphalt site for convenience. The recent R/V Meteor Cruise M67/2 revisited Chapopote and further located gas and oil seeps at the asphalt site [Bohrmann *et al.*, 2008].

#### 4.4. Data Acquisition and Processing

A 2D high resolution seismic grid covering Chapopote was shot during the M67/2 cruise. Two primary seismic sources were used: a 4.1 L GI gun and a 0.16 L watergun. This work presents exclusively the GI gun data. An 8-section streamer was used as the recording equipment, with a total active length of 400 m and 64 high resolution channels. The streamer was towed by a lead-in and a stretch section, and thus the maximum gun-receiver offset is ~480 m. The dominant frequency range of the collected dataset is 50 – 200 Hz, indicating a vertical

resolution of 10 – 2.5 m [Yilmaz, 1991], assuming an average sediment acoustic velocity of 2000 m/s.

The dataset was processed with a multichannel seismic processing method, using the Vista seismic processing software package. It was filtered with a broad band-pass filter of 30/60-600/800 Hz to preserve both the high resolution and the deeper penetration signals, while still filtering out the greater part of the frequency dependent noise. Subsequently, the entire dataset was binned with 10 m common mid-point (CMP) spacing. The binned data were then normal move-out (NMO) corrected and stacked, based on picked velocities. The stacked profiles were time migrated with the finite difference method. Furthermore, for those profile sections where reflectors are steeply inclined, smaller CMP-bin spacing (5 or 3 m) was applied, to ensure a better NMO correction, and to improve stacking and migration quality.

Our bathymetric data were collected with a Simrad EM120 multibeam system mounted on the R/V Meteor. The data processing was carried out with Caribes software. Procedures include sound-velocity modelling, motion correction, trace editing and gridding with a spacing of 40 m. The GMT software [Wessel and Smith, 1991] was used for displaying the bathymetry grid and seismic line locations.

#### 4.5. Observations and Descriptions

In this data presentation, we first briefly outline some key observations on the bathymetry data, then focus on the description of the seismic features, including defining seismic reflector and sediment units. These definitions are worthwhile because reflectors in the surrounding basins can be mostly traced into Chapopote except in its narrow centre. Based on this definition, other seismic features observed among different profiles can also be correlated according to their stratigraphic levels, which then makes it possible to reveal their lateral extent and variation in their characteristics. In the end, having correlated our reflector units with those defined by earlier seismic studies in the deep GoM basin, an age control of the sediment units will be established to reconstruct the depositional and deformational history of Chapopote.

##### 4.5.1. Bathymetric features of Chapopote and the location of the asphalt site

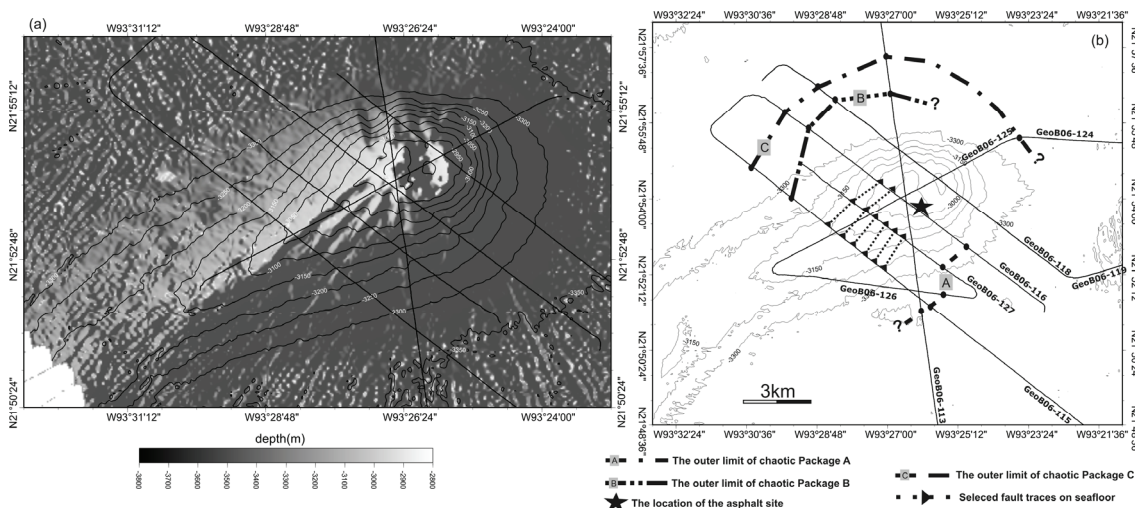


**Figure 4.2.** a) A shaded relief for Chapopote. b) A sketch map for the distribution of the chaotic packages and part of the fault traces on the seafloor.

Our bathymetric data show that Chapopote is a ridge-knoll system made up of a knoll and a small ridge extending southwestwards. In this study, we will name the knoll as Chapopote Knoll and the small ridge as Chapopote Ridge (Fig 4.1b). The term 'Chapopote' will be used to refer to the entire ridge-knoll system. The knoll is about 7 km wide across the strike of Chapopote. It is uplifted to about 400 m above surrounding seafloor, with a 50 m-deep, 500 m-wide depression in the center of the knoll. The asphalt site is located on the outer rim of the depression, and south to the center of the knoll (Fig 4.2b). The Chapopote Ridge extends southwestward about 6 km from the knoll, with the elevation gradually dropping to 150 m above seafloor. Further southwestwards, the ridge elevation increases again, probably connecting to another knoll. A series of seafloor offsets, probably fault traces, are visible on the crest of the ridge, but fade out at the knoll (Fig 4.2a).

#### 4.5.2. Seismic reflector units and their general characteristics

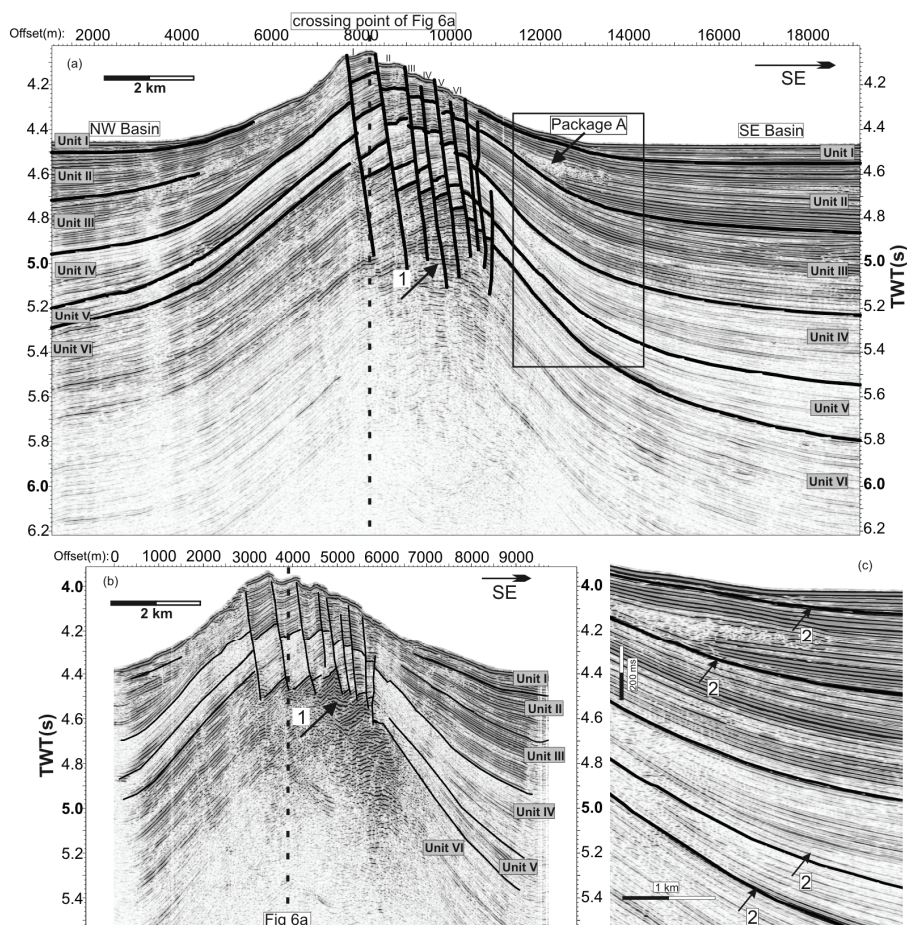


**Figure 4.3.** a) The profile GeoB06-115 with the picking of the 6 units and faults. The profile is 10 m CMP binned. The box shows the area for Fig 3c close-up. b) The profile GeoB06-127 with the picking of the 6 units and faults. The profile is 10m CMP binned. c) The close-up of the ridge flank of Fig 3a, showing the onlaps in different depth levels.

Arrow Group 1 points to those sections in Unit VI with higher amplitudes than their vicinity. Arrow Group 2 marks the onlap events at the base of every unit.

A distinct observation seen in all profiles is that seismic reflectors onlap to the flank of Chapopote. The onlaps do not just appear at one depth level, but instead they repeat several times from deep to shallow (Arrow Group 2, Fig 4.3). An “onlap event” denotes onlaps at one depth level. Since these events consistently occur in the seismic dataset, they provide clear markers to trace reflectors among different profiles. Thus, we divided the seismic reflector units according to these onlap events (Fig 4.3). Typically, each unit is comprised of an upper and a lower section. In the lower sections, reflectors dominantly onlap at the flank of Chapopote, while the upper sections tend to drape upon the entire structure. There are, however, two exceptions: One is that Unit I does not seem to have an upper section, and the entire unit terminates at the ridge and knoll flank; the other is for the deepest unit (Unit VI), which extends laterally into the ridge-knoll system without any apparent onlapping or reflector convergence.

The top of Unit VI is thus the deepest reflector upon which onlaps can be observed. However, the most obvious onlap events are recorded in Units I to III. Almost their entire lower sections onlap to the ridge flank. These three units also show relatively strong reflectivity almost everywhere. Moreover, a small scale chaotic package can also be observed inside these units (e.g. Package A, Fig 4.3a). Compared to Units I to III, the onlap events in Units IV and V are relatively subtle. These two units also reveal relatively low reflection amplitudes. Although some individual stronger reflective intervals appear inside these two units in the undeformed basin area, they either terminate or decrease in amplitude at the flank and the centre of Chapopote.

Unit VI is distinctive because of the absence of onlap events and because of its higher reflection amplitude, compared to the overlaying Units IV and V, except in the basin away from the southeastern flank of the ridge in Fig 4.3a (called SE basin hereafter). Since we did not use any amplitude-depth compensation method during the data processing, the high amplitudes within Unit VI cannot be the result of overcompensation. The lower boundary of Unit VI is not defined, because it is the deepest unit seen in our data.

#### **4.5.3. Observations on the Chapopote Ridge profiles**

Compared to Chapopote Knoll, Chapopote Ridge is a much less prominent topographic feature in the bathymetry. The ridge rises to 150 m above the basin floor, while the knoll reaches maximum elevation of 400 m. Such a difference implies the degree of deformation is also quite different between the ridge and the knoll, as are other features that can be observed in the seismic profiles. In this section, we define and describe major features observed in the Chapopote Ridge area and demonstrate their character variations from the ridge to the knoll in the next section.

##### **4.5.3.1 High amplitude patches**

In this study, we distinguish two different kinds of high amplitude reflection features. One is the high amplitude characteristic just described for Units I, II, III and VI. They show consistently higher amplitudes at both Chapopote and in the surrounding undeformed basin. The other kind of high amplitude feature is restricted to the core of Chapopote (Arrow Group 1, Fig 4.3). These short reflector sections with high amplitudes will be called high amplitude patches.

In the two profiles of Fig 4.3, these patches appear as strong reflector sets, several hundred milliseconds of two way travel time (TWT) beneath the top of the ridge. In most cases, their amplitudes range from 50% to 100% of the reflection amplitude of the undeformed basin floor, but they are brighter than the normal sediment reflectors in the same subsurface depth. Furthermore, the high amplitude patches appear as amplitude enhancement of the upper Unit

VI reflectors. They are either sectionized by fault blocks (Fig 4.3a and 4.3b) and clustered directly under the upper boundary of Unit VI (Fig 4.3b) or have sharp lateral boundary with normal sediments (Fig 4.3b). Some of these patches show clear negative polarity of their wave forms, while others are more ambiguous in their polarity.

#### 4.5.3.2 Shallow faults

A set of faults on the shallow subsurface is clearly imaged at the summit of Chapopote Ridge (Figs 4.3a and 4.3b), which confirms that the offsets seen in the bathymetry (Fig 4.2a) are the result of faulting. They are roughly parallel to each other and dip steeply (~45°) towards the southeast, stepwise down-throwing the SE ridge flank. All of these faults show bigger throws with increasing sub-bottom depth, suggesting that they are syn-depositional to the shallow sediments. Since the sediment units can be traced across the ridge, the thickness variation of a unit at different fault blocks can also be measured. Surprisingly, at first glance, Units II to VI do not display the smallest thickness in the highest uplifted fault block of the present day. Instead, the thinnest part is in the block IV of the Fig 4.3a.

The close spacing of these faults (800-200 m) makes it difficult to correlate individual faults between pairs of 2D profiles. We suggest a rough correlation made on the two profiles (GeoB06-115 and 127 in Fig 4.3a and 4.3b respectively) at Chapopote Ridge (Fig 4.2). The defined fault surfaces indicate a slight trend of convergence from Chapopote Ridge to Chapopote Knoll, but they lack the clear central convergence characteristic of radiation faulting.

#### 4.5.3.3 Asymmetrical internal structure

The definition and picking of the six seismic units clearly demonstrate the highly asymmetrical internal structure of the ridge. The SE flank and the SE basin have subsided significantly more deeply compared to their NW counterparts. Larger subsidence results in thicker sediments in the SE basin. At present, the surface of the SE basin is still slightly deeper than the one northwest of the ridge (~ 15 ms TWT).

#### 4.5.3.4 Chaotic packages in the flank

In Fig 4.3a and 4.3c, an acoustically chaotic package can be observed in Unit II on the SE flank of Chapopote Ridge (Package A). The reflectors in the package have much lower reflection amplitude than the neighbouring sediment reflectors, and they appear rather discontinuous. This package has concordant contact with upper and lower sediment reflectors, pinching out towards the direction of the ridge crest, while grading into continuous reflectors away from the crest. Thus, it appears wedge-shaped.

### 4.5.4. Comparison of the Chapopote Knoll profiles with those in Chapopote Ridge

#### 4.5.4.1 The sediment units and the high amplitude patches

As already mentioned, one of the fundamental differences between Chapopote Knoll and Ridge is the magnitude of uplift. Our profiles show that the higher elevation of Chapopote Knoll is accompanied by a higher uplifted Unit VI. For example at Chapopote Ridge, Fig 4.3a shows that the upper boundary of Unit VI is located below the adjacent basin floor, being buried by ~500 ms TWT of shallower sediments. But at Chapopote Knoll, the upper boundary of Unit VI is uplifted high above the adjacent basin seafloor, with much thinner sediment above it (Fig 4.4 and 4.5). Furthermore, the unit is steeply inclined and the dip reaches to 25° at the flank of the knoll. Despite this more intense uplift, no reflector onlap is observed within this unit. Thickness

measurements between any two arbitrary reflectors within Unit VI also do not reveal any significant thickness variation.

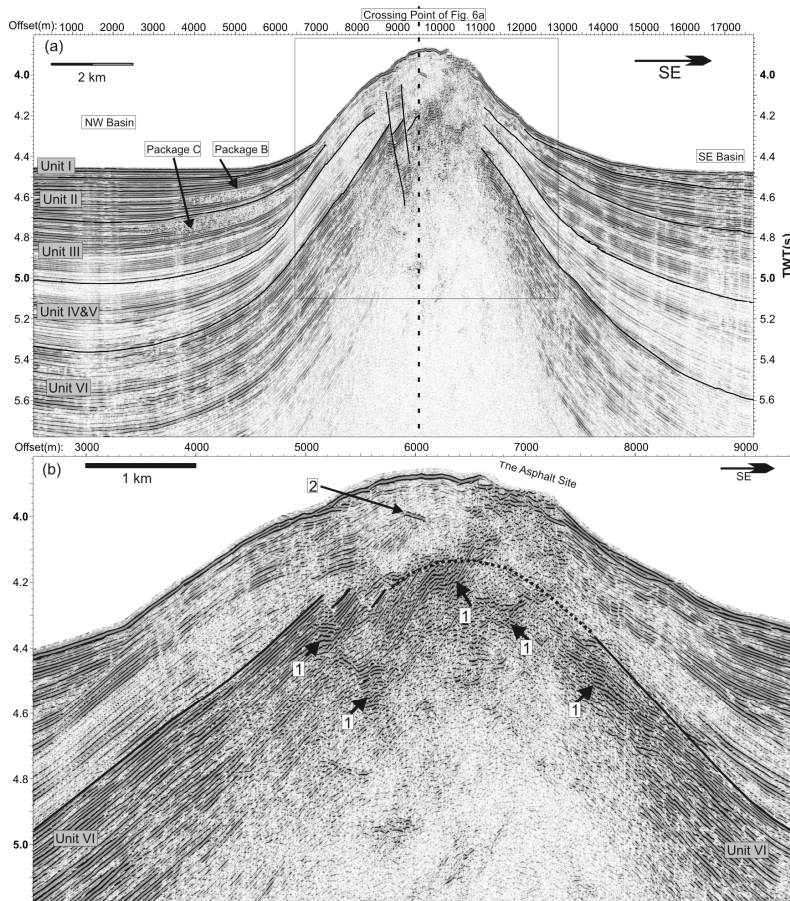


*Figure 4.4 a) An overview of the profile GeoB06-116 with the picking of the 6 units and 2 faults that can be recognized. The box marks the close-up area shown in Fig 4b. The profile is 5 m CMP binned. b) The close-up of the profile under the asphalt site. The dashed lines mark the inferred upper boundary of Unit VI. The profile is 3 m CMP binned.*

*Arrow Group 1 points to the high amplitude patches. Arrow 2 points to a reflector indicating 3D effect in the crest of Chapopote Knoll.*

Units I to V are also uplifted, but they become thinner or even pinch out on the flank, which is more obvious at Chapopote Knoll. Fig 4.3 shows that at Chapopote Ridge, these units can be individually recognized across the structure and have an accumulative thickness of ~500 ms TWT, despite onlaps and unit thinning. However, at Chapopote Knoll, they thin to a total thickness of only about 200 ms TWT at the flank of the knoll. At the crest of the knoll, the seismic reflectors become rather discontinuous, ruling out picking of reflectors or recognition of individual units.

The high amplitude patches at Chapopote Knoll also show several significant differences compared with those in Chapopote Ridge. Instead of appearing as amplitude enhancement of Unit VI reflectors, these patches form short sections of reflectors, sub-horizontally dipping, and thus cross-cutting the steep sediment reflectors in the same location. Together with the higher uplifted Unit VI, they are also closer to the sea floor. Wherever the top of Unit VI can be picked, the high amplitude patches seem to be confined beneath it.

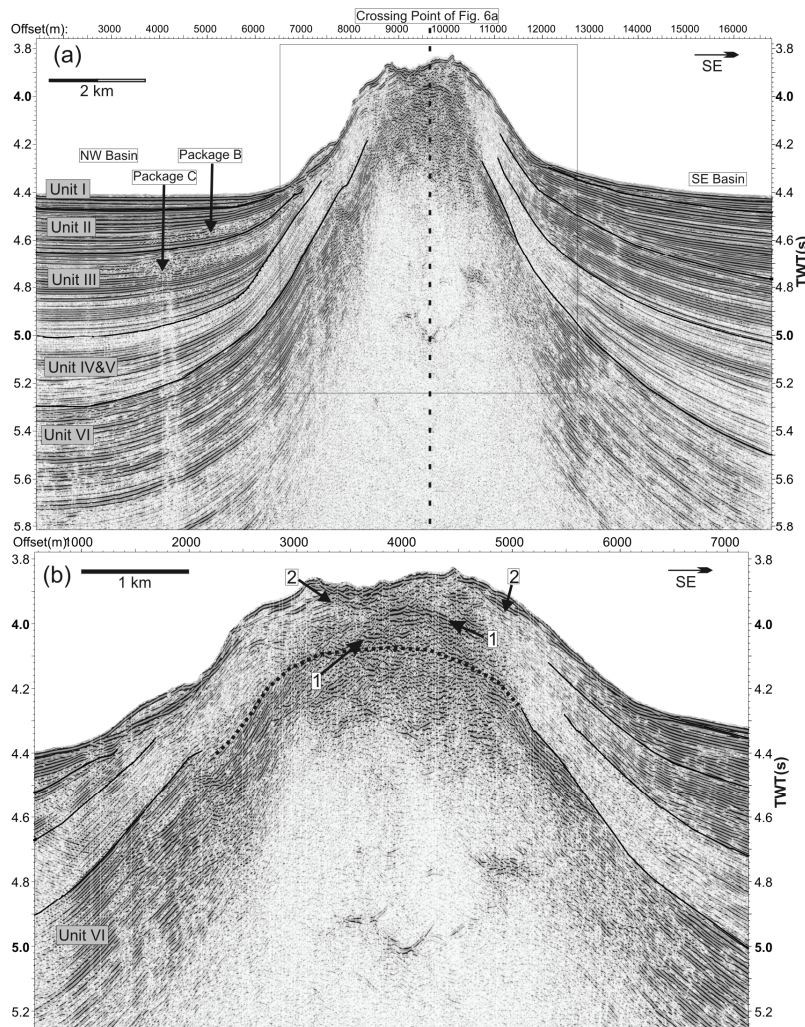


**Figure 4.5** a) An overview of the profile GeoB06-118. The box marks the close-up area shown in Fig 5b. The profile is 5 m CMP binned. b) The close-up of the profile around the crest of Chapopote Knoll, with CMP binning spacing of 3m. The dashed lines mark the inferred upper boundary of Unit VI.

Arrow Group 1 points to the high amplitude patches; Arrow Group 2 shows possible 3D effect of the seafloor.

Only at the right part of the knoll crest in Fig 4.4a, and across the entire crest area in Figs 4.5a and 4.6a, the stratigraphic relation between Unit VI and the high amplitude patches does become unclear, because the top of Unit VI cannot be picked there. In the same location, the high amplitude patches seem to extend up to seafloor. However, their amplitudes do not become stronger with shallower depth. The lone exception is seen in Fig 4.6, where a high amplitude patch has extremely low frequency and 1 – 2 times higher amplitude than that of the seafloor.

#### 4.5.4.2 The asymmetrical internal structure and the shallow faults

The asymmetrical geometry of the internal sediment structures with a more deeply subsided SE flank is clearly recognized at Chapopote Ridge, but is much less pronounced at Chapopote Knoll. Around Chapopote Knoll, the SE basin is also less subsided. If we use the basin NW of the ridge-knoll system (called NW basin hereafter) as a reference, then at Chapopote Ridge the top of Unit VI in the SE basin appears ~450 ms TWT deeper than the one in the NW basin (Fig 4.3). To the northeastern end of the ridge-knoll system, that depth difference gradually decreases (~300 ms TWT in the profile GeoB06-116, Fig 4.4a; ~200 ms TWT in GeoB06-118, Fig 4.5a).

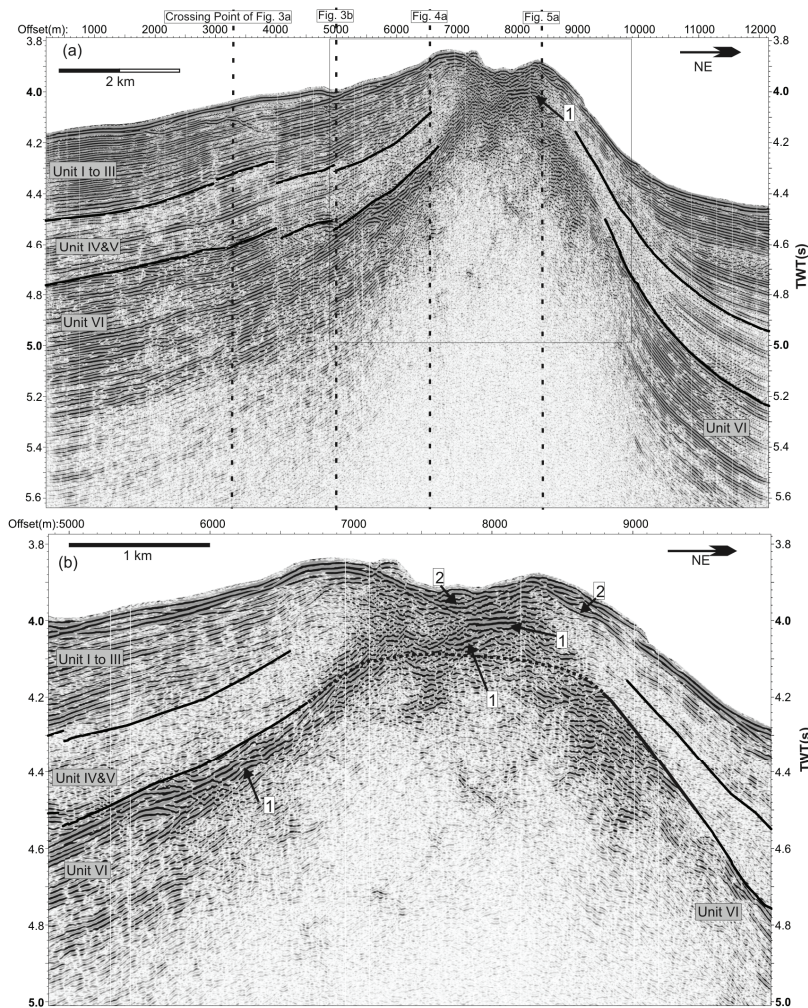


**Figure 4.6** a) The profile GeoB06-125. The box marks the close-up area shown in Fig 6b. b) Close-up of the profile. Both figures are binned with 5 m CMP spacing. The dashed lines mark the inferred upper boundary of Unit VI.

Arrow Group 1 points to the high amplitude patches, the sub-horizontal reflector has twice the amplitude of the seafloor reflector; Arrow Group 2 shows possible 3D effect of the seafloor.

The shallow faults, clearly visible at Chapopote Ridge, cannot be clearly traced on the top of Chapopote Knoll. We can only pick two small displacements of Unit VI in Fig 4.4a. They fall close to the projected positions of the western-most fault surfaces defined at the ridge (Fig 4.2b). Projection of the eastern-most fault surfaces, on the other hand, is in a ~750 m wide vertical chaotic zone (Fig 4.4b) below the asphalt site (noted in Fig 4.1b). This zone is distinguished from the sediments at the SE side by a transition from continuous reflectors to a chaotic zone, and differs from the sediments at the NW side because it contains higher amplitude reflectors. The chaotic zone extends from the asphalt site downwards to Unit VI. Thus, it is embedded in the sediment Units II to V.

If these small displacements in Fig 4.4 are the true continuation of the western-most faults defined at Chapopote Ridge, then the seismic profiles indicate that the fault throws become smaller towards the knoll. The fault displacements to the seafloor also fade out on the knoll crest (Fig 4.2a), which supports this conclusion. These observations suggest that the reduced visibility of these faults inside the knoll is due to their having smaller offsets in this area and not simply to imaging problems.

Thus, the cumulative offset of the faults apparently varies in conjunction with the amount of subsidence of the SE basin. At Chapopote Knoll, the smaller subsidence of the SE basin is accompanied by smaller fault offsets and more symmetrical internal structure. At Chapopote

Ridge, the SE basin subsidence increases, as do the total fault offsets. Since most of the faults are imaged in Fig 4.3a, we can use this profile to make a simple restoration experiment by moving the faulted blocks along the fault planes until the top of Unit VI reveals no offset. The resultant profile shows that the depth difference of this unit between SE and NW basins (Fig 4.7) almost completely disappears.

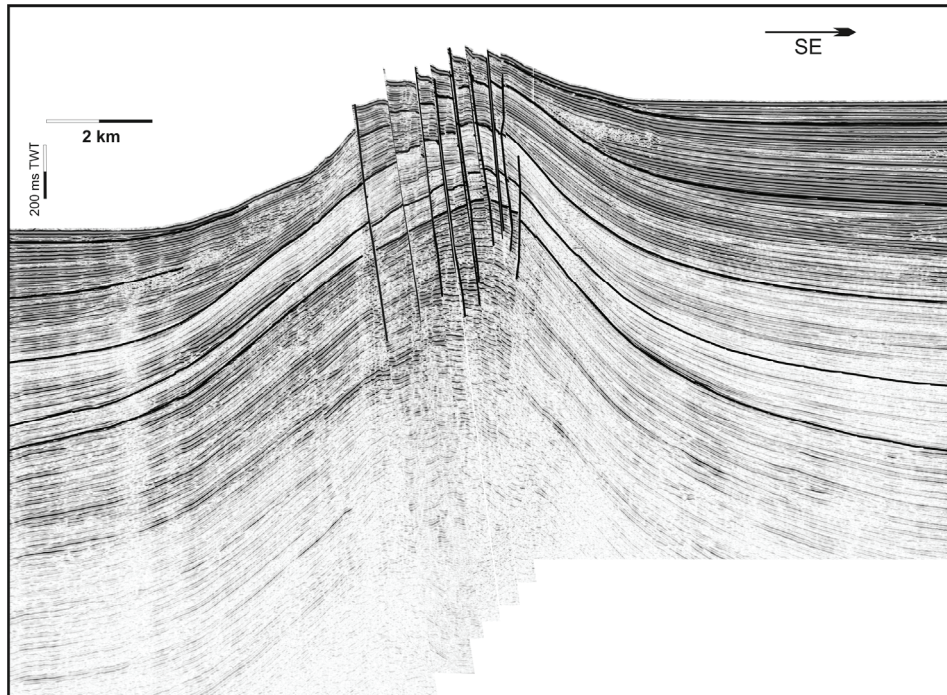


**Figure 4.7** A simple restoration experiment by moving faulted blocks until Unit VI has no offset. The SE-most fault is not used in the restoration because it does cut to the surface.

#### 4.5.4.3 The chaotic packages in the flank

Chaotic packages with geometry and internal reflectivity similar to Package A at the SE flank of Chapopote Ridge (Fig 4.3a and 4.3c) are also observed at the flank of Chapopote Knoll (Package B and C, Fig 4.4 and 4.5). However, they appear only on the NW flank and occur in Units II and III, respectively. This indicates that they are not the continuation of Package A, instead they represent two different packages distributed exclusively at the NW flank of the knoll. Thus, these two chaotic packages are denoted as Package B and C (Fig 4.4 and 4.5). In contrast, Package A in Fig 4.3a has a small lateral extent only around the ridge (Fig 4.2b). The spatial extent of the outer boundaries of these three packages is marked in Fig 4.2b.

#### 4.5.5. Age of the seismic units

Although our seismic lines did not run through any published deep penetration drill sites, an age estimate can be derived from comparison of our data with previous seismic studies in the deep GoM, which date back to the 1960s. For a detailed summary of early academic seismic surveys in the deep GoM basin, readers may refer to Buffler [1991]. We will use the seismic units of the deep GoM basin modified by Shaub et al. [1984], which were correlated to DSDP Leg 10 sites [Worzel et al., 1973]. Most of the age definitions for the units in Shaub et al. [1984] are interpolated or extrapolated, due to limited recovery rate and penetration of these early drill sites. These ages were later refined by Feng [1995]. However, although Feng [1995] presented a

more detailed unit division, we decided to use [Shaub et al. \[1984\]](#)'s units, as our correlation method targets simplicity and is limited in accuracy.

The correlation is based mainly on the identification of the distinctive low reflection amplitudes in some intervals of Units IV and V. It is commonly observed that there is a typically transparent or low amplitude unit in the shallow sediments of the deep GoM basin [[Worzel and Bryant 1973](#); [Watkins et al., 1978](#); [Shaub et al., 1984](#)]. [Shaub et al. \[1984\]](#) assigned this unit as Cinco de Mayo, late Miocene to Pliocene in age. Higher sea level at this time prevented coarse-grained sediment from reaching the deep gulf basin, resulting in hemipelagic-dominated sedimentation with finer grain-size and lower reflection amplitude [[Shaub et al., 1984](#); [Ladd et al., 1976](#); [Worzel and Bryant 1973](#)]. Since our Units IV and V are the only low amplitude units in our profiles, especially in the morphologic highs, they look rather like the counterpart of Cinco de Mayo in the study area.

	Age (Ma)	Shaub[1984] Units	Bertagne[1984] Units	Our units	
Holo.	0.01	Sigsbee	Unit 5	Unit I to III	
Pleisto.	2.8		1.7		Unit 4(D)
			2.8		Unit 4(C)
Pliocene	4.2#	Cinco de Mayo	9	?	
	5.3			5.5#	Unit 4(B)
Miocene	Late	Upper Mexican Ridge	12	?	
			Unit 4(A)	Unit VI	
	Middle		15.5		
Early			23.7		
			30#		

# The age values are taken from Feng [1995]'s modification  
The age durations are not to the length scale of the figure

**Figure 4.8** An age correlation of our seismic units to some previous seismic studies relevant to the study area

Although Cinco de Mayo is very thin (< 200 m) in most parts of the deep GoM basin, the isopach maps of [Shaub et al. \[1984\]](#) show this unit to be around 200 – 250 m thick in our study area. The same thickness is also shown in [Bertagne \[1984\]](#)'s seismic unit of similar age interval in Veracruz Tongue, the abyssal plain west to the study area ([Fig 4.1a](#)). In our profiles, although the total thickness of Units IV and V can reach 600 ms TWT in some locally strongly subsided places (the SE basin, [Fig 4.3a](#)), these two units normally show a total thickness of ~300 ms TWT (300 m with an acoustic velocity 2000 m/s of the sediment) in most of the undeformed locations. This is rather similar to the thickness of Cinco de Mayo in this area. Thus, both the reflection amplitude and thickness comparison suggest that Units IV and V are correlated with the Cinco de Mayo unit, late Miocene to early Pliocene in age ([Fig 4.8](#)). Therefore, Units I to III were deposited from the Pliocene to Pleistocene, but we do not have further control for their

respective ages. The Unit VI should correspond to the upper part of the Upper Mexican Ridge unit in [Shaub et al. \[1984\]](#), late Miocene or older in age ([Fig 4.8](#)).

Our seismic stratigraphy is subject to uncertainties because our dataset does not cross other seismic profiles. If the total thicknesses of Units IV and V are truly thicker than Cinco de Mayo, then either the lower boundary of Unit V may further extend into the late Miocene, or the upper boundary of Unit IV may extend into the later Pliocene. Nevertheless, the principal result of our age correlation should still be valid: The seismic appearances, thicknesses, and the depth levels of Units IV and V all suggest these two units should correspond to the high sea-level stand and fine-grained sedimentation episode from the late Miocene to the early Pliocene. Accordingly, Unit VI should correspond to the upper part of the Upper Mexican Ridge unit, when coarse or sandy sediments dominated even in abyssal basin settings [[Worzel et al., 1973](#); [Worzel and Bryant, 1973](#); [Bertagne, 1984](#); [Shaub et al., 1984](#)].

## 4.6. Interpretation and Discussion

### 4.6.1. Evolution of the knoll uplift and the ridge faulting

With the detailed observations on the seismic units inside Chapopote, it is possible to gain some insight into the evolution history of the system. Starting with the deepest imaged sediment unit (Unit VI), we found it displays onlap neither at Chapopote Knoll nor at Chapopote Ridge, although it might slightly become thinner into the knoll. At the time of deposition of Unit VI (upper part of the Upper Mexican Ridge unit of [Shaub et al. \[1984\]](#)), the southern deep Gulf of Mexico basin should have been in a stage of extensive turbiditic sedimentation [[Worzel et al., 1973](#); [Worzel and Bryant, 1973](#); [Bertagne, 1984](#); [Shaub et al., 1984](#)]. Around the study area, this time period corresponds to the development of Campeche Apron of [Galloway et al. \[2000\]](#). The sediments should be able to 'feel' any significant morphological variations. The absence of onlaps can only mean the absence of topographic variation when Unit VI was deposited. Likewise, the presence of onlap events in the lower section of Unit V (the late Miocene to Pleistocene) indicates that Chapopote Knoll and Ridge started to present a seafloor expression (or underwent its latest uplift event) during the deposition of Unit V. It also implies that although Chapopote Knoll is more highly uplifted, and thus appears to be a much more mature feature, it was not uplifted earlier than Chapopote Ridge.

The onlap events in different depth levels from Units V to I indicate the presence of positive morphology during the deposition of these sediments. Since the knoll and the ridge share the same onlap events in Units I to V, they probably also share similar uplift history since the late Miocene. However, detailed uplift history in this time period cannot be reconstructed from the stratigraphic information alone, because it may have been controlled by both sedimentation and local tectonics. The repetition of the onlaps in the different depth levels could be either due to episodic uplift of the system or to variation between turbiditic and hemipelagic sedimentation. In general, pelagites tend to drape across positive morphologies, while turbidites tend to onlap. For the same reason, the less pronounced onlaps and thickness variations of Units IV and V could be due to either a less elevated ridge-knoll system or to the domination of hemipelagic sedimentation at that time.

The combined thickness of Units II to V (Unit I completely terminates at the flank) becomes rather decreased at the flank of Chapopote Knoll. Although we cannot pick the thickness of these units at the crest of the knoll, in principle, the thickness should not be larger than that at the flank where no erosion is observed. Sediment onlaps and failure may have both contributed

to the thinning of these units, but we suggest that the thinning is predominantly accomplished by onlaps and reflector convergence.

The degree and extent of erosion and slumping at Chapopote are assumed to be limited because of the following: We observe few erosional features (e.g. toplaps, scarps or head walls), except for the NW flank in Fig 4.5a. The missing of toplaps, particularly on the crest of the knoll, argues against preferential erosion by currents on the topographic high. Slumps did occur: the chaotic packages (Packages A, B and C) are interpreted as slump units, according to their shapes and internal reflection pattern (Fig 4.3, Fig 4.4 and Fig 4.5), suggesting the slumps occurred as episodic events. Nevertheless, the slump packages are limited in area (Fig 4.2), and limited indications of scarps additionally suggest the three slumps mapped in Fig 4.2 may have originated from even more limited sediment failure sites. The lack of slump sites might be explained by jointly considering knoll uplift, SE basin subsidence, and sedimentation. The SE flank of Chapopote receives more sediments than the NW flank because the SE basin is subsiding and because it faces the regional sediment source. Thus, even during the uplift of Chapopote and the subsidence of the SE basin, the SE flank is still gentler in slope than the NW flank, preventing sediment failure. Sediments only fail where sedimentation smoothing cannot prevent slope over-steepening either from more significant uplift, such as in the cases of Packages B and C (Fig 4.4 and 4.5), or from a larger magnitude of SE basin subsidence, such as in the case of Package A in Fig 4.2.

Sediment faulting is another component of activity during the knoll uplift. It is not clear which mechanism initiated these faults, but the fault offset magnitudes seem to be controlled by the subsidence of the SE basin. With the decreasing subsidence from Chapopote Ridge to Chapopote Knoll, the cumulative offset of the faults also becomes smaller. Thus, these faults down-throw the SE flank of the ridge-knoll system, technically accommodate the more significant subsidence at the SE basin, and result in the asymmetric structure of Chapopote. This can also explain why the thinnest sediment package in Fig 4.3a is in fault block IV instead of in the present-day crest of the ridge, since the gradual subsidence in the SE basin could have caused the crest of the ridge to retreat northwestwards to its current position.

To summarize the evolution of the Chapopote ridge-knoll system, we suggest Chapopote started to uplift around the deposition time for the top of Unit VI in the late Miocene. The structure must have had a significant elevation when Units III to I were deposited during the late Pliocene to Pleistocene times, especially in the case of Chapopote Knoll. As a result, a large part of these younger sediments onlap to the flank of the knoll. Several sediment slump events occurred during the deposition of Units III and II, but their scales are limited and occur only where flank steepening exceeded sedimentation smoothing. Because of the onlaps and erosion, the sediment cover above Unit VI is rather thin at the crest of the knoll, and likely has been so ever since the uplift. The shallow faults may have been continuously active during the uplift, accommodating the subsidence in the SE basin.

## **4.6.2. A hydrocarbon trap-leakage model**

### **4.6.2.1 A reservoir-seal combination at Chapopote**

As mentioned, we distinguish two kinds of high amplitude reflections seen in our profiles. One is the high amplitude appearance of Units I to III and Unit VI, the other is the high amplitude patches. We regard the persistent high amplitude of Units I to III and VI in most parts of the study area as an indication of their lithological nature, with higher reflectivity due to a coarse

grain-size. (The exception is found at the crest of Chapopote Knoll, where Units I to III become less clearly imaged and lower in amplitude (Fig 4.4 and Fig 4.5), as will be discussed below.) This should be particularly reasonable for Unit VI, because at its time of deposition (the late Miocene) the deep GoM basin and study area were dominated by coarse-grained turbiditic sedimentation [Worzel et al., 1973, Worzel and Bryant, 1973; Shaub et al., 1984, Bertagne 1984, Galloway et al., 2000].

Likewise, the low reflection amplitude appearance of Units V and IV, especially in the topographic highs, suggests finer grain-size. Their deposition time (the early Pliocene) is also a sea level high stand period, when the continental clastic source was hindered in reaching the deep Gulf basin [Worzel and Bryant, 1973; Shaub et al., 1984]. Shale deposition was also dominating further south at the near-shore, onshore Marcuspana basin during this period [Ambrose et al., 2003]. Because the fine-grained Units V and IV overlie coarser Unit VI, these three units form a lithologic reservoir-seal combination.

Despite the fact that the southern GoM is believed to have been sediment-starved in the later Pliocene and Pleistocene [Shaub et al., 1984; Galloway et al., 2000], the high amplitude appearance of Units I to III may indicate their coarse grain-size, and their turbiditic origin could be inferred from the pronounced onlaps recorded in these units. On the other hand, we note that Chapopote Knoll is presently ~400 m above the nearby basin floor, and it also should have been well elevated when these three units were deposited, as has been just discussed. It is reasonable to consider that such high elevation may have prevented turbiditic deposition on the top of the knoll and may have led to finer hemipelagic sedimentation there. This scenario is exemplified in other deep water turbiditic provinces [e.g. Spinelli et al., 2004; Stow and Mayall, 2000]. It may also partially explain the weak amplitude appearance of these units at the top of the knoll, due to finer grain-size sediment having lower reflectivity (Fig 4.4 and Fig 4.5). In addition, because these units were deposited in the latest stage of the knoll's evolution, they should have milder deformation, and thus gentler dipping angles, compared to those of Unit VI underneath. Conventionally, a dipping unit has a higher vertical permeability than that of a horizontal one with the same lithology, due to permeability anisotropy of stratified sediments. Based on these considerations, Units I to III may also behave as seals on the crest of the knoll, although in most of the basin they would be relatively coarse-grained turbiditic sediments.

#### 4.6.2.2 Trap formation and its timing

The uplift of Chapopote Knoll and Ridge not only caused the possible lithology changes within Units I to III, but also resulted in a dome structure and a typical four-way structural trap, with Unit VI forming a reservoir and the shallower sediments forming seals. This trap would have started to evolve soon after the deposition of Unit VI (the late Miocene). This occurred at some time corresponding to the early part of the oil generation window for the Bay of Campeche's major source rock of the Latest Jurassic, the Cretaceous and the Cenozoic [Ambrose et al., 2003; Magoon et al., 2001]. Compared to those near-shore or onshore fields, the study area is further north in the deep basin, with lower sedimentation rates and thus slower thermal maturation. The hydrocarbon generation window of the local source rocks is likely shifted to a later time. Hence, the trap was formed before, or in the early part of the local petroleum generation window. As long as there are migration pathways tapping into the source rock or deeper reservoirs, petroleum can migrate and accumulate in the reservoir: i.e. Unit VI.

#### 4.6.2.3 Hydrocarbon accumulation in the reservoir

Since the high amplitude patches defined in our seismic profiles either have sharp boundaries with nearby sediment reflectors, or cross-cut the dipping sediment reflectors in the knoll, they cannot be caused by lithological transitions of the original sediments. In addition, they are also confined within the top of Unit VI, except in the very crest area of Chapopote Knoll. The close stratigraphic relationship between the high amplitude patches and sedimentary Unit VI precludes the possibility that these patches represent a cap rock of salt diapirs. Because Chapopote Knoll is a hydrocarbon seep site, any abnormal reflection features inside a reservoir unit are most probably caused by hydrocarbon accumulations such as free gas, gas hydrates, oil, asphalt etc. One or more of them may be responsible for these high amplitude patches.

Although it is difficult to fully characterize the seismic attributes of these high amplitude patches with our dataset, some of these patches seem to indicate gas accumulations beneath the reservoir unit. For example, in Fig 4.3b, the high amplitude patches appear as part of the Unit VI reflectors, but have reversed polarity on their tops, and lower frequency than neighbouring sediments. These features are typical of free gas accumulations along sediment strata [e.g. Bünz and Mienert, 2004; Gay et al., 2006; Tréhu et al., 2003]. Furthermore, the horizontal bright section in the north-eastern end of the knoll, with an amplitude twice that of the basin seafloor (Fig 4.6), particularly resembles free gas assemblages seen in seismic profiles. Although the bright section is extremely shallow in depth, and thus may fall within the regional gas hydrate stability zone (GHSZ), free gas migration or even accumulation inside GHSZ is possible, as indicated by recent geochemical and geophysical surveys elsewhere [Milkov et al., 2004; Pecher et al., 2007]. If these interpretations are correct, then the reservoir-seal combination of the shallowest six units has already trapped hydrocarbons, although it is not possible to provide further constraints on their nature.

### 4.6.3. Hydrocarbon leakage and seepage at Chapopote

#### 4.6.3.1 Depth of the reservoir unit under the crest of Chapopote Knoll

Because the shallow sediment units above the reservoir unit become significantly thinner primary by onlapping on the flank of the knoll, the proposed seal interval (Units II to V) must be very thin under the crest of the knoll and cannot be well consolidated. Furthermore, as we discussed in the evolution scenario of Chapopote, such sediment cover above the reservoir must have been always thin since Chapopote started the uplift, instead of being later thinned by erosion.

However, we cannot directly measure the thicknesses of these shallow units at the crest of the knoll because the boundaries between sediment units cannot be recognized there. The most straightforward explanation for the absence of sediment structure is pronounced 3D effects on our 2D profiles, particularly around the crest of the knoll. Many unusual reflectors at that location can be attributed to side-reflections from nearby seafloor (Arrow Group 2 in Figs 4.4, 4.5 and 4.6). Nevertheless, the total thickness of these seal units should not vary greatly from the highest point of the flank, where sediment units can be recognized, to the crest, assuming no major erosion.

It seems unlikely that sediments on the crest would be preferentially eroded, except for what can be indicated from the depression on the crest (Fig 4.2a). The depression's exact origin cannot be constrained yet, but we infer it should be caused either by normal faulting in this micro extensional environment or by sediment collapse after fluid release, similar to pockmarks' behaviour [Judd and Hovland, 2007]. If the first possibility is true, then the depression does not

necessarily indicate presence of erosion. When the latter possibility is true, sediment was lost during pockmark formation. However, such erosion would only occur inside the depression, and does not extend to the locations of the profiles in [Figs 4.4 and 4.5](#). For these profiles, one can still assume the thickness of the shallow sediments (Units II to IV) to be the same as that on the highest point of flank where these sediments are still recognizable. With this assumption of seal sediment thickness, the depth of the reservoir unit can also be estimated, as is shown in [Figs 4.4b, 4.5b and 4.6b](#) by dashed lines.

#### **4.6.3.2 Presence of seepage in the crest of Chapopote Knoll**

As discussed, the high amplitude patches should represent hydrocarbon accumulations inside Chapopote. When the high amplitude patches and the inferred depth of the reservoir are compared, we find these patches are no longer confined beneath the reservoir unit. This in turn indicates that hydrocarbons are no longer confined inside the reservoir unit under the crest of the knoll. Instead, they have broken through into the seal cover. The asphalt site ([Fig 4.4](#)) shows an example of the high amplitude patches making the transition from confinement in the reservoir to invading into overlying strata. The high amplitude chaotic zone under the site is embedded in Units II to V, with seismic features different from the shallow sediment units on either side, appearing more like the high amplitude patches in the more centre part of the crest ([Fig 4.5](#)). The penetration of hydrocarbons into the seal unit explains the observation of hydrocarbon seepage at the asphalt site.

Because the presence of the high amplitude packages in the seal unit is indicated to be common in the entire crest of Chapopote Knoll, we suggest hydrocarbon breakthrough is a common feature in the crest, and is not restricted to just beneath the asphalt site. Although extensive asphalt pavement is localized at the asphalt site, and thus it represents the most active seep at Chapopote, seepage is not completely quiescent across the remainder of the crest. During the M67/2 survey, weathered asphalt gravels and gas flares were also discovered on the crest of the knoll far from the asphalt site [[Bohrmann et al., 2008](#)]. Free gas flares further suggest the over-saturation of methane gas in subsurface of the knoll crest. How these hydrocarbons broke into the seal sediments cannot be indicated by our data, but it does not seem to be caused directly by the shallow faults, even though they cut through the entire seal-reservoir sequence. There is no amplitude abnormality along the fault planes imaged on our profiles.

Even if the fine-grained sediment (Units II to V) failed to seal the reservoir, solid phase hydrocarbons could still clog, and temporally seal possible fluid pathways, although a complete closure of the system is not likely because of the thin sediment cover above the reservoir. In the case of Chapopote, solid asphalt could act as a seal. Furthermore, because the seafloor lies within the regional GHSZ, if methane gas is largely oversaturated, then high concentrations of gas hydrates precipitated in seepage pathways could also behave as a sealing material [[Kleinberg et al., 2003](#); [Tryon et al., 2002](#)]. Incomplete hydrocarbon seals may inhibit hydrocarbon accumulation to be totally exposed, and may episodically fail, resulting in episodic seepage. [Fig 4.9](#) summarizes the processes we infer to occur at Chapopote Knoll.

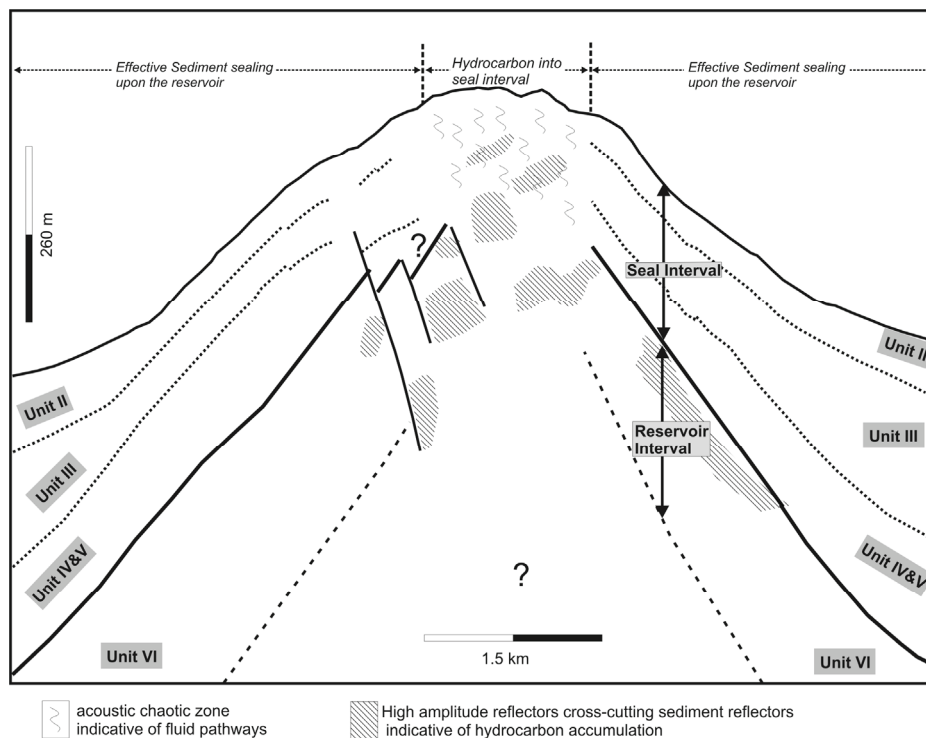


**Figure 4.9** An idealized structure and fluid processes under Chapopote Knoll

At the flank of the knoll or less deformed areas, hydrocarbons are trapped inside the reservoir Unit VI, and sediment seal upon the reservoir is relatively thick. Under the crest of the knoll, hydrocarbons have invaded into the thin seal interval (some 100 m thick). Solid phase hydrocarbons may still incompletely seal fluid pathways in this interval. The resultant seepage is episodic. The faults have limited offsets to the knoll, and their role as fluid leakage pathways is argued to be limited.

#### 4.6.4. Inference for deep sediment and salt structure under Chapopote

The deep structure of Chapopote is not imaged by our seismic data. However, previous seismic studies in Campeche Knolls and Sigsbee Knolls [e.g., Garrison and Martin, 1973; Watkins et al., 1978; Buffler, 1991], and the analogy of Challenger Knoll [Ewing et al., 1969] suggest that diapirs in the deep southern GoM may all be individual salt stocks extending from the autochthonous or deep allochthonous salt level. Large development and lateral movement of salt canopies, similar to Sigsbee Escarpment, is absent in this region. The salt at Chapopote should likewise stem from a rather deep mother unit, i.e. the autochthonous salt from Challenger Unit of Shaub et al. [1984], presently ~5 km deep and ~ 4 km during the late Miocene. Assuming this to be the case, there are two main possibilities for the structure of deeper sediment and the depth of the salt at Chapopote.

One possibility is that the top of the salt was very close to the seafloor during most of the basin history. Immediately prior to the uplift of Chapopote, the salt may only have been covered by the 200 - 400 m of sediments imaged below the top of Unit VI in our profiles. The salt stock started to pierce the shallowest sediment when the sedimentation rate slowed down after the deposition of Unit VI. The latest deformation stage is possibly what is imaged in our seismic profiles. In earlier times, it behaved more like a passive diapir, down-building depositing sediments and keeping itself close to the seafloor.

The second possibility is that the top of the salt is still buried by kilometres of sediments. In this case, deeply buried salts could not have caused the uplift of Chapopote alone, because although such thick sediment cover provides a large density inversion [Nelson, 1991], the mechanical strength of the thick sediment prevents diapirs from piercing it [Schulz-Ela et al., 1993; Jackson et al., 1994]. Extra forces would be therefore required to mobilize the salt and to uplift Chapopote. For the deep water Campeche Knolls, one likely candidate is a regional lateral compression of the sediment column starting in the late Miocene [Watkins et al., 1978; Pérez-Cruz, personal communication 2007], which is indicated by folds and thrust faults in the area. These two possibilities for the deep sediment structure are both compatible with the shallow sediments structure in our profiles. The width where the top of Unit VI is upturned is over 14 km, extending several kilometres from the crest of the knoll. Such a particularly wide deformation zone can be explained either by an active diapir piercing thick roof-sediment, or by a lateral sediment shortening with a folding wave-length independent of salt activity [Rowan et al. 2003].

We propose these two possibilities as principle structures present in the deeper depth of Chapopote. Both imply mechanisms for migration of fluids from the source rock level to the shallow depth. In the first case, the near salt deformation zone can provide pathways for migration. In the second case, a large anticline structure under Chapopote is able to focus fluids and support their migration through its crest. These possible mechanisms directly connect the deeper level hydrocarbons to those in the shallow reservoir discussed in this study.

#### **4.6.5 occurrence of the asphalt seepage on the seafloor**

The rather shallow reservoir under Chapopote facilitates the seepage of not only light fluids, but also heavy hydrocarbons. It makes it possible that hydrocarbons began migrating through the sediment column as mobile petroleum phases, but might have become heavier and less mobile in the Miocene reservoir due to processes such as phase separation and biodegradation. Note also that the petroleum produced in the area is heavy (API 22, e.g. Magoon et al. [2001]), which facilitates formation of asphalts or tars by additional processes. Such heavy hydrocarbons may still be mobile enough to break through some 100 m of seal sediments above the shallow reservoir. They solidify only at the seafloor or in the very shallow subbottom, as a result of near-surface and surface chemical or physical processes, such as biodegradation, consolidation at low temperature conditions around bottom water, or evaporation of remaining light components.

Thus, a very shallow reservoir, which can receive and trap abundant petroleum, is the key in our speculation for formation of surface asphalt deposit. Such petroleum becomes heavier in this shallow reservoir by physical and chemical processes, and finally reaches seafloor as asphalt. If a reservoir is too deep, then heavy petroleum formed in it cannot move through a long pathway to the surface. If a reservoir is too small or volume of trapped petroleum is not sufficient, then, even if asphalt deposits on seafloor, its extension may be too small to be discovered by current deep sea survey technologies.

Finally, we must allow that our dataset and the interpretation of it do not exclude other hypotheses for the forming of surficial asphalt deposits. For example, the supercritical water hypothesis in principle requires a narrow and vertical chimney under the asphalt site for transportation of asphaltenes dissolved in supercritical water [Hovland et al. 2005, 2006]. The chimney would have to extend down to a crustal-level chamber where supercritical water forms. Our dataset has very limited depth penetration at the asphalt site, and thus can neither prove nor disprove the existence of such a structure. Our inference for deeper structures is based on general salt and sediment features in the region, and cannot exclude special cases.

Nevertheless, our dataset does provide evidences for a gradual deformation of Chapopote and an extensive hydrocarbon accumulation beneath the knoll, which fits better with the model we propose. Our ongoing chemical investigations on the composition of the asphalts may cast light on its source and degree of biodegradation for a more advanced discussion on the origin of the asphalts.

#### 4.7. Conclusion

1. The presented seismic dataset shows a relatively highly reflective thick sediment unit (Unit VI) overlain by an acoustically more transparent interval (Units IV and V), especially on the morphologic high. Our age model suggests that Unit VI is deposited in the late Miocene, while Units IV and V are of the late Miocene to early Pliocene age. Both their seismic characteristics and their depositional age indicate that Unit VI is a coarse-grained turbiditic deposit covered by a fine-grained hemipelagic sediment interval: Units IV and V. Such a sediment sequence forms a reservoir-seal combination. Units I to III may also act as a seal on the top of the knoll.

2. These units are significantly uplifted and domed to form the sediment core of Chapopote. The reservoir-seal sequence combines with a dome structure to accomplish a four-way hydrocarbon trap. The structure would have started to evolve later than the deposition of Unit VI, but uplifted to high elevation at least before the deposition of the late Pliocene to Pleistocene sediments (Units I to III). Because of the elevated structure, a large portion of these shallower units onlap to the flank of the ridge-knoll system, especially where Chapopote is most uplifted. The onlaps of Units I to V result in a thin sediment seal above the reservoir unit (Unit VI). These sediments occasionally slumped during the deposition of Units II and III, but the scales of the slumps are limited, and thus are not the major cause of the thin seal cover.

3. This trap structure formed during the main petroleum generation window for the major source rocks of the Jurassic, the Cretaceous and the Tertiary age. As long as there are pathways connecting the trap with the source rock or with deeper reservoirs, the trap is able to accumulate petroleum. The high amplitude patches, which are mostly confined inside the reservoir unit, indicate accumulation of hydrocarbons inside the reservoir. Some of these patches show seismic features characteristic of gas accumulation.

4. The thin seal cover above the reservoir unit facilitates hydrocarbon leakage. On the crest of Chapopote Knoll, quite a few high amplitude patches extend above the reservoir unit. This suggests hydrocarbons are invading into shallower seal sediment. This invasion is a ubiquitous phenomenon at the crest of the knoll, not just restricted to beneath the asphalt site. Fossil asphalt gravels and some gas seeps in other parts of the crest were also discovered during the M67/2 survey, but the asphalt site is currently the most active seep. The rest of the area might be temporarily sealed by solid phase hydrocarbon.

5. The shallow faults imaged in our seismic profiles have decreasing total offsets in the direction from Chapopote Ridge to Knoll. The amount of their total offsets appears to be controlled by the magnitude of the subsidence in the SE basin. Because the degree of such subsidence is smaller towards Chapopote Knoll, these faults also have smaller offsets accordingly. Although the faults cut through the entire reservoir-seal combination, they do not seem to directly provide pathways for hydrocarbon seepage.

6. According to our understanding of regional geology, we infer that the deeper part of Chapopote could represent a buried fossil passive diapir that is now actively piercing the relatively thick roof sediments. Or, it could be a small scale anticline initiated by a regional

compression in the late Miocene, with salt in the core of Chapopote, especially in the knoll. Both possibilities provide pathways for hydrocarbon migration from greater depth up to the reservoir unit in this study.

7. The presence of a shallow reservoir, a thin seal cover, hydrocarbon accumulations, and leakage implies that petroleum might have migrated into the reservoir as a mobile fluid. It was then reworked to lose its lighter components during the accumulation and seepage processes discussed in this study, which occur in a depth level of 100 – 200 m below the seafloor. These mechanisms are sufficient to explain the deposition of the asphalts on the seafloor of Chapopote.

#### 4.8 Acknowledgements

Thanks are given to the crew of the R/V Meteor during the cruise M67/2, for their excellent cooperation with our onboard scientific work. We are grateful to the Mexican government and Pemex for the permission to survey Mexican national waters during the cruise M67/2. Special acknowledgements are given to G. Préz-Cruz and G. Basurto of Pemex Deep Water Exploration, for their inspirational discussions with us. We sincerely thank Elva Escobar and Jaime U. Fucugachi of UNAM for their generous helps during the M67/2 cruise and our visits in Mexico. Gratefully acknowledged are Ian MacDonald, Martin Hovland, and William Waite for their valuable reviews. F.D.'s research visits in Mexico are supported by Bremen International Graduate School for Marine Sciences (GLOMAR). The M67/2 cruise and this study are funded through DFG-Research/Exzellenz Cluster, "the ocean in the earth system", No. Marum0569.

#### References

- Ambrose, W. A., T. F. Wawrzyniec, K. Fouad, S. C. Talukdar, R. H. Jones, D. C. Jennette, M. H. Holtz, S. Sakurai, S. P. Dutton, D. B. Dunlap, et al., (2003),** Geologic framework of upper Miocene and Pliocene gas plays of the Macuspana Basin, southeastern Mexico, *AAPG Bull.*, 87(9), 1411-1435, doi: 10.1306/04140302022
- Bertagne, A. J., (1984),** Seismic stratigraphy of Veracruz Tongue, deep southwestern Gulf of Mexico, *AAPG Bull.*, 68(12), 1894-1907
- Bohrmann, G. and S. Schenck, (2004),** *R/V Sonne Cruise Report SO 174, GEOMAR Report*, pp. 40-50, IFM-GEOMAR, ISSN 0936-5788
- Bohrmann, G., V. Spiess, and cruise participants, (2008),** *Report and preliminary results of R/V Meteor Cruise M67/2a and 2b, Balboa -- Tampico -- Bridgetown, 15 March - 24 April, 2006. Fluid seepage in the Gulf of Mexico, Berichte, No. 263, Fachbereich Geowissenschaften, Universität Bremen, ISSN 0931-0800*
- Bryant, R. B., J. Lugo, C. Córdova, and A. Salvador, (1991),** Physiography and bathymetry, in *The geology of North America, The Gulf of Mexico Basin vol. J*, edited by Salvador, A., pp. 160-196, Geological Society of America
- Buffler, R. T., (1991),** Seismic stratigraphy of the deep Gulf of Mexico Basin and adjacent margins, in *The geology of North America, The Gulf of Mexico Basin vol. J*, edited by Salvador, A., pp. 353-387, Geological Society of America
- Bünz, J. and J. Mienert, (2004),** Acoustic imaging of gas hydrate and free gas at the Storegga Slide, *J. Geophys. Res.*, 109, B14102, doi: 10.1029/2003JB002863

- Ewing**, M., J. L. Worzel, A. O. Beall et al., (1969), Site 2, in *Initial reports of Deep Sea Drilling Project, vol. 1*, US Government Printing Office, Washington
- Feng**, J., (1995) Post mid-Cretaceous depositional history, Gulf of Mexico, Ph.D. thesis, Univ. of Tex. at Austin, Austin
- Galloway**, W. E., P. E. Patricia, X. Li, and R. T. Buffler, (2000), Cenozoic depositional history of the Gulf of Mexico basin, *AAPG Bull.*, 84(11), 1743-1774, doi:10.1306/8626C37F-173B-11D7-8645000102C1865D
- Garrison**, L. E. and R. G. Martin, (1973), Geologic structures in the Gulf of Mexico Basin, *US Geological Survey Professional Paper*, 773, US Government Printing Office, Washington
- Gay**, A., M. Lopez, P. Cochonat, D. Levaché, G. Sermondadaz and M. Seranne, (2006), Evidences of early to late fluid migration from an upper Miocene turbiditic channel revealed by 3D seismic coupled to geochemical sampling within seafloor pockmarks, Lower Congo Basin, *Marine and Petroleum Geology*, 23, 387-399, doi: 10.1016/j.marpetgeo.2006.02.004
- Hovland**, M., I. MacDonald, H. Rueslåtten, H. K. Johnsen, T. Naehr and G. Bohrmann, (2005), Chapopote asphalt volcano may have been generated by supercritical water, *EOS*, 86 (42), 397, 402
- Hovland**, M., H. G. Rueslåtten, H. K. Johnsen, B. Kvamme and T. Kuznetsova, (2006), Salt formation associated with sub-surface boiling and supercritical water, *Marine and Petroleum Geology*, 23(8), 855-869, doi:10.1016/j.marpetgeo.2006.07.002
- Jackson**, M. P. A., C. B. Vendeville, and D. D. Schultz-Ela, (1994), Structural dynamics of salt systems, *Annu. Rev. Earth Planet. Sci.*, 22, 93-117
- Judd**, A. and M. Hovland, (2007), *Seabed fluid flow, the impact on geology, biology, and the marine environment*, pp. 190 – 194, Cambridge University Press
- Kleinberg**, R. L., C. Flaum, D. D. Griffin et al., P. G. Brewer, G. E. Malby, E. T. Peltzer and J. P. Yesinowski, (2003), Deep sea NMR: Methane hydrate growth habit in porous media and its relationship to hydraulic permeability, deposit accumulation, and submarine slope stability, *J. Geophys. Res.*, 108, B10, doi:10.1029/2003JB002389
- Kholodov**, V. N., (2002), Mud Volcanoes, their distribution regularities and genesis: communication 1. Mud volcanic provinces and morphology of mud volcanoes. *Lith. Min. Resour.*, 37(3), 197-209, doi: 10.1023/A:1015425612749
- Ladd**, J. W., R. T. Buffler, J. S. Watkins, J. L. Worzel and A. Carranza, (1976), Deep seismic reflection results from the Gulf of Mexico, *Geology*, 4, 365-368
- MacDonald**, I. R., G. Bohrmann, E. Escobar, F. Abegg, P. Blanchon, V. Blinova, W. Brückmann, M. Drews, A. Eisenhauer, X. Han, et al. (2004), Asphalt Volcanism and Chemosynthetic Life in the Campeche Knolls, Gulf of Mexico, *Science*, 304 (14 May), 999-1002, doi:10.1126/science.1097154
- Magoon**, L. B., T. L. Hudson, and H. E. Cook, (2001), Pimienta-Tambra(!) – A giant supercharged petroleum system in the southern Gulf of Mexico, Onshore and Offshore Mexico, in *The western Gulf of Mexico Basin: Tectonics, sedimentary basins, and petroleum systems*, edited by Bartolini, C., R. T. Buffler and Cantú-Chapa, pp. 83-125, AAPG Memoir 75

- Milkov**, A. V., G. R. Dickens, G. E. Claypool, Y. Lee, W. S. Borowski, M. E. Torres, W. Xu, H. Tomaru, A. M. Tréhu and P. Schultheiss, (2004), Co-existence of gas hydrate, free gas, and brine within the regional gas hydrate stability zone at Hydrate Ridge (Oregon margin): evidence from prolonged degassing of a pressurized core, *Earth Planet. Sci. Lett.*, 222, 829-843, doi:10.1016/j.epsl.2004.03.028
- Nelson**, T. H., (1991), Salt tectonic and listric-normal faulting, in *The Gulf of Mexico Basin, The Geology of North America, vol. J.*, edited by Salvador, A., pp. 73-89, Geological Society of America
- Pecher**, I., S. Henrys, G. Crutchley, A. Gorman, W. Wood, R. Coffin, N. Kukowski and CHARMNZ Working Group, (2007), Seismic evidence for free gas in the regional gas hydrate stability zone beneath an anticline on the Hikurangi margin, New Zealand, *Geophysical Research Abstracts*, v9, 02103
- Pequegnat**, W., W. Bryant and J. Harris (1971), Carboniferous sediments from Sigsbee Knoll, Gulf of Mexico. *AAPG Bull.* 55(1), 116-123
- Rowan**, M. G., T. F. Lawton, K. A. Giles and R. A. Ratliff (2003), Near-salt deformation in La Popa basin, Mexico, and the northern Gulf of Mexico: A general model for passive diapirism. *AAPG Bull.* 87(5), 733-756
- Salvador**, A., (1991), Origin and development of the Gulf of Mexico basin, in *The Gulf of Mexico Basin, The geology of North America vol. J.*, edited by Salvador, A., pp. 389-444, Geological Society of America
- Schulz-Ela**, D. D., M. P. A. Jackson and B. C. Vendeville (1993), Mechanics of active salt diapirism, *Tectonophysics*, 228, 275-312
- Shaub**, F. J., T. R. Buffler and G. J. Parsons, (1984), Seismic stratigraphic framework of deep central Gulf of Mexico basin, *AAPG Bull.*, 68(12), 1790-1802
- Spinelli**, G. A., L. Zühlsdorff, A. T. Fisher, C. G. Wheat, M. Mottl, V. Spieß and E. R. Giambalvo (2004), Hydrothermal seepage patterns above a buried basement ridge, eastern flank of the Juan de Fuca Ridge, *J. Geophys. Res.* 109, B01102, doi:10.1029/2003JB002476
- Stow**, D. A. V. and M. Mayall, (2000), Deep-water sedimentary systems: new models for the 21<sup>st</sup> century, *Marine and Petroleum Geology*, 17, 125-135, doi:10.1016/S0264-8172(99)00064-1
- Tissot**, B. P. and D. H. Welte, (1984), Petroleum formation and occurrence, pp. 375-414, Springer, Berlin
- Tréhu**, A. M., D. S. Stakes, C. D. Bartlett, J. Chevallier, R. A. Duncan, S. K. Goffredi, S. M. Potter and K. A. Salamy, (2003), Seismic and seafloor evidence for free gas, gas hydrates, and fluid seeps on the transform margin offshore Cape Mendocino, *J. Geophys. Res.*, 108, B5, 2263, doi:10.1029/2001JB001679
- Tryon**, D. M., K. M. Brown and M. E. Torres, (2002), Fluid and chemical flux in and out of sediments hosting methane hydrate deposits on Hydrate Ridge, OR, II: Hydrological processes, *Earth Planet. Sci. Lett.*, 201, 541-557, doi:10.1016/S0012-821X(02)00732-X
- Viniegra**, F., (1981), Great carbonate bank of Yucatán, southern Mexico, *Journal of Petroleum Geology*, 3(3), 247-278

**Watkins**, J. S., J. W. Ladd, R. T. Buffler, F. J. Shaub, M. H. Houston and J. L. Worzel, (1978), Occurrence and evolution of salt in deep Gulf of Mexico, in *Framework, facies and oil-trapping characteristics of the upper continental margin*, edited by Bouma, A.H., Moore, G.T., and Coleman, J.M., pp. 43-65, AAPG studies in Geology 7

**Wessel**, P. and W. H. F. Smith, (1991), Free software helps map and display data. *EOS*, 72, 445-446

**Worzel**, J. L., Bryant, W., et al., (1973), Site 89 and Site 90, in *Initial Reports of Deep Sea Drilling Project, vol. X*, edited by Worzel, J.L., W. Bryant et al., pp. 71-115, U.S. Government Printing Office, Washington

**Worzel**, J. L., and W. Bryant, (1973), Regional aspects of Deep Sea Drilling in the Gulf of Mexico Leg 10, in *Initial Reports of the Deep Sea Drilling Project, vol. X*, edited by Worzel, J.L., W. Bryant et al., pp. 737-748, U.S. Government Printing Office, Washington

**Yilmaz**, Ö., (1991), *Seismic data processing*, pp. 468 – 473, Society of Exploration Geophysics, Tulsa

## Chapter 5. Shallow sediment deformation styles in north-western Campeche Knolls, Gulf of Mexico and their controls on the occurrence of hydrocarbon seepage

Feng Ding<sup>1</sup>, Volkhard Spiess<sup>1</sup>, Ian R. MacDonald<sup>2</sup>, Markus Brüning<sup>1</sup>, Noemi Fekete<sup>1</sup>, Gerhard Bohrmann<sup>1</sup>

1. Zentrum für Marine Umweltwissenschaften (Marum), Universität Bremen, Klagenfurter Strasse, 28359 Bremen, Germany

2. Texas A&M University - Corpus Christi, 6300 Ocean Dr. HRI-121, Corpus Christi, TX, USA

*Submitted to Marine and Petroleum Geology*

### 5.1 Abstract

During German R/V Meteor M67/2 expedition to Campeche Knolls, southern Gulf of Mexico, a set of 2D high resolution seismic data were acquired to study the near-surface sediment structure and its relationship with hydrocarbon seepages in this salt province. The comprehensive survey covered 18 individual bathymetric highs or ridges and identified three principle structural types: Passive Type, Chaopote Type, and Asymmetric Flap Type. The first type is the result of passive diapirism, while the latter two would be both initialized by a regional compressional event in the late Tertiary, but are differently modified by salt tectonism. Chapopote Type structures appear as symmetric domes, with uplifted coarse-grained Tertiary sediments in their cores and rather thin syn-kinematic covering sediments. Asymmetric Flap Type structures are also first folded as domes or ridges, but one flap later subsides due to salt evacuation, resulting in single uplifted monoclines. With the coarse-grained pre-kinematic sediments as reservoir units, both structural types can focus and accumulate hydrocarbons. The geometries of the structures and gas-indicating seismic features both suggest hydrocarbons are accumulated in the centre of the Chapopote Type structures and the subsided flaps of the Asymmetric Flap Type structures. Hydrocarbon leakage from these thinly sealed reservoirs occurred in the majority of the seep sites in the study area. The seep locations suggested by analysis of sea surface oil slick images of SAR satellite data are also examined in this study. These independently derived seep locations confirm that seepage occurs at sites predicted by our seismic interpretation and structural analysis.

### 5.2 Introduction

Campeche Knolls is one of the physiographic provinces in the southern Gulf of Mexico (GoM) continental slope, west to Banco de Campeche and east to Veracruz Tongue. It is so named because of its numerous knolls and ridges on the seafloor, which are mostly related to salt tectonics (Garrison and Martin, 1973; Bryant et al., 1991). Aside from salt activity, Campeche Knolls is also a region of active hydrocarbon seepage. Natural oil slicks on sea surface have long been known to be present in this area. Recent camera-, video-sledge and ROV investigations also demonstrated the existence of oil and free gas seeps and discovered massive asphalt and gas hydrate deposits on the seafloor at some knolls, e.g., Chapopote (MacDonald et al., 2004).

Mature petroleum and asphalt seeps clearly suggest a thermal-genic origin of the seeping fluids. Thus, they could be used to indicate the presence of prolific hydrocarbon reservoirs in the area. Detection and analysis of surface petroleum seeps is gradually being recognized as an important approach to reduce the risk in oil explorations (Abrams, 2005). On the other hand,

shallow subsurface processes may greatly alter the character of seeping fluids, ranging from chemical composition to geographic distribution (Abrams, 1996, 2005; Macgregor, 1993; Thrasher et al., 1996). In particular, near-surface sediment deformation and resultant structures (Thrasher et al., 1996; Naeth et al., 2005), as well as intermediate stratigraphic reservoirs (e.g. Gay et al., 2006), can provide migration pathways which deviate fluid geographically away from deep feeding reservoirs. Thus, shallow subsurface processes must be considered before the link between surface seeps and deep feeding reservoirs can be established.

One purpose of this study is to reveal shallow subsurface sediment and salt structures in north-western Campeche Knolls, and to discuss their controls on the occurrence of hydrocarbon seeps. Based on observation and interpretation of high resolution seismic and bathymetry data from R/V Meteor Cruise M67/2, we first try to understand shallow subsurface salt and sediment structure patterns, spatial distribution of different structure types and their evolution scenarios. This knowledge makes it possible to discuss the influence of these structures on migration, accumulation and leakage of hydrocarbon fluids. Thus, prospective seepage areas can be predicted, if these shallow structures impose a primary influence on seep occurrence.

Furthermore, the seep locations can also be independently inferred from sea surface data. Natural oil slicks on the sea surface originating from petroleum seeps can be resolved in satellite images, which are now being used to trace back the source positions of these slicks, and thus locations of seeps. The inferred seep positions in north-western Champeche Knolls are available from Nigel Press Associates (see the dataset section), which indicated over 200 seep locations in the area. These inferred positions of seep sites are considered reliable because they led to the discovery of Chapopote (MacDonald et al., 2004), and about six of the locations over a broad reach of the area were found to include seeps during a recent ground-truth survey (MacDonald et al., 2007).

If these inferred seep locations are consistent with the prospective positions predicted from our structural analysis, it should first suggest the reliability of both results, because they are based on totally independent datasets. More importantly, it indicates that the occurrence and spatial distribution of hydrocarbon seeps in the study area are overprinted by characteristics of the shallow subsurface structures and their spatial pattern. This study makes a detailed comparison of these two independent results and discusses the implications.

### 5.3 Regional Geology

Campeche Knolls is one of the two active salt provinces in the southern Gulf of Mexico. Together with the Sigsbee Knolls, it makes up the salt regime in southern GoM, which is separated from Mississippi-Texas-Louisiana salt province by the Sigsbee Abyssal Plain (Bryant et al., 1991; Buffler, 1991). The two regions are described as knolls because previous seismic surveys had indicated a widespread occurrence of uplifted domes. The Sigsbee Knolls are located to the northeast of the Campeche Knolls, and are bounded by the carbonate Banco de Campeche (Campeche Bank) and the Sigsbee Abyssal Plain. The Campeche Knolls are bounded by the Banco de Campeche to the east, and the Bay of Campeche to the south (Fig 5.1a). A salt-free abyssal plain called Veracruz Tongue (Bertagne, 1984; Bryant et al., 1991) is located between the Campeche Knolls and the Mexican Ridges further west. Northwards, the Campeche Knolls are linked to the Sigsbee Knolls. The salt activity in the southern deep GoM basin is believed to be an analogue to that of the Texas-Louisiana shelf in the northern GoM (Garrison and Martin 1973). Most of the salt is inferred to have deposited in the Late Jurassic

(Challenger Unit of [Watkin et al. 1978](#)), during the rifting stage of the gulf ([Salvador, 1991](#)), equivalent to the Louann salt of the northern gulf.

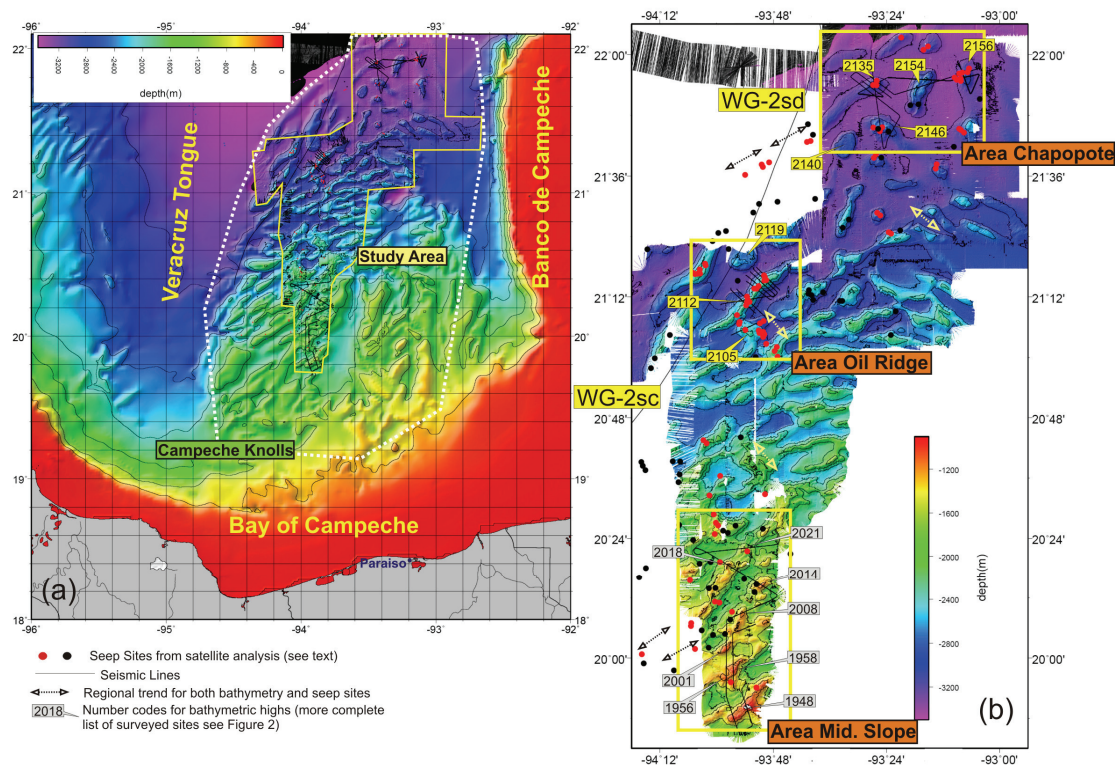


**Figure 5.1** a) Campeche Knolls and the study area. b) Three sub-study-areas and number coding of bathymetric highs.

The yellow polygon in Figure 1a marks our bathymetry data coverage. The seep sites inferred from SAR satellite analysis (see the text) can further infer seepage rate of individual sites. Thus, the seep sites are plotted in different colors. Because such a result is not explored in the study, the rating criteria are not introduced here.

As typical for basins in Gulf of Mexico, the Campeche Knolls has been covered with a thick column of sediments, most of it above the salt unit. The total sediment thickness reaches 5 – 10 km, varying with water depth and distance from the southern coast. The sediments are even thicker in the near-shore Bay of Campeche and onshore areas (e.g. [Ambrose et al., 2003](#); [Vinięgra, 1981](#)). The thick sediments provided prolific petroleum source rocks with the most productive one being of latest Jurassic and Cretaceous age. (e.g., [Magoon et al., 2001](#); [Santamaria-Orozco et al., 1998](#)). But most of the sediments are deposited during Cenozoic times, controlled by both orogenic events in Mexico and sea level changes.

Hydrocarbon generation makes Campeche Knolls a high-ranked and prolific petroleum region ([Magoon et al. 2001](#)) and studies have long shown that salt activity supports leakage of gas and oil. During DSDP Leg 10, at Site 88, drilling into the crest of one of the knolls had to be abandoned because of indication of highly pressurized gas ([Worzel et al., 1973a and b](#)). Oil seepages can also be indicated by widespread natural oil slicks on the sea surface of the region, which are quite similar to the oil slicks in northern Gulf of Mexico ([MacDonald et al., 1996](#); [De Beukelaer et al., 2003](#)). More recently, remote sensing results in Campeche Knolls guided R/V Sonne Cruise SO174 ([Bohrmann and Schenck, 2004](#)) to a discovery of gas, oil and asphalt

seepage on the top of one knoll in the northern tip of the province: Chapopote (MacDonald et al., 2004). The recent multi-disciplinary R/V Meteor Cruise M67/2 revisited Chapopote (Bohrmann and Spiess, 2008; Ding et al., 2008), and also surveyed a border area in north-western Campeche Knolls to collect the major seismic dataset for this study.

## 5.4 Dataset and processing

### 5.4.1 Seismic and bathymetry data

The seismic source in the cruise M76/2 was a 4.1 L GI gun. The recording equipment was an 8-section streamer, with total active length of 400 m and 64 high-resolution channels. The streamer was towed by a stretch and a lead-in section and thus the maximum gun-receiver offset was ~480 m. The dominant frequency range of the collected dataset is 50 – 200 Hz, indicating a vertical resolution of 10 – 2.5 m (Yilmaz, 1991), assuming an average velocity of 2000 m/s.

The dataset was processed with a multichannel processing procedure using Vista processing software package. It was filtered with a bandpass filter of 30/60-600/800 Hz. The goal was to preserve both high resolution and deep penetration signal while still filtering frequency-dependent noise. Subsequently, the entire dataset was binned with 5 m common mid-point (CMP) spacing. The binned data were then normal-move-out (NMO) corrected and stacked, based on picked velocities. The stacked profiles were time migrated with a finite difference method. For those profile sections where highly dipping reflectors were recorded, the CMP bin spacing was reduced to 3m, to ensure better NMO and stacking quality and thus better imaging of dipping features. Additionally, two regional profiles (WG-2sc and -2sd, Shipley et al., 2005) from the western margin of the study area were also incorporated into the study. These are airgun multichannel seismic data collected in 1974 during Cruise IG-1202. The stacked data with 50 m CMP distance were downloaded from the Seismic Data Center of University of Texas (Shipley et al., 2005). The seismic interpretation was carried out using Kingdom Suit software package.

The bathymetry data was collected with an EM120 multibeam system mounted on R/V Meteor. The data processing was carried out with the Carabes™ software. Major procedures include water velocity modelling, trace editing, motion correction and gridding with a spacing of 50 m. GMT software (Wessel and Smith, 1991) was used to display the bathymetry grid, the locations of seismic lines, and the locations of seeps inferred from satellite images.

### 5.4.2 Locations of seep sites from satellite image interpretation

Floating oil that disperses over active hydrocarbon seeps is readily detected using satellite synthetic aperture radar (SAR) because the resultant surfactant layer dampens capillary waves and decreases radar backscatter, thus creating areas of water that appear radar-dark in SAR images (Espedal and Wahl, 1999). Although many marine processes can generate surfactant layers (Huhnerfuss et al., 1989), SAR targets over oil seeps are distinctive because they emanate from the discrete points on the sea surface where oil drops and bubbles arrive from the seafloor. The oil subsequently drifts down-wind and down-current, forming linear “slicks” (MacDonald et al., 1993; MacDonald et al., 2002). Repeated presence of seep-derived oil slicks in separate SAR images of a given area provides a means to survey the numbers of hydrocarbon seep sites across oil-producing regions (Kornacki et al., 1994). The seep survey data used to target seafloor exploration (MacDonald et al., 2004) and the seismic surveys described in this study were obtained from Nigél Press Associates (NPA) and form a portion of

their world-wide archive of offshore petroleum prospects (de Faragó Botella et al., 2004; Williams et al., 2006).

## 5.5 Results and Observations

### 5.5.1 Positive bathymetry features

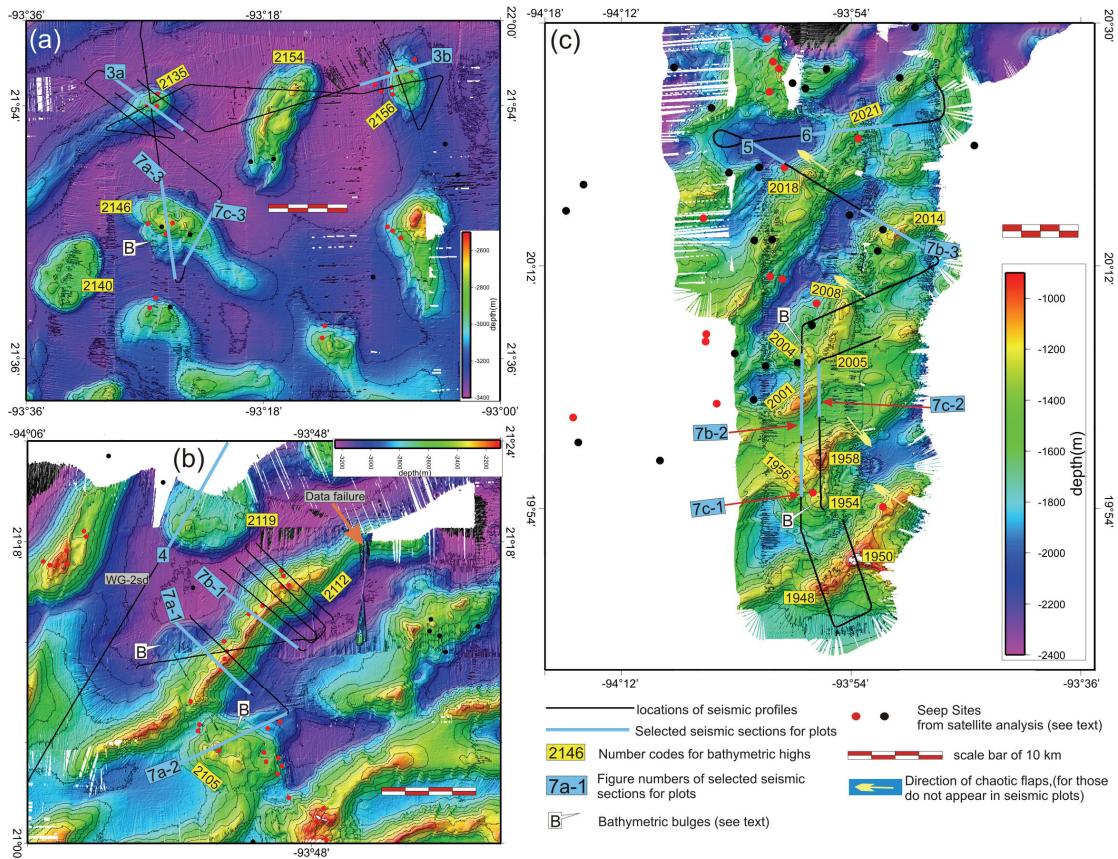


**Figure 5.2** Focus on the three sub-study-areas.

Although our bathymetry data is restricted to the north-western part of Campeche Knolls, it nonetheless shows a distinct change of topographic characteristics, i.e., from knolls in the north (in water depths of around 3300 m) to ridges in the South (up to water depth of around 1000 m), (Fig 5.1b). The knolls in the North are typically 5 – 15 km in diameter and rise 400 – 800 m above the surrounding basins. Within the scope of our dataset, the ridges indicate a dominating directional trend from SW to NE, and a minor trend of SE to NW (Fig 5.1b). The ridges are mainly linear, positive features extending tens of kilometres in length and rising to several hundred meters in elevation. Most of them comprise along-strike peaks, which are high in elevation but limited in length. A few others seem to be equally elevated along their entire strike length (Fig 5.2b). The high elevations of these bathymetric highs and absence of bathymetric scarps at the foot of continental slope offer a clear distinction between this area and the Texas-Louisiana Slope of the northern GoM. There, the topography is dominated by salt-withdrawal basins and scarp features at the toe of the slope (Liu and Bryant, 2000).

For consistency, we adapted the numbering system used during Cruise SO174 (Bohrmann and Schenck, 2004; MacDonald et al. 2004) to refer to all the bathymetric highs in this study. The system assigns the first 4 digits of latitude of the tip of a bathymetric high as the numeric

identifier for the high. For example, if the tip of a high is located at latitude 21° 20' 32", then its identifier is 2120. We add prefix "H" (for bathymetric high) to the identifiers in our text to more clearly indicate them as references to highs. So the high in this example would be coded as H2120. In our figures, the prefix is omitted, because there the numerical identifiers cannot be confused with other parameters. If a high is a continuously elevated ridge, then the 4 digits are taken from the latitude of the mid-point of its strike. We give individual numbers for those peaks along ridges (Fig 5.1b).

### 5.5.2 Shallow subsurface features of the bathymetric highs

The seismic survey during M67/2 was carried out in three separate areas: one at Chapopote (H2135) and surrounding knolls, one around H2112, and one across several ridges further south (Fig 5.1b). For convenience, we name these three areas as Area Chapopote, Area Oil Ridge (the area seems to be particularly rich in oil seeps) and Area Middle Slope (Fig 5.1b). The latter two largely overlap Pemex exploration blocks Hunahpu and Temoa, respectively (G. Pérez-Cruz and G. Basurto, personal communication, 2007). In this section, several traceable seismic horizons in the study area will be first introduced, and then subsurface seismic signatures of the bathymetric highs will be presented in detail.

#### 5.5.2.1 Sediment reflector groups and their correlation in the study area

The major challenge to pick and trace reflectors results from the fact that the seismic lines mostly run across the steepest and most deformed part of ridges and knolls. The reflectors tend to lack continuity and cannot be easily correlated between lines. Thus, the reflector picking was mainly based on recognition of their reflectivity appearance and patterns. We note the existence of a weak reflective interval in virtually all the northern part of the study area and used this as marker for correlation between profiles. However, this approach only enabled the picking of a limited number of reflectors across the entire region.

As a result, only two reflectors could be correlated in parts of the study area: the top and bottom of the weak reflective unit, Reflector X and Y respectively (Fig 5.3), which correspond to the upper boundaries of Unit IV and Unit VI, respectively, in a detailed seismic study of Chapopote (Ding et al., 2008). Nevertheless, some stratigraphic and age control of sediments for the study area can be established. Because the top of the weakly reflective interval (Reflector X) corresponds to the top of Unit IV at Chapopote, it has a Pliocene age (Ding et al. 2008). The bottom of the weak reflectivity interval (Reflector Y) corresponds to the top of Unit VI of late Miocene age.

#### 5.5.2.2 High Amplitude Patches

High amplitude patches (HAPs) are reflector sections that are discontinuous and appear relative high in amplitude (Fig 5.3). They are observed beneath many bathymetric highs, with reflection amplitude higher than in their surrounding, but the absolute amplitude actually lower than that of the seafloor. Their depths range from several hundred milliseconds of two way travel time (TWT) below seafloor to directly beneath the seafloor. These HAPs often blank-out the reflections underneath, similar to seismic wipeouts (e.g., Wood et al., 2000), but as will be discussed, the implication of HAPs may be more than gas and gas hydrates signatures, which the term "seismic wipeouts" tend to suggest. More detailed observations of their character and its variations will be introduced together with the seismic descriptions of the bathymetric highs.

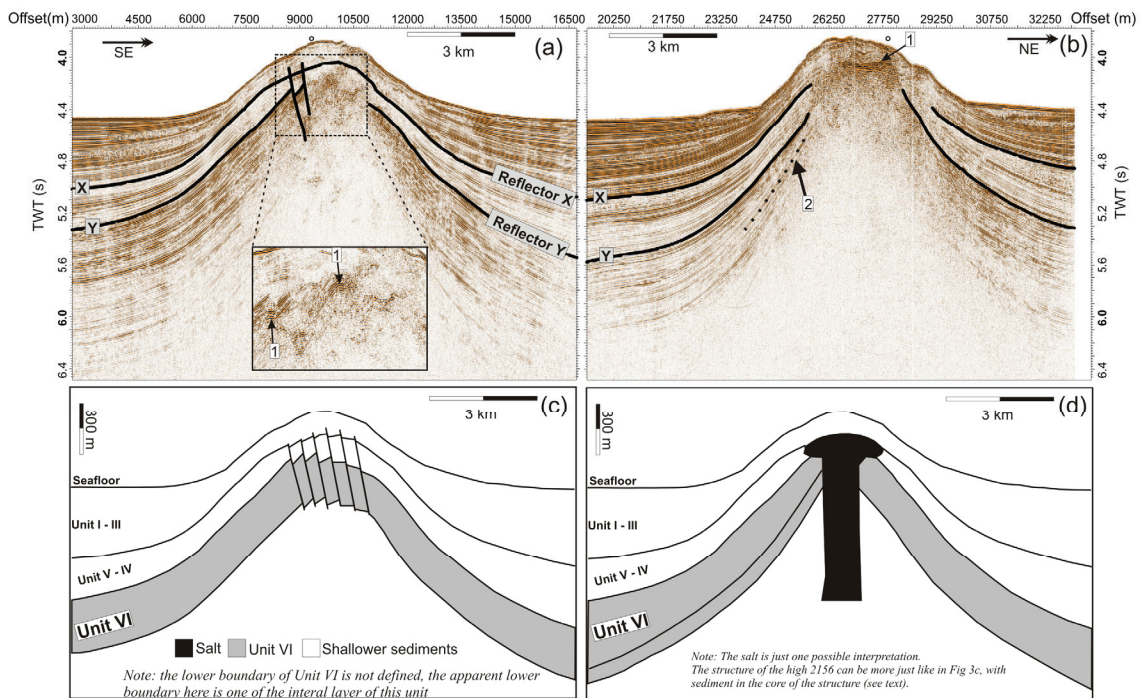


**Figure 5.3** Internal structures for the two knolls defined as Chapopote Type. **(a)** Line GeoB06-116 for Chapopote (H2135). **(b)** Line GeoB06-119 for H2156. **(c)** Interpretation of the general structure of shallow sediments of Chapopote Type. **(d)** An alternative interpretation for H 2156.

Arrow 1 points to HAPs. Arrow 2 points to the onlap in side Unit VI. The locations of these two profiles are shown in Fig 5.5.2a, The faults in the center of Fig 5.3c are interpretative. They have minor offsets to the seafloor and do not seem to assist fluid leakage (Ding et al., 2008). The geometry of the salt in Figure 3d is interpretative.

### 5.5.2.3 Categorization of seismic features of the bathymetric highs

Our seismic lines cross more than twenty bathymetric highs, which are located in various water depths (800-3000 m) with rather different map view appearances. It is not surprising that their internal seismic character also varies significantly. Nevertheless, common features could be found among the different highs, which allowed us to classify three types, as well as a buried structure type, for the purposes of discussion.

**1. Chapopote Type.** This type shows very similar internal structure to that of Chapopote. The bathymetric highs H2135 (Chapopote) and H2156 are assigned to this type. Their surface expressions appear to be knolls, whilst small ridges seem to be attached to them. In the subsurface, deep sediments, particularly Unit VI, are domed up. At H2135, no onlap is observed in Unit VI, but at H2156, an onlap event seems to exist (Fig 5.3). Many reflectors in shallower sediments onlap towards the flank of the knolls, and thus these units' thicknesses are significantly reduced towards the highest uplifted parts the knolls (Fig 5.3), where seismic signal penetration also drops significantly, and continuous seismic reflectors become more chaotic and overprinted by HAPs at shallow sub-bottom depth.

In spite of the general similarity of H2135 and H2156, their HAPs are quite different in appearance. In the case of Chapopote (H2135), HAPs are small in size and mostly constrained

within Unit VI. Only under the crest of the knoll do they seem to extend into shallower sediments and approach the seafloor. However, at H2156, the stratigraphic relationship between HAPs and Unit VI is more uncertain, because the sediment reflectors mostly become invisible at the flanks of the knoll, and the core of the knoll is left for HAPs only (Fig 5.3). Furthermore, these HAPs seem much more extensive in size and form a continuous belt. However, in the entire knoll, they are clearly buried under several hundred milliseconds TWT of sediments.

2. *Passive Type*. The surface expression of this type of structure is also a knoll. In the available seismic data, only one bathymetric high is assigned to this type: H2119. A zone of HAPs is buried in shallow depth under the seafloor. These HAPs are widely distributed under large parts of the knoll. Apparently no other internal structure can be observed. Sediment reflectors in the vicinity basin seem to sharply terminate at the flanks of the knoll without any significant deformation. Since these seismic features are quite similar to typical passive salt diapirs, this type is named as Passive Type (Fig 5.4).

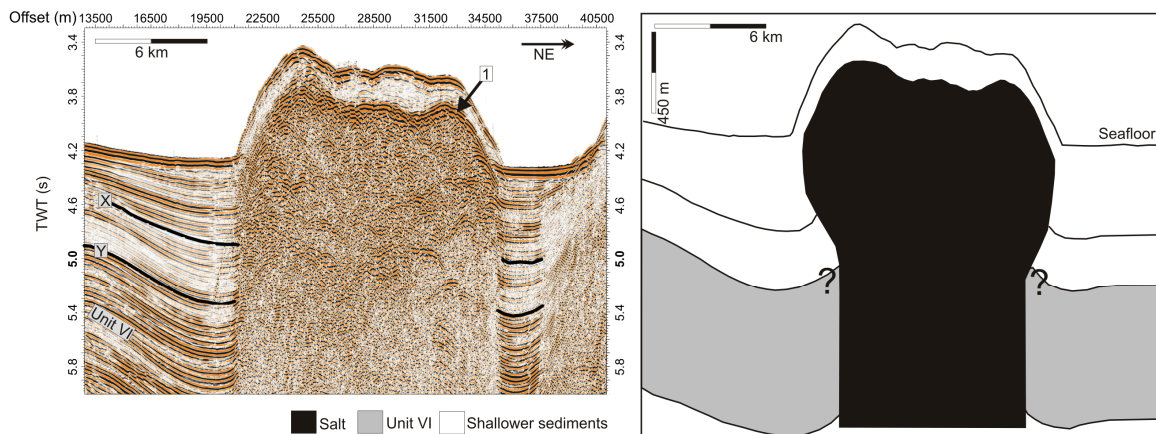


**Figure 5.4.** The example of Passive Type H2119.

The profile from line WG-2sd (Shipley et al. 2005). The Arrow 1 points to the HAPs.

3. *Perdido Type*— a buried structure. Strictly speaking this is not an internal structure of a bathymetry high, because it is totally buried. The sole example in our data is slightly west to H2018 (Fig 5.5). It is a broad and low amplitude anticline, folding Unit VI and deeper structures (Fig 5.5). The limb of this anticline is a kink-band, with a steep dipping short section connecting the top of fold and undeformed sediment away from the fold. Such a structure is strikingly similar to the folds in the Perdido fold belt (Fiduk et al. 1999; Trudgill et al. 1999), and thus is named as Perdido Type.

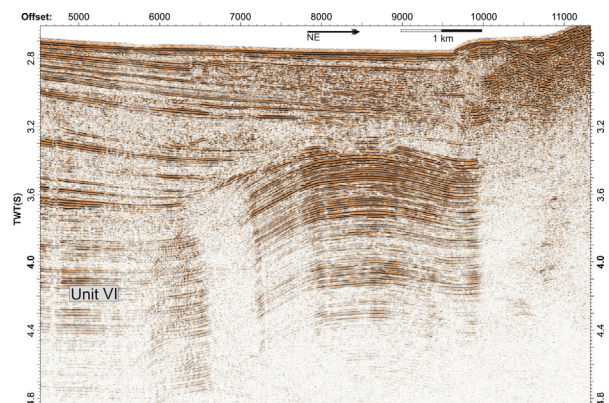


**Figure 5.5** The example of Perdido Type, Line GeoB06-087.

4. *Asymmetric Flap Type*. This type mostly appears either as ridges or as peaks along ridges on map view. It is the dominant type of highs in the study area (Table 5.1). In a typical example H2021 (Fig 5.6), the most noticeable character is the dramatic change in internal structure across the strike of its ridge. At one side of the strike, a continuous sediment unit is uplifted to a steep dip angle (Fig 5.6). No onlap is observed inside this unit. In contrast, sediments above this unit show significant onlap at the flank, and thin to a veneer on the highest uplifted part of the high. We call this side *uplifted flap* for convenience. We suggest that the uplifted flap is the essential part of this structure type. We will classify a structure as Asymmetric Flap Type so long as there is a unit with relative constant thickness that is more strongly uplifted at one side of its strike than at the other.

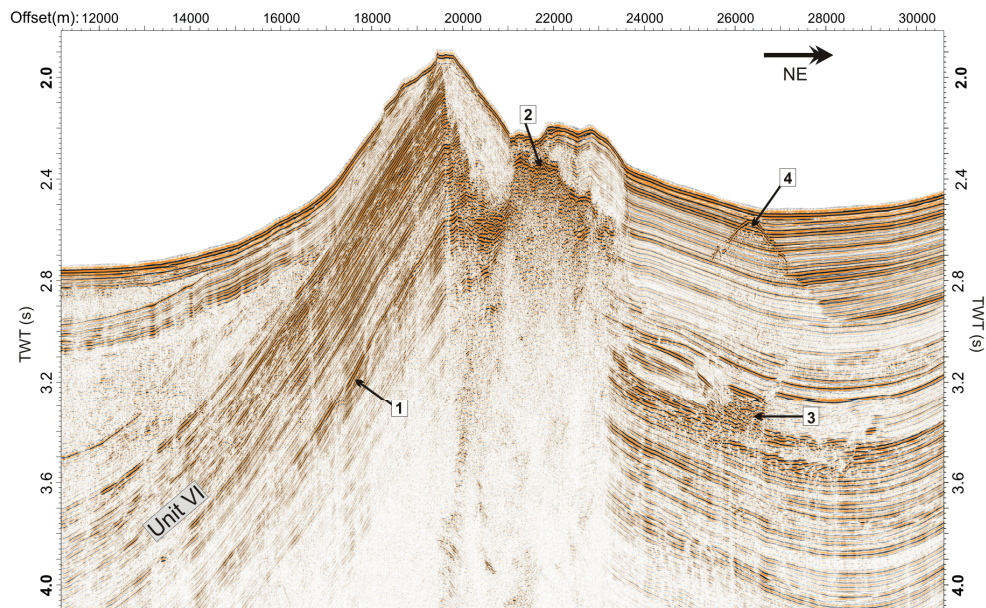


**Figure 5.6** An example of Asymmetric Flap Type, Line GeoB06-086 for H2021.

The Arrow 1 points out the Unit VI. The Arrow 2 points out the HAPs. The Arrow 3 points to a possible paleo-channel. The Arrow 4 points to an artifact, which should be caused by a highly reflective object close to but not exactly crossed by the seismic line. The reflector pickings are not shown, in order to highlight the contrasting seismic features between Unit VI and shallower sediments.

At the other side of strike, HAPs appear at shallow burial depth. Seismic signals are “blacked out” below this zone, and thus no deeper structures were imaged. Since there is no continuous sediment reflector and clear structure can be observed, we call this side *chaotic flap* hereafter. The sediment reflectors in the vicinity basin seem to terminate sharply at the chaotic flap, without deformation. Detailed observations on individual cases, which will be described in the next section, show that HAPs may not be present at some chaotic flaps and hence sediment structures may be observed (although they are still called chaotic flaps for the consistence of terminology).

It is uncertain if the unit with constant thickness in the uplifted flap is a same unit at all these highs, because defined sediment units cannot be trace to the entire study area. Only in some cases (e.g. H2146, H2021 in Fig 5.2), it can be identified as Unit VI. The identification is

impossible for most other highs (Table 1). In the following, such a sediment unit will be called *constant thickness unit*, but they may or may not be a same unit.

#### 5.5.2.4 Detailed internal structure and its spatial variations of the Asymmetric Flap Type

The Asymmetric Flap Type makes up the majority of the highs in the study area, with water depths ranging from 1000 m to 3000 m. Although most of these highs are located along ridges, their lateral extent along the strike of the ridges is not much longer than their across-strike extent. Its numerical predominance among the bathymetric highs and its distribution in a broad reach of the study area may indicate that the structure also varies significantly between different cases. Furthermore, its short along-strike extent may suggest that the structure changes significantly along-strike. This section summarizes these variations of seismic features both among different highs and along individual highs, where our data coverage allows such effort.

Area	Bathymetric Highs	Structure Type	Stratigraphic nature of constant thickness unit(s)	Largest extent of HAPs, seen in our data
Chapopote	Chapopote(2135)	Chapopote	Unit VI	N/A
	2154	uncertain	N/A	N/A
	2156	Chapopote	Unit VI	N/A
	2146	Chapopote	Unit VI	N/A
	2140	Passive	N/A	N/A
Oil Ridge	2119	Passive	N/A	N/A
	2112	Asymmetric Flap	Cannot be defined	Extended
	2105	Asymmetric Flap	Cannot be defined	Extended
Middle Slope	2021	Asymmetric Flap	Unit VI	Limited
	2018	Asymmetric Flap	Cannot be defined	Extended
	2014	Asymmetric Flap	Cannot be defined	Limited
	2008	Asymmetric Flap	Cannot be defined	Extended
	2004	Not Applicable (N/A)	N/A	Part of bulge from H2005
	2005	Asymmetric Flap	Cannot be defined	Extended
	2001	Asymmetric Flap	Cannot be defined	Limited
	1958	Asymmetric Flap	Cannot be defined	Extended
	1956	Asymmetric Flap	Cannot be defined	Extended
	1954	N/A	N/A	Part of bulge from H1968/H1958
	1950	Asymmetric Flap	Cannot be defined	No HAPs
1948	Asymmetric Flap	Cannot be defined	No HAPs	

**Table 5.1** Summarization of several structure features of the studied bathymetric highs.

As mentioned, the uplifted flap comprises a constant thickness unit which appears to be upturned, but it abruptly terminates under the peak of the highs. This is the most consistent feature for all the highs of the Asymmetric Flap Type. But besides this, structures show many differences. To us, one of the most obvious variations occurs in the chaotic flaps: the spatial extent of HAPs across the strike of the structures.

In many cases, the HAPs appear to stretch out several kilometres away from the peaks of respective highs, and extend into some small *bulges* at the foot of their chaotic flaps (Fig 5.7a). These bulges are also clearly visible in map views (Fig 5.2). Mostly, no clear seismic signal is visible beneath the HAPs. In some of the other cases (Fig 5.7b and Fig 5.6), the HAPs are spatially more limited, occurring only under the proximity to the peaks of these highs. There is also no bulge-like feature at the foot of the chaotic flaps. Possibly because the HAPs are

smaller, occasionally some sediment reflectors are observed below the HAPs (Fig 5.7b-2). Interestingly, there are also some other cases where the expected HAPs do not occur at all in the chaotic flaps (Fig 5.7c), and both flaps seem to be made up of stratified sediments.

**Fig 6a, Appearance with Extended HAPs**

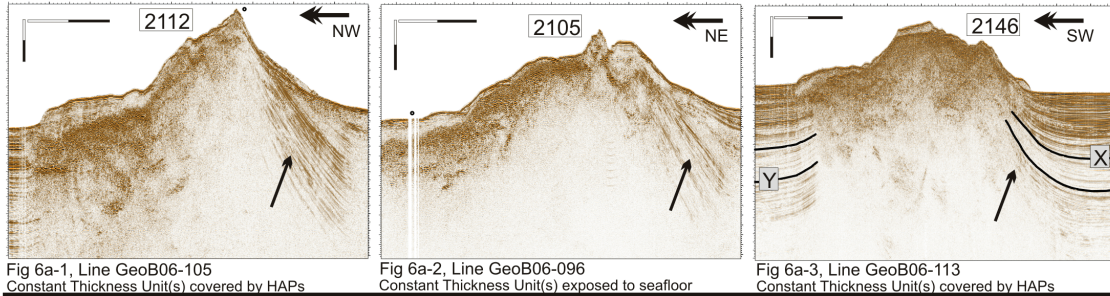


**Fig 6b, Appearance with Limited HAPs**

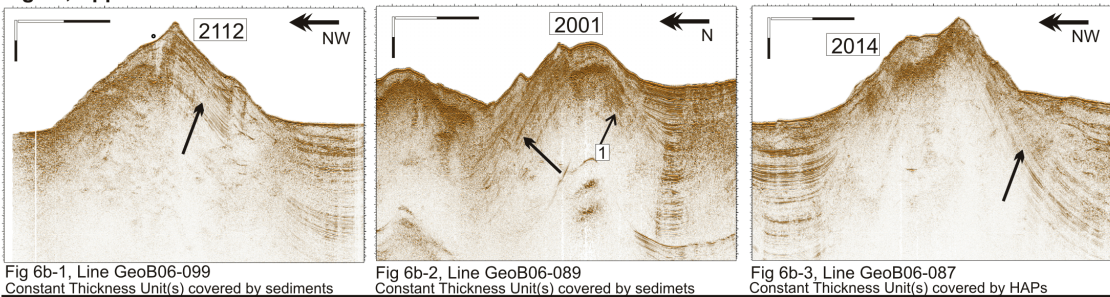


**Fig 6c, Appearance with no HAPs**

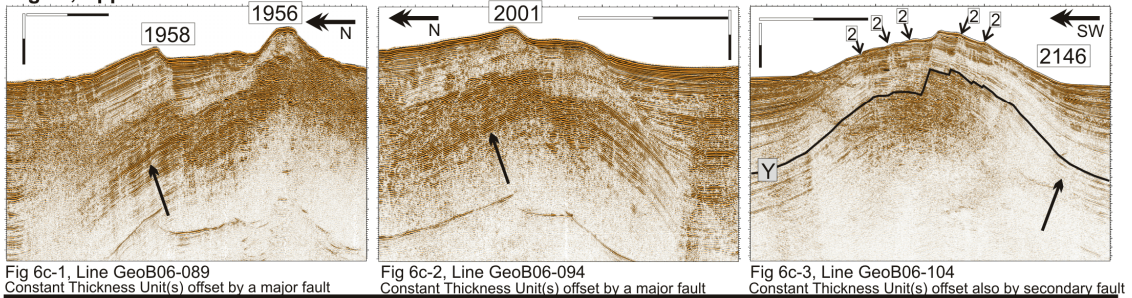


**Figure 5.7.** Different seismic appearances of Asymmetric Flap Type in our dataset. (a) Appearance with extensive HAPs. (b) Appearances with limited HAPs. (c) Appearances with no HAPs.

The scale bars in all the frames represent 3 km and 500 ms TWT in horizontal and vertical direction, respectively. The numbers in each frame are the number codes of bathymetric highs. The bold arrows point out the constant thickness unit. Arrow 1 points to uplifted sediments in the chaotic flap. Arrow Group 2 points to the secondary faults (see text). Where regional reflector tracing is possible, Reflector X and Y are marked.

Note that these differences can occur not only among different bathymetric highs but also along the strike of a same high. We interpret these differences as different seismic appearances of the Asymmetric Flap Type, namely *appearance with extended HAPs*, *appearance with limited HAP* and *appearance with no HAP* (Fig 5.7). Together with the changes in the spatial extent of the HAPs, many other features are also different.

When the HAPs are present (appearance with extended HAP and limited HAP), the uplifted flaps show no faults causing visible offsets. Although the constant thickness unit always terminates at the peak of the highs, it is mostly not directly truncated at the seafloor. Instead, it

is either covered by a weakly reflective unit that also covers the HAPs (Fig 5.6) or it is directly covered by HAPs (Fig 5.7b-3). When the HAPs are absent, the entire structure appears as a faulted anticline and the constant thickness unit is easy to recognize at both flaps. The two flaps are separated by an apparent normal fault (Fig 5.7c). The down-thrown chaotic flap accumulates slightly thicker sediment above the constant thickness unit(s), indicating that the faulting is syn-depositional. In some more complicated cases (Fig 5.7c-3), besides the large offset fault, there are also several small faults visible on both flaps, cutting the entire high into blocks of less than 1 km wide. The constant thickness unit(s) in such cases reveals gradually gentler dipping angles towards the centre of the highs.

Our data indicate that most bathymetric highs of the Asymmetric Flap Type show a seismic appearance with extended HAPs (Table 5.1). Some apparently independent bathymetric highs in map views are actually bulges in association with the extended HAPs (H2004 and H1954, Figs 5.2b and 5.2c). Only at those highs that are small in size or more isolated along the ridges (H2021, H2014 and H2001), no extended HAPs can be observed. HAPs totally disappear only at the very margin of some highs (Figs 5.7c and Fig 5.2), where the structures do not seem to be fully uplifted, or at the southern most highs (H1948 and H1950). We note again that different seismic appearances can occur in different parts of a same bathymetric high. One example is H2112 (Fig 5.2b), where extended HAPs only appear at its south-western end, while showing limited HAPs at its north-eastern end (Figs 5.7a-1 and b-1). Both appearances with limited HAPs and with no HAPs can also appear at a same bathymetry high (H2001, Figs 5.7b-2 and 7c-2).

### 5.5.3 Occurrence of seep sites at different types of bathymetric highs

The inferred seep sites from the analysis of satellite SAR images (called the satellite analysis for convenience) are plotted in Figures 5.1 and 5.2. We found that these sites dominantly occur in elevated locations. They either cluster at or around knolls or line up along the strike of ridges. Because the ridges have regional strikes of SW-NE and SE-NW, the seep sites also seem to be arranged in these two directions (Fig 5.1). Only very few sites appear in undeformed basins. The exact number of these exceptions cannot be provided as it would require a specific definition of the boundary between elevated and undeformed areas, which is out of the scope of this study. However, it seems obvious that these exceptions should not be dominant.

In addition, there are also several notable detailed observations. One is that positive bathymetric features do not guarantee the occurrence of seepage. Most of the seeps seem to be concentrated on three defined blocks: Area Chapopote, Area Oil Ridge and Area Middle Slope, which had been therefore seismically surveyed during the Cruise M67/2. Some ridge areas outside of our seismic coverage appear to be particularly barren of seeps (Fig 5.1b).

Furthermore, seeps do not occur randomly upon the bathymetric highs, rather they occur in patterns that seem to be related to different structural types. For the Chapopote type, many seep sites are indicated at both H2135 (Chapopote) and H2156. On the other hand, at H2135, seeps seem to focus on the center of the high, while those at H2156 form an outer ring around the high. The Passive type H2119 is apparently seep-inactive. Only one seep site is indicated at the outer ring of the high (Fig 5.2b).

The Asymmetric Flap Type comprises uplifted flanks and chaotic flanks. Among all the positive features in this study, no seep is located at the uplifted flank. Some of the seeps occur at the highest tips of the bathymetric highs, as exemplified at Area Oil Ridge (H2112 and H2105).

Others are distributed on the chaotic flanks. However, on those bathymetric bulges associated with extended HAPs, seepage seems rather rare (e.g. of bulges of H2112, H2105 in Fig 5.2b, H2004 and H1954 in Fig 5.2c), but seeps do occur around their margins. These patterns of seep occurrence will be further discussed in relation to our structural interpretation.

## 5.6. Discussion

### 5.6.1. The nature of HAPs

HAPs occur at most of the studied bathymetric highs, but are absent in undeformed basins. Their discontinuity and high reflection amplitudes indicate that they do not represent normal sediment interfaces. In our study area, where salt activity and hydrocarbon accumulation are well expected in shallow sediments, the most possible candidates to seismically appear as HAPs are the upper surface of salt bodies, accumulations of free gas, or gas hydrates.

In order to distinguish salt and hydrocarbon accumulations, it could be helpful to first refer to a bathymetric feature: Virtually all the bathymetric highs have tip-like or elongated peaks, while H2119 (Passive Type) has a rather flat top extending over 12 km (Fig 5.2b). Similar flat-top positive features, with smaller lateral size make up the bulges (H2004 and H1954) at chaotic flaps with extended HAPs (Asymmetric Flap Type) (Fig 5.2a, b and c).

When a salt stock or tongue is uplifted above or close to the adjacent seafloor, the salt tops tend to spread out laterally, because of there is virtually no confinement from the upper end of the salt (Schultz-Ela, 2003, Rowan et al., 2003). As a result, these structures appear as flap-topped highs on a map view. In the deep Gulf basin, the Challenger Knoll, with very shallow salt (Ewing et al., 1969), also shows a wide flat top of nearly 10 km in diameter. The flat-topped map views of H2119 and those bulges in Figure 5.2 seem to hint to the same salt-spreading process in the shallow subsurface, which in turn suggests that the HAPs beneath these highs represent the tops of salt units. Furthermore, we note the small wavelength folds above several extended HAPs (Figs 5.7a-1 and 5.7a-3). They are restricted to the extent of the HAPs and are not found in undeformed basins or at other bathymetric highs. This indicates that they may not represent depositional sediment waves caused e.g., by bottom currents. Such small wavelength folding of shallow sediments in a basin of several kilometres sediment thickness can only be explained if these folded sediments are underlain by a shallow detachment layer, e.g., salt units in this case. Hence, we interpret laterally extended HAPs at the chaotic flaps of Asymmetric Flap Type highs and those under Passive Type highs as top of salt units.

The HAPs in other highs may not all be indicative of salts. Detailed observations of HAPs in Chapopote (H2135) (Ding et al., 2008) suggest that they are signatures of hydrocarbons, particularly free gas, in the shallowest sediment level. For HAPs at other highs, the current dataset cannot distinguish between salt units and hydrocarbon fluids.

### 5.6.2 Shallow Subsurface Structures for Different Types of Bathymetric Highs

#### 5.6.2.1 Chapopote Type

For Chapopote (H2135), a detailed interpretation has been carried out by Ding et al. (2008), which can be outlined as the following: (1) The sediment deposited in the late Miocene (Unit VI) is a permeable coarse-grained unit according to both its deposition time and its reflectivity. In comparison, younger sediments have finer grain size and are thus of lower permeability. (2) Unit VI is domed up to 400 m above the surrounding seafloor. Since onlap is absent in this unit, the doming must have started after its deposition. Such uplifting subsequently caused onlaps of

shallower sediments at the flank of Chapopote, and thus the sediment seal cover upon Unit VI is very thin. (3) The doming could be caused by either an active diapir piercing thick roof sediments or by a regional compressional event, which mobilized deeply buried salt. If the first is true, the salt cap should be relatively shallow to allow active diapirism. Otherwise, the salt would still be buried by thick Cenozoic sediments. (4) In places where the sediments are mildly deformed, the HAPs are well confined within Unit VI. Such stratigraphic relationship between Unit VI and the HAPs suggests that the latter are signatures of free gas and gas hydrates, confined in the reservoir unit, instead of a salt cap. Only at the very crest of Chapopote do the HAPs extend up to the seafloor, indicating the breaking of the sediment seal in the entire crest area.

Such scenario should also be largely true for the other bathymetric highs categorized as Chapopote Type (H2156), but with two major differences. First, at H2156, a clear onlap event is also visible within Unit VI (Fig 5.3b), indicating that it started uplifting earlier than Chapopote (H2135). Furthermore, the HAPs in the core of H2156 have a continuous and clear boundary with the sediments above, and thus seem to be buried by thin sediments even at the peak of the knoll (Fig 5.3b). The fewer available seismic lines (compared to the data coverage at Chapopote, Fig 5.2a) cannot unequivocally reveal if the HAPs are confined by the reservoir unit: Unit VI. Thus, the exact nature of the HAPs in H2156, whether they are salt or hydrocarbons, remains uncertain.

The idealized structural model for the Chapopote Type is sketched in Figure 5.3c, integrating the characteristics of H2135 and H2156. Whether salt is present in the shallow structures is not clear for H2156, thus Figure 5.3d also outlines an alternative interpretation with HAPs in H2156 being interpreted as salt.

#### 5.6.2.2 Passive Type

Shallowly buried HAPs extend across almost the entire width of the only example (H2119) of the Passive Type. As just discussed, the broad and flat HAPs may indicate its being the top of a salt unit. Any deeper structures seem to be totally blanked and the sediments just beside this blanking zone appear almost undeformed. All these features fit well into the character of a passive diapir under a mild sedimentation rate environment (Jackson et al., 1994b; Rowan et al., 2003). Thus, we interpret this structural type as the result of passive diapirism. If shallowly buried passive diapirs always have flat tops on map view, the similarly flat-topped H2140 in Area Chapopote (Fig 5.2a) may also imply its passive diapir nature.

The structural interpretation is sketched in Figure 5.4b. The salt-sediment interface at the flank of the salt stock is however, speculative. A narrow sediment deformation zone just beside the flank may exist, as apparent “drag folds” or stacked onlap events would be the result of passive diapirism (Schultz-Ela, 2003, Rowan et al., 2003). Nevertheless, these structures are not observable in the seismic data, probably due to the blanking of salt top.

#### 5.6.2.3 Asymmetric Flap Type

1. *An idealized near-surface structural model and its along-strike variations.* The Asymmetric Flap Type displays three kinds of appearances in our seismic profiles (Fig 5.7). Extended HAPs are seen in most highs of the Asymmetric Flap Type (Table 5.1). When a bathymetric high is relatively small or isolated from other highs, it may show HAPs confined in its centre. At the less deformed periphery of a high, HAPs are absent (Fig 5.7c). So, the extent of HAPs and

size/elevation of the bathymetric highs seem to be linked: a higher degree of deformation is coupled with a larger extent of HAPs.

Fig 7a, Structural model for appearance with extended HAPs

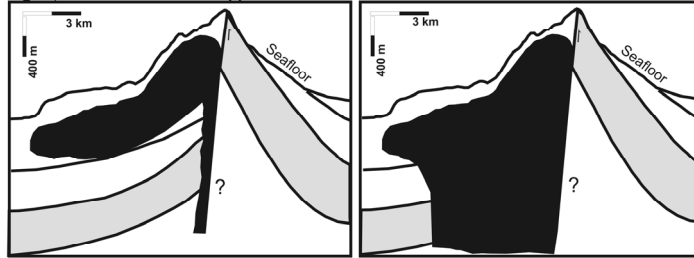


Fig 7a-1, Extrusive Salt Case

Fig 7a-2, Broad Salt Unit Case

Fig 7b, Structural model for appearance with limited HAPs

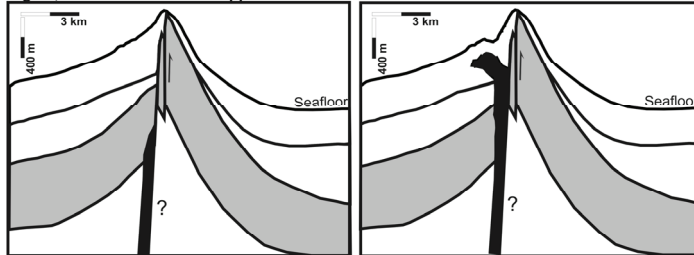


Fig 7b-1, Deep Salt Case

Fig 7b-2, Shallow Salt Case

Fig 7c, Structural model for appearance with no HAPs

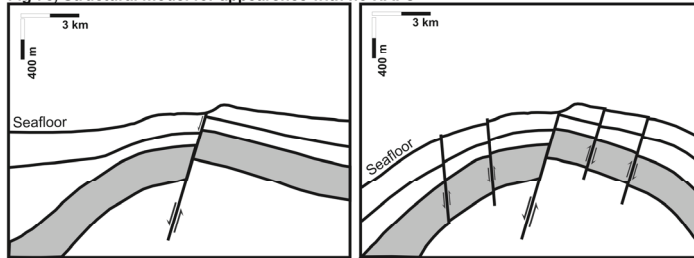


Fig 7c-1, Simple Major Fault Case

Fig 7c-2, Major Fault and Secondary Fault Case

■ Salt □ Deep constant unit(s) □ Shallower Sediments

**Figure 5.8** Structural interpretations for different seismic appearances of Asymmetric Flap Type. (a) The most deformed structure with extended HAPs occurrence. (b) The intermediate deformed structure with limited HAPs extent. (c) The most immature structure, where HAPs are absent.

In both Figures 8a and 8b, two kinds of salt geometries cannot be excluded (see text). The salt bottom and subsalt structures are interpretative. These models are the integration of structure elements of Asymmetric Flap Type (see text), and thus are not direct interpretations of any specific seismic lines. The scale bars are only suggestive of approximate sizes of these structures.

Extended HAPs are always associated with bulges at the foot of chaotic flaps (Fig 5.7a). As discussed, these bulges would be caused by shallowly buried salt, the tops of which caused the HAPs in seismic profiles. The sediments covering the salt are rather thin. Subsalt structures are mostly not imaged. Thus, it is uncertain if the salt represents extruded salt sheets, with a feeder rooted in the centre of the high, or a wide salt stock across the entire chaotic flaps. Because of this uncertainty, Figure 5.8a, as a structural interpretation for Asymmetric Flap Type with extended HAPs, presents two possibilities.

When the HAPs are restricted under the peak of a high (Fig 5.7b), they may indicate that the salt extent is limited and does not reach the foot of the chaotic flaps. Thus, Fig 5.8b shows a small salt stock restricted in the centre of the structure. The salt is plotted as an extruded salt tongue, although a wider salt stock, as wide as the horizontal extent of the HAPs, is also possible. Because these HAPs may alternatively be signatures of gas accumulations, Figure 5.8b-2 provides an alternative structural interpretation. In such cases, salt is absent in the penetration range of our seismic signal. Because HAPs have limited extent, they occasionally do not blank the sediment reflection beneath them (Fig 5.7b-2). These sediments indicate that although the chaotic flaps frequently appear to be structureless in their immediate subsurface, their deeper sections may be composed of stratified sediments that are upturned, similar to those in the uplifted flaps.

Steeply upturned sediments at the chaotic flaps are most clearly seen when HAPs are totally absent (Fig 5.7c). A large offset normal fault separates chaotic and uplifted flaps, and causes most of the offset between the two. The offsets of the secondary faults are minor (Fig 5.7c-3). Figure 5.8c shows our structural interpretation for this case. Note when HAPs appear in the chaotic flaps, there is no indication of faults between the uplifted and chaotic flaps, except in a few highs (Figs 5.6 and 5.7b-2). However, because the sediments of the uplifted flaps are much more elevated than those of the chaotic flaps (Figs 5.7a and 5.7b), a large offset must be accommodated. This could be accomplished by a major fault between an uplifted and its corresponding chaotic flap, by a set of faults at the chaotic flap, or by collapse of salt underlying the chaotic flaps. We infer that the first two possibilities may be applicable when the salt volume in the shallow subsurface of the chaotic flaps is limited, while the third possibility can be applied when extensive salt bodies occupy the chaotic flaps.

The idealized bathymetric high of the Asymmetric Flap Type in Fig 5.8 displays all three structural appearances along-strike. At its most developed part, the constant thickness unit is highly elevated in the uplifted flap and extended salt bodies occur in the chaotic flap (Fig 5.8a). Away from the maximum uplift, the salt extent becomes substantially limited (Fig 5.8b), at least in the depth range under discussion. The constant thickness unit at the uplifted flap remains highly elevated. At the end of the strike, sediment deformation becomes mild and salt is absent in shallow depth (Fig 5.8c). A complication derives from the small offset faults, which occasionally occur at less elevated parts and fragment both the uplifted and chaotic flaps. Similar minor faults are not observed at the uplifted flap where the structure is more deformed (Figs 5.8a and 5.8b).

*2. Initiation of the structure development.* The absence of onlaps in the constant thickness unit suggests it to be a pre-kinematic sediment unit, deposited before the uplift of the bathymetric highs. As a sharp contrast, the shallower sediments onlap and show clear thickness variation across the bathymetric highs, typical for syn-kinematic sediments. Thus, these highs should have been uplifted right after the deposition of the constant thickness unit, and their elevations are then maintained until the present day.

The time of uplift of these highs is not well constrained, because of the difficulties to regionally trace reflectors. Only in a few cases, the constant thickness unit can be picked as Unit VI (Table 5.1), which then indicates that they are uplifted at the same time as Chapopote (H2135) in the late Miocene (Ding et al., 2008). However, for the other highs the timing of their uplift is basically unknown.

On the other hand, the seismic study by Bertagne (1984) on the Veracruz Tongue, a basin neighbouring our study area (Fig 5.1), indicates that only during and after Miocene times did this basin become starved of turbiditic sediment input and instead received slumping sediment from the West (our study area). If the uplift of the bathymetric highs blocked turbiditic sediment transport to the Veracruz Tongue and caused slumping into this basin, then those highs should started uplift during and after Miocene times (Bertagne, 1984). In our study area, the top of constant thickness unit can often be traced into neighbouring mini-basins, which indicate the unit to be buried at relatively shallow depth in these basins (1-1.5 s TWT, about 750 to 1125 m). Considering the total thickness of sediments in this study area between 5 km and more than 10 km (Shaub et al., 1984; Buffler, 1991), the shallow stratigraphic position of this unit may suggest its relative young age (around late Miocene). Thus, a relatively recent formation of these bathymetric highs is reasonable.

3. *Evolution of the structure.* Our seismic observations and interpretations suggest that the sediments at both the uplifted and chaotic flaps are upturned to form an anticline. In an active salt region, such a folding of sediments can be accomplished by either lateral shortening or uplift of roof sediments through active diapirism. The first case would indicate a regional compression event, while for the second case no external deformation force is necessary. Nevertheless, a regional shortening, started around the time for the top of Unit VI is particularly favoured by the presence of the Perdido Type in our study area. For this type, Unit VI and underlying sediments are at least 1.5 km thick (Fig 5.5), and such thick roof sediments prohibit active diapirism (Schulz-Ela et al., 1993). Furthermore, the kink-band fold or pop-up structure of the Perdido Type rather resembles those folds typically observed at Perdido Fault Belt, being triggered by gravitational compression at the lower Rio Grande slope (Trudgill et al., 1999; Camerlino and Benson, 2006). We thus suggest that the Perdido Type in our study area indicates a lateral compressional event. Because both Perdido Type and Asymmetric Flap Type have similar youngest pre-kinematic strata (Unit VI or the constant thickness unit), it is reasonable to infer that the same compressional event also triggered the development of the Asymmetric Flap Type. Compression on regional scale also explains the NE-SW and NW-SE regional trends of the Asymmetric Flap Type (Fig 5.1b). Because the age of the constant thickness unit is uncertain, the exact timing of this event may vary at different locations, but lies very likely around late Miocene, as just discussed.

Unlike the Perdido Type, the Asymmetric Flap Type is active until the present day, and thus has not been buried. This is probably due to continuous supply of salt from the evacuation of salt from the mini-basins in between the bathymetric highs, which keeps this structural type being inflated and uplifted. Such a salt evacuation also causes the subsidence of mini-basins and associated with it, of the chaotic flaps. This would be the reason for the development of normal faulting between the uplifted and chaotic flaps. Dissimilar to salt rollers, the centre of subsidence and salt evacuation is not at the hanging wall of normal faults (the chaotic flaps in our case) (Jackson et al., 1994a; Jackson, 1995; Rowan et al., 1999), but instead in the mini-basins some distance away from the chaotic flaps. So, the overall structure resembles the asymmetric diapir of Nelson (1991), and the shallow sediments at chaotic flaps are still upturned, even when the flap as a whole subsided.

The subsidence of the chaotic flaps and the mini-basins does not necessarily require a regional extension of supra-salt sediments. It can be simply caused by salt evacuation, and when the elevation difference of the uplifted and chaotic flaps becomes large enough, the salt in the core would be exposed and flow out. In this case, the interpretation in Fig 5.8a-1 is more likely. Such a scenario implies that the salt out-flow occurred at relative late stage of the structural evolution. In turn, the sediments on the top of the salt are recent sediments after the out-flow, instead of a condensed section of entire syn-kinematic section: sediments deposited since the constant thickness unit. This is supported by the observation that at nearby mini-basins, the syn-kinematic sediments are up to ~800 ms TWT thick, while the sediments on the top of the salt are veneer-thin. If a regional extension does occur after the initial uplift, it may open and widen the gap between the chaotic and uplifted flaps, and a widened salt stock may result (Fig 5.8a-2). Note that in both cases, ample salt supply to the chaotic flaps can be expected by continuous subsidence of the mini-basins and thus evacuation of salt from underneath. The folding of these salt-covering sediments may be a local feature, because there is no indication of very recent compression elsewhere. In all, our Asymmetric Flap Type evolution scenarios indicates that the

deformational style changed from compression to tectonic relaxation since late Miocene, apparently similar to the Bay of Campeche (Mitra et al., 2005).

### 5.6.3 Implications for the occurrence of seeps

#### 5.6.3.1 Possible seep areas indicated by the shallow structures and comparison with seeps locations indicated by the satellite analysis

As mentioned, the purpose of our structural analysis is to further discuss the influence on the seepage of fluids. The observations of seismic features and knowledge about the internal structures of the bathymetric highs, which were laid out in detail in previous sections, are here applied to infer the prospective areas for seepage.

1. *Chapopote Type*. Bathymetric highs H2135 (Chapopote) and H2156 are grouped as Chapopote Type. Their most common character is the dome structure of sediment Unit VI and shallower sediments. Unit VI is suggested to be a coarse-grained unit of late Miocene age, while the younger sediments contain many fine grained sediment intervals (Ding et al., 2008). The high permeability of Unit VI and the dome geometry enable the Chapopote Type to focus and accumulate hydrocarbons, a classical structural trap.

For H2135 (Chapopote), detailed observations on the HAPs suggest that they are signatures of gas, and expectedly other fluids, trapped in the reservoir (Ding et al., 2008). Only under the crest of the knoll, these fluids seem to break through seal sediments, with chaotic reflections reaching seafloor on the seismic profiles. Such a break-through of fluids may have directly led to seepage on Chapopote. Thus, seeps are most likely to occur at those break-through spots: at the crest of H2135. Three seep sites were identified by the satellite analysis at the crest, and some of them were ground-truthed by the Cruise SO-174 and M67/2 (Bohrmann and Schenk, 2004; Macdonald et al., 2004; Bohrmann and Spiess, 2008).

For H2156, on the other hand, the nature of the HAPs is still uncertain. Gas, gas hydrates and/or salt signatures can be possible explanations. Nevertheless, these HAPs appear to be well buried by fine-grained sediments. This observation discredits that any fluids have broken through to the surface at the crest of H2156. Namely the crest is well sealed, regardless of various possibilities for nature of the HAPs here. This may not necessarily mean that the thin cover sediments provide an effective seal, but may rather indicate that the sediments were deposited in lieu of fluid activity. Seeps most likely occur around the outer flank of the HAPs, where seismic signatures are chaotic and often blanked. The satellite analysis also indicates that the seep sites ring around the high, at locations where HAPs are absent.

2. *Passive Type*. Because the geometry of salt and sediments beneath the salt cap is unconstrained by the seismic data, some sediment and salt traps could exist close to the salt flank. Nevertheless, unlike the Chapopote Type, the sediments around the broad circus of a Passive Type high is largely undeformed, and thus do not have a fluid-focusing structure. The extensive salt cap and the sediments covering the cap also prohibit leakage of hydrocarbons on the top of the high. Only when deep structures and petroleum generation could supply these highs with sufficient hydrocarbon fluids, hydrocarbons would be guided by the seal and seep at the outer ring of the highs. Otherwise, the Passive Type should be quiescent in seepage. The satellite analysis suggests only one seep site on the flank of H2119 and no seep is indicated for H2140, matching well with our interpretation.

3. *Asymmetric Flap Type*. A geometry that can focus fluids is expected for the Asymmetric Flap Type. At the uplifted flaps, the constant thickness unit is almost exposed at the seafloor, but the

unit is well stratified and minimally faulted. Because of permeability anisotropy of stratified sediments, any fluids inside will most likely migrate along the beds towards the peaks of the bathymetric highs or into the chaotic flaps. At the chaotic flaps, we have interpreted that if the constant thickness unit is under the HAPs, it would be also upturned similar to that of the uplifted flaps (Fig 5.8). This upturned unit should also focus fluids to the highest points of the chaotic flaps. In all, for the Asymmetric Flap Type fluids may be mostly accumulated in the peaks and the highest points of the chaotic flaps. Accordingly, the chaotic flaps and the possible faults between the chaotic and uplifted flaps are our expected locations for fluid seepage. At the less developed parts (the case of Fig 5.7c), secondary faults on both uplifted and chaotic flaps may provide some seepage pathways.

Whether such geometries can focus fluids also depends on the conductivity of the constant thickness unit. According to the Cenozoic depositional history of the deep GoM basin (Galloway et al., 2000), only sediments equivalent to or older than the late Miocene would be coarse enough to be likely conductive units, but the age of most of the constant thickness unit is uncertain. However, as discussed, most of it is likely to have a Miocene age, and its relative high amplitude also indicates its coarse grain size, and thus may behave as carrier beds. Note that the structures of both Asymmetric Flap Type and Chapopote Type can possess very shallow reservoirs of significant size, a critical requirement for the seafloor occurrence of massive asphalt (Ding et al., 2008). Hence, it is not surprising that such asphalt deposits were also found above Asymmetric Flap Type structures (MacDonald et al., 2007).

When extended HAPs occur (the case of Fig 5.8a), salt should be widely present at shallow depth in the chaotic flaps. Salt is usually an effective seal, preventing seepage directly above it. Like the discussion at H2156 of Chapopote Type, if HAPs are buried by well stratified sediments (e.g., Fig 5.6, offset 22,000 to 24,000 m), these intact sediments should indicate quiescence of seeps above them. These two considerations suggest that if extended salt units occur or well stratified sediments cover the HAPs, seepage is unlikely to occur at these locations, although in general, the chaotic flaps are seep-promising areas.

Our principal expectation that the seeps only occur on the chaotic flaps or the peaks of the highs matches unexceptionally with the satellite-indicated seep locations. Furthermore, the interpretation that salt units may prevent the occurrence of seepage is well witnessed in the Area Oil Ridge. The locations of shallow salt (south part of chaotic flap of H2112 and chaotic flap of H2105) both show absence of seepage. The seep sites largely do occur at these two highs, and only (1) on the peak of the highs, where the uplifted flaps terminate (H2105 and south part of H2112), (2) where shallow salt becomes limited in extent (north part of H2112) and (3) outer ring of the salt units (H2105). Other bathymetric highs also show similar patterns. H2001 (Fig 5.2b and Fig 5.7b) exemplifies our interpretation that when well stratified sediments cover the HAPs, seeps should also be absent. On the other hand, no seeps are indicated on the secondary faults. Their role in fluid leakage seems limited.

#### *5.6.3.2 Possible uncertainties of the interpretation*

During our discussion above, we presented that the knowledge of the seismic features and the internal structure in the study area largely explains the distribution patterns of seep sites indicated by the satellite analysis. But we also admit such knowledge cannot provide exact geographic positions of seep sites, as the satellite analysis does. Also at some locations where our profiles crossed some seep sites indicated by the satellite analysis, direct seismic indications for fluid pathways (blanking zone, gas/fluid chimney) are rare.

We consider this issue by referring to the nature of our work, which is different from those site-specific surveys, focusing in a single or a single group of seep sites (e.g. Reilly et al., 1996; Zühlsdorff and Spieß, 2004). Only in those studies, with 3D or densely spaced 2D seismic datasets, detailed characterization of seismic features and their spatial variation is possible. Furthermore, in structurally complicated locations, 3D seismic datasets are theoretically necessary to reduce side echoes. Our work, however, is to address the general near-surface structural styles and their regional distribution in the north-western Campeche Knolls. Methodologically, the study focuses on these structural patterns to identify locations of shallow hydrocarbon accumulations. At these locations, shallowly buried salt indicates locations of effective sealing and/or undisturbed sediments indicate locations of seepage inactive. The areas without these two features are thus seepage promising areas. The consistency between these areas and the seep sites independently predicted by the satellite analysis should demonstrate the reliability of both approaches.

Near-surface sediment structures only account for presence of traps and leakage pathways. These features are not necessarily charged with hydrocarbon fluids, which, in this petroleum-prolific region, are mainly supplied from greater depth. Furthermore, instead of a straight leakage pathway, many of the structures may encompass fluid structure traps, and fluids' mobility could be compromised by chilling and gas-hydration at near surface low temperatures. After all, we regard that the locations with stratified sediments upon possible hydrocarbon accumulations are quiescent in seepage, but in these locations, how the hydrocarbon accumulations are sealed is not addressed. Beside salt, gas hydrates and chilled heavy petroleum may serve as seal materials. Thus, seepage is only possible when fluid supply is ample to overcome these retention factors. This could help to explain the concentrated seepage occurrence in the Area Chapopote, Oil Ridge and Middle Slope (Fig 5.1b), and relative seepage quiescence in the rest of the study area, especially that between Area Oil Ridge and Middle Slope. Deep processes, which control the petroleum generation, migration, accumulation and leakage in deep reservoirs need to be incorporated to discuss this broader perspective.

## 5.7 Conclusion

This study incorporates bathymetry, high resolution seismic and inferred hydrocarbon seep locations from analysis of satellite images from the north-western Campeche Knolls, in order to characterize (1) regional bathymetric features, (2) the spatial distribution pattern of seep sites, (3) shallow subsurface structures of bathymetric highs, (4) structural evolution of these highs, and (5) the control of these structures on the occurrence of seepage.

Our bathymetry data reveals that the study area is characterized by a knoll-dominated northern part and ridge-dominated southern one. The ridges can have relatively high and uniform elevation along most of their strike, but more commonly, they are made of highly elevated peaks with limited along-strike extent. Both ridges and knolls are arranged in a clearer regional NE-SW trend and a less pronounced NW-SE trend. The seep sites indicated by satellite analysis show that they are mostly clustered on the knolls or lineated along the ridges. As a result, these seep sites also show the two regional trends.

The investigation on over 20 knolls and peaks along the ridges indicates three types of shallow subsurface structures: Chapopote Type, Passive Type and Asymmetric Flap Type. The first two types are distributed in the northern part of the study area, appearing as knolls and being limited in numbers. The Asymmetric Flap Type is the dominant structural style in the entire study area: virtually all the peaks along the ridges and some knolls represent this structural style.

The Chapopote Type has a bathymetric appearance and internal structure similar to domes, with permeable sediments of late Miocene or older age composing the deep strata of the domes. The Passive Type is recognized as comprising passive salt diapirs with wide salt stocks in their centre. An Asymmetric Flap Type structure is made up of an uplifted flap and a subsided chaotic flap. The deep sediments at the uplifted flap are synthetically upturned, so the younger sediments largely onlap at this flap. Upturned sediments and salt may both exist in the chaotic flap. These different types of structures also suggest different sediment deformation history. The Passive Type, as expected for passive diapirs may be present in the area since the time of salt deposition. The Chapopote Type and the Asymmetric Flap Type should have developed during the late Tertiary (possibly since the late Miocene). The deformation could be initiated by lateral contraction in the study area.

The dome-like structure of the Chapopote Type supports a focusing effect of hydrocarbon fluids into its core. The permeable sediments of late Miocene or older age both provide fluid pathways to bolster such effect. Thus, hydrocarbon accumulation in the structure is well expected. However, the trap in H2135 (Chapopote) is sealed by fine-grained Pliocene and younger sediments. Seepage occurs only on the highest point of the structure where break-through of hydrocarbons through the seal is indicated seismically. The highest point of H2156 seems to be inactive, and could be possibly sealed by salt, gas hydrates or high viscosity heavy petroleum, e.g., asphalt. Thus, seepage occurs only at the flank of the structure, where such sealing is absent.

Both extended distribution of salt and featureless sediments on the flank underscore the Passive Type to be an efficient fluid-focusing structure. The satellite analysis also suggests that this type is largely seepage inactive. A fluid-focusing effect is promised for the Asymmetric Flap Type, with the upturned sediments in both chaotic and uplifted flaps being capable of guiding fluids into the centre of the structure and the late Miocene or similar sediments acting as aquifers. Thus, fluid accumulations, provided they occur, should be on the chaotic flaps of the structure and/or at the peak of the bathymetric highs. However, salt and other sealing materials in the upper parts of chaotic flaps tend to prevent fluids to escape to the seafloor. Seepage only occurs when such seals fail or are absent. These seepage promising areas are well consistent with seep sites identified from the analysis of satellite SAR images by NPA.

We have presented that the shallow sediment and salt structures, which are the expressions of the salt tectonics in the southern GoM, largely control the locations of seepage in our study area. Regionally, the general trends of the structures: NE-SW and NW-SE result in the same regional trends of seep sites. In smaller scale, the structural types of individual bathymetric highs control more specific locations of seepage. Considering all these imprints of shallow structures on the fluid seepage, we suggest that expected deep reservoirs can only be directly indicated by these seep sites when both the shallow and the deep sediment column are shaped by the same set of tectonic processes. Furthermore, the concentrated seepage occurrence in the three sub-study-areas: Area Chapopote, Area Oil Ridge and Area Middle Slope cannot be explained by shallow structure styles and trends alone. This might be the expression of petroleum generation and deep reservoir distribution in these areas.

## 5.8 Acknowledgments

We thank the crew of the R/V Meteor during the cruise M67/2, for their excellent cooperation with our onboard scientific work. We are grateful to the Mexican government and Pemex for the permission to survey Mexican national waters during the cruise M67/2. Special

acknowledgements are given to G. Pérez-Cruz and G. Basurto of Pemex Deep Water Exploration, for their inspirational discussions with us. Elva Escobar and Jaime U. Fucugachi of UNAM have generously helped us during the M67/2 cruise and our visits in Mexico. F. D.'s research visits in Mexico were supported by Bremen International Graduate School for Marine Sciences (GLOMAR). The M67/2 cruise and this study are funded through DFG-Research/Exzellenz Cluster, "the ocean in the Earth system".

## References

- Abrams, M. A.**, 1996. Distribution of subsurface hydrocarbon seepage in Near-surface marine sediments. In Schumacher, D. and Abrams, M. A. (eds.) Hydrocarbon migration and its near-surface expression. AAPG Memoir No. 66, pp. 1 – 14.
- Abrams, M. A.**, 2005. Significance of hydrocarbon seepage relative to petroleum generation and entrapment. *Marine and Petroleum Geology*, 22, 457-477
- Ambrose, W. A.**, Wawrzyniec, T. F. and Fouad, K. et al., 2003. Geologic framework of upper Miocene and Pliocene gas plays of the Macuspana Basin, southeastern Mexico, *AAPG Bulletin* 87(9), 1411-1435, doi: 10.1306/04140302022
- Bertagne, J. A.**, 1984. Seismic stratigraphy of Veracruz Tongue, deep southwestern Gulf of Mexico, *AAPG Bulletin* 68(12), 1894-1907
- De Beukelaer, S. M.**, MacDonald, I. R., Guinnasso, N. L. Jr., Murry, J. A., 2003. Distinct side-scan sonar, Radarsat SAR, and acoustic profiler signatures of gas and oil seeps on the Gulf of Mexico slope. *Geo-Marine Letters* 23, 177-186.
- Bryant, R. B.**, Lugo, J., Córdova, C. and Salvador, A., 1991. Physiography and bathymetry. In Salvador, A. (Ed.) *The geology of North America, The Gulf of Mexico basin vol. J.* Geological Society of America. pp. 160-196.
- Bohrmann, G.** and Schenck, S., 2004. R/V Sonne Cruise Report SO 174. GEOMAR Report, ISSN 0936-5788, IFM-GEOMAR, Kiel, Germany.
- Bohrmann, G.**, Spiess, V., and cruise participants, 2008. Report and preliminary results of R/V Meteor Cruise M67/2a and 2b, Balboa -- Tampico -- Bridgetown, 15 March - 24 April, 2006. Fluid seepage in the Gulf of Mexico, *Berichte*, No. 263, Fachbereich Geowissenschaften, ISSN 0931-0800, Universität Bremen, Bremen, Germany.
- Buffler, T. R.**, 1991. Seismic stratigraphy of the deep Gulf of Mexico basin and adjacent margins. In J. Salvador, A. (Ed.) *The geology of North America, The Gulf of Mexico basin vol. J.* Geological Society of America. pp. 353-387.
- Camerlo, R. H.** and Benson, E. F., 2006. Geometric and seismic interpretation of the Perdido fold belt: Northwestern deep-water Gulf of Mexico. *AAPG Bulletin*, 90(3), 363 – 386.
- Espedal, H.** and Wahl, T., 1999. Satellite SAR oil spill detection using wind history information. *International Journal of Remote Sensing*, 20(1), 49-65.
- Ewing, M., J. L.** Worzel, A. O. Beall et al., 1969. Site 2, Initial reports of Deep Sea Drilling Project, vol. I. US Government Printing Office, Washington
- de Faragó Botella**, Holguin Quiñones, N. M. and Williams, A. K., 2004. New Petroleum Systems Detected in the Deep-water Mexican Gulf by Satellite Radar Imagery. AAPG International Conference, Cancun, Mexico, American Association of Petroleum Geologists October 24-27
- Ding, F.**, Spiess, V., Brüning, M., Fekete, N., Keil, H. and Bohrmann, G., 2008. A conceptual model for hydrocarbon accumulation and seepage processes around Chapopote asphalt site, southern Gulf of Mexico: from high resolution seismic point of view. *Journal of Geophysical Research*, 113, B08404, doi:10.1029/2007JB005484

- Fiduk, J. C.**, Weimer, P., Trudgill, B. D., Rowan, M. G., Gale, P. E., Phair, R. L. Korn, B. E., Roberts, G. R. Gafford, W. T., Lowe, R. S. and Queffelec, T. A., 1999. The Perdido Fold Belt, Northwestern Deep Gulf of Mexico, Part 2: seismic stratigraphy and petroleum systems. *AAPG Bulletin*, 83(4), 578 – 612
- Galloway, W. E.**, Patricia, G. E., Li, X. et al., 2000. Cenozoic depositional history of the Gulf of Mexico basin, *AAPG Bulletin* 84(11), 1743-1774, doi:10.1306/8626C37F-173B-11D7-8645000102C1865D.
- Garrison, L.E.** and Martin, R. G., 1973. Geologic structures in the Gulf of Mexico Basin. US Geological Survey Professional Paper, 773. US Government Printing Office, Washington
- Gay, A.**, Lopez, M., Cochonat, P. et al., 2006. Evidences of early to late fluid migration from an upper Miocene turbiditic channel revealed by 3D seismic coupled to geochemical sampling within seafloor pockmarks, Lower Congo Basin. *Marine and Petroleum Geology* 23, 387-399, doi: 10.1016/j.marpetgeo.2006.02.004.
- Huhnerfuss, H.**, Alpers, W. and Witte, F., 1989. Layers of different thicknesses in mineral-oil spills detected by grey level textures of real aperture radar images. *International Journal of Remote Sensing* 10(6), 1093-1099.
- Jackson, M. P. A.**, Vendeville, C. B. and Schultz-Ela, D. D., 1994a. Structural dynamics of salt systems, *Annual Review of Earth and Planetary Science* 22, 93-117.
- Jackson, M. P. A.**, Vendeville, C. B. and Schultz-Ela, D. D., 1994b. Salt-related structures in the Gulf of Mexico: A field guide for geophysicists. *The Leading Edge* 8.1994, 837-842.
- Jackson, M. P. A.** 1995., Retrospective salt tectonics. In Jackson, M. P. A., Roberts, D. G. and Snelson, S. (Eds.) *Salt tectonics: a global perspective*. AAPG Memoir No. 65, pp.1-28.
- Kornacki, A. S.**, Kendrick, J. W. and Berry, J. L., 1994. The impact of oil and gas vents and slicks on petroleum exploration in the deepwater Gulf of Mexico. *Geo-Marine Letters* 14(2/3), 160-169.
- Liu, J.** and Bryant, W. R., 2000. Seafloor morphology and sediment paths of Northern Gulf of Mexico deep water. In Bouma, A. H. and Stone, C. G. (eds.) *Fine-grained turbidite systems*. AAPG Memoir No. 72/SEPM Special Publication No. 68, pp. 33 – 46.
- MacDonald, I. R.**, Guinasso, N. L. Jr., Ackleson, S. G., Amos, J. F., Duckworth, R., Sassen, R. and Brooks, J. M., 1993. Natural oil slicks in the Gulf of Mexico visible from space. *Journal of Geophysical Research* 98 C9, 16351-16364.
- MacDonald, I. R.**, Reilly, J. F. Jr., Best, S. E., Venkataramaiah, R., Sassen, R., Guinasso, N. L. and Amos, J., 1996. Remote sensing inventory of active oil seeps and chemosynthetic communities in the Northern Gulf of Mexico. In Schumacher, D. and Abrams, M. A. (eds.) *Hydrocarbon migration and its near-surface expression*. AAPG Memoir No. 66, pp. 27 – 37.
- MacDonald, I. R.**, Leifer, I., Sassen, R., Stine, P., Mitchell, R. and Guinasso, N. L. Jr., 2002. Transfer of hydrocarbons from natural seeps to the water column and atmosphere. *Geofluids* 5, 95-107.
- MacDonald, I. R.**, Bohrmann, G., Escobar, E. et al., 2004. Asphalt Volcanism and Chemosynthetic Life in the Campeche Knolls, Gulf of Mexico, *Science* 304 (14 May), 999-1002, doi:10.1126/science.1097154.
- MacDonald, I. R.**, Escobar, E., Naehr, T., Joye, S., Spiess, V., Chapopote III cruise participants, 2007. The Asphalt Ecosystem of the Gulf of Mexico: Results from the Chapopote III Cruise. *EOS*, 88(52), AGU Fall Meeting Supplements, Abstract B43E-1660 INVITED
- Macgregor, D. S.**, 1993. Relationships between seepage, tectonics and subsurface petroleum reserves. *Marine and Petroleum Geology*, 10(6), 606 – 619.

- Magoon, L. B.**, Hudson, T. L. and Cook, H. E., 2001. Pimienta-Tambra(!) – A giant supercharged petroleum system in the southern Gulf of Mexico, Onshore and Offshore Mexico. In Bartolini, C., Buffler, R. T. and Cantú-Chapa (Eds.) The western Gulf of Mexico Basin: Tectonics, sedimentary basins, and petroleum systems. AAPG Memoir No. 75, pp. 83 - 125.
- Mitra, S.**, Figueroa, G. C., Garcia, J. H. And Alvarado, A. M., 2005. Three-dimensional structural model of the Cantarell and Sihil structures, Campeche Bay, Mexico. AAPG Bulletin, 89(1), 1 – 26.
- Naeth, J.**, di Primio, R., Horsfield, B., Schaefer, R. G., Shannon, P.M., Bailey, W.R. and Henriot, J.P., 2005. Hydrocarbon seepage and carbonate mound formation: A basin modelling study from the Porcupine Basin. Journal of Petroleum Geology 28(2), 147-166
- Nelson, T.H.**, 1991. Salt tectonic and listric-normal faulting, in Salvador, A. (Ed.) The Gulf of Mexico Basin, The Geology of North America, vol. J. Geological Society of America. pp. 73-89.
- Reilly, J. F.**, MacDonald, I. R., Biegert, E. K. and Brooks, J. M., 1996. Geological controls on the distribution of chemosynthetic communities in the Gulf of Mexico, in *Hydrocarbon migration and its near-surface expression: AAPG Memoir 66*, edited by Schumacher, D. and M.A. Abrams., pp.39-62, American Association of Petroleum Geologists
- Rowan, M. G.**, Jackson, M. P. A. and Trudgill, B. D., 1999. Salt-Related fault families and fault welds in the northern Gulf of Mexico. AAPG Bulletin 83(9), 1454-1484.
- Rowan M. G.**, Lawton, T. F., Giles, K. A. and Ratliff, R. A., 2003. Near-salt deformation in La Popa basin, Mexico, and the northern Gulf of Mexico: A general model for passive diapirism. AAPG Bulletin 87(5), 733-756.
- Salvador, A.**, 1991. Origin and development of the Gulf of Mexico basin, in Salvador, A. (Ed.) The Gulf of Mexico basin, The geology of North America vol. J. Geological Society of America. pp. 389-443.
- Santamaria-Orozco, D.**, Horsfield, B., Di Primio, R. and Welte, D. H., 1998. Influence of maturity on distributions of benzo- and dibenzothiophenes in Tithonian source rocks and crude oils, Sonda de Campeche, Mexico. Organic Geochemistry 28(7-8), 423-439.
- Schultz-Ela, D. D.**, Jackson, M. P. A. and Vendeville, B. C., 1993. Mechanics of active salt diapirism. Tectonophysics 228, 275-312.
- Schultz-Ela, D. D.**, 2003. Origin of “drag” folds bordering salt diapirs. AAPG Bulletin 87(5), 757-780.
- Shaub, F. J.**, Buffler, T. R. and Parsons, G. J., 1984. Seismic stratigraphic framework of deep central Gulf of Mexico basin. AAPG Bulletin 68(12), 1790-1802.
- Shipley, T.**, Gahagan, L., Johnson, K. and Davis, M., (Eds.) 2005. Seismic Data Center. University of Texas Institute for Geophysics. URL: <http://www.ig.utexas.edu/sdc/>.
- Thrasher, J.**, Fleet, A. J., Hay, S. J., Hovland, M., Düppenbecker, S., 1994. Understanding Geology as the key to using seepage in exploration: the spectrum of seepage styles. In Schumacher, D. and **Abrams, M. A.** (Eds.) Hydrocarbon migration and its near-surface expression. AAPG Memoir No. 66, pp.223-241.
- Trudgill, B. D.** Rowan, M. G., Fiduk, J. C., Weimer, P., Gale, P. E. Korn, B. E., Phair, R. L., Gafford, W. T., Roberts, G. R. and Bobbs, S. W., 1999. The Perdido Fold Belt, Northwestern Deep Gulf of Mexico, Part 1: structural geometry, evolution and regional implications. AAPG Bulletin, 83(1), 88 – 113.
- Viniegra, F.**, 1981. Great carbonate bank of Yucatán, southern Mexico. Journal of Petroleum Geology 3(3), 247-278.
- Watkins, S. J.**, Ladd, W. J., Buffler, T. R. et al., 1978. Occurrence and evolution of salt in deep Gulf of Mexico, In Bouma, A.H., Moore, G.T., and Coleman, J.M., (Eds.) Framework, facies and

oil-trapping characteristics of the upper continental margin. AAPG studies in Geology No. 7, pp. 43-65.

**Williams, A. K.**, Lawrence, G. M., and King, M., 2006. Exploring for Deepwater Petroleum Systems with SAR (Synthetic Aperture Radar) – Fact or Fiction?: Comparing Results from Two of Today's Hot-Spots (Congo Fan and Santos) with Two of Tomorrow's (Campeche and Cariaco). AAPG Annual Conference and Exhibition Houston, Texas, April 10-12, 2006.

**Wessel, P.** and Smith, W. H. F., 1991. Free software helps map and display data. EOS 72, 445 – 446.

**Wood, W. T.**, Gettrust, J. F., Chapman, N. R. Spence, G. D. and Hyndman, R. D., 2002. Decreased stability of methane hydrates in marine sediments owing to phase-boundary roughness. Nature, 420(12), 656 – 660.

**Worzel, J. L.**, Bryant, W., et al., 1973a. Site 89 and Site 90. In Worzel, J.L., Bryant, W. et al. (Eds.) Initial Reports of Deep Sea Drilling Project, vol. X. U.S. Government Printing Office, Washington. pp. 71-115.

**Worzel, J. L.**, and Bryant, W., 1973b. Regional aspects of Deep Sea Drilling in the Gulf of Mexico Leg 10. In Worzel, J.L., W. Bryant et al. (Eds.) Initial Reports of the Deep Sea Drilling Project, vol. X. U.S. Government Printing Office, Washington. pp. 737-748.

**Yilmaz, Ö.**, 1991. Seismic data processing. Society of Exploration Geophysics, Tulsa

**Zühlsdorff, L.** and Spieß, V., 2004. Three-dimensional seismic characterization of a venting site reveals compelling indications of natural hydraulic fracturing. Geology 32(2), 101-104.

## **Chapter 6. Interaction between accretionary thrust faulting and slope sedimentation at the frontal Makran Accretionary Prism, their resultant shallow sediment structures and some implications for hydrocarbon fluid seepage**

**Feng Ding<sup>1</sup>, Volkhard Spiess<sup>1</sup>, Noemi Fekete<sup>1</sup>, Bramley Murton<sup>2</sup>, Markus Brüning<sup>1</sup> and Gerhard Bohrmann<sup>1</sup>**

1. Marum, University of Bremen, Klagenfurter Strasse, 28359 Bremen, Germany

2. National Oceanography Centre Southampton, Empress Dock, Southampton, SO14 3ZH, UK

### **6.1 Abstract**

During the Meteor Cruise M74/2 to the Makran accretionary prism, a set of high resolution seismic data was collected to study the shallow sediment structure evolution at the deformation front and lower slope, and influences of this process on cold fluid seepage occurrence. At the deformation front, the accreted sediments are imbricated by upward-propagating thrust faulting, which further induces secondary thrusts segmenting the hanging-walls of the primary thrusts. Shallower sediments above these thrust are folded under the strain of deep sediment offset, until the thrusts reach seafloor. The anticlines in shallow sediment, as the result of the primary and secondary thrusts, can also be recognized in the sediment ridges of the lower slope. These folds remain active at the lower slope, and folding the newly deposited slope basin sediments. Furthermore, the slope sediments, deposited at the less elevated foot-walls of primary and secondary thrusts, prevent the uplifted hanging-walls from being suspended and failing. This also means the slope sediments wedge apart imbricate slices at their upper ends, causing the various hanging-walls to be steeper in dip than they otherwise would be.

These folded imbricate slices and slope sediments in the lower slope form near-surface structural traps for fluids escaping from the greater depth. The accumulations of hydrocarbon fluids in these traps, especially free gas, are suggested by various seismic anomalies. When these traps are sufficiently charged they can induce diatremes, gas chimneys above them. Seepage atop these features are ground-truthed by ROV diving of the same cruise. Thus, focused seepage around Fifth Ridge are supplied by hydrocarbons, possibly thermogenic and accumulated in shallow traps. The study area does not indicate mud volcano-like features caused by vigorous ascending of overpressured fluids.

### **6.2 Introduction**

The Makran Accretionary Prism stands as one of thickest accreted sediment complexes in the world (e.g., White and Klitgord, 1976; Gaedicke et al., 2002). Immediately land-ward of the accretion deformation front (called the frontal Makran), the prism is also distinguished by its spectacularly high and steep sediment ridges (e.g., Fruehn et al., 1997; Kukowski et al., 2001; Schlüter et al., 2002). They are surface expressions of thrust faulting and imbricate slices, which may be continuously active after their formation at the toe of the prism. Moreover, the sediment ridges are also subjected to fast deposition of new slope sediments, supplied from the subaerial Makran Prism.

Tectonic shortening is the major driving force for the thrust faulting. Thus, most of the studies on the frontal Makran focus more on the deep, décollement level thrust faulting and under-plating,

and simply assume or imply that new sediments passively infill thrust-resulted morphologic lows. However, thrust faulting uplifts hanging-walls and propagate upwards. The newly deposited slope sediments, in many cases more than 1 km thick, may be eventually incorporated into the faulted units. In this process, they would be deformed and would change the geometric configuration of the thrusts, influencing their further activity. However, little is known about how thrust faulting evolves at its upper end, incorporating the growing slope sediments.

Furthermore, tectonic thickening and under-plating of sediments at convergent margins facilitates generation of excess fluids, which are either squeezed-out pore waters, diagenetic water or hydrocarbon fluids. Fluid expulsion is witnessed as pervasive occurrence of mud volcanoes in the subaerial or shallow water part of the Makran Prism. At the deeply submerged frontal Makran, expulsion is indicated by pronounced bottom simulating reflectors (BSR) in seismic profiles, carbonate crusts on the seafloor etc. (e.g., [Minshull and White, 1989](#); [von Rad et al. 2000](#)). Moreover, 15 new seep sites were discovered in the frontal Makran during the recent Cruises M74/2 and /3 ([Spiess et al., 2008](#); [Bohrmann et al., 2008](#)). Thrust faults are long assumed to be the sole fluid pathway for seeps, but the discovered seep sites do not seem to occur along the surface traces of these thrusts ([Bohrmann et al, 2008](#)). Instead, many are located on top of the sediment ridges. Therefore, patterns of seep distribution may be better understood by investigating shallow subsurface structures of the frontal Makran, addressing their influence on fluid migration in the near-surface.

High resolution seismic and swath bathymetry data collected during Cruise M74/2 to the frontal Makran may provide hints to the issues above. With these datasets, we will focus on both the deformation front and an internal ridge at the frontal Makran. The study first addresses how thrust faults and imbricate slices initiate at the deformation front. It then investigates how the faults and related shallow structures further evolve at that internal ridge, which receives fast deposition of slope sediments. The detailed understanding of shallow structures around the internal ridge, together with seismic anomalies, may then provide new hints for fluids accumulation and seepage around that ridge.

### 6.3 Data

The 2D high resolution seismic dataset was acquired during the M74/2 Cruise. The seismic source was a 4.1 L GI gun. The streamer had a total active length of 400 m, with 64 high resolution channels. Additional lead-in and stretch sections increased the maximum gun-receiver offset to ~480 m. During part of the acquisition, the streamer was towed parallel to the TOBI deep tow sidescan sonar. The collected seismic dataset has a dominant frequency range of 50 – 200 Hz, indicating a vertical resolution of 10 – 2.5 m ([Yilmaz, 1991](#)) at sediment acoustic velocity of ~2000 m/s. The dataset was processed with a multichannel seismic processing method, using the Vista seismic processing software. It includes band-pass filtering, common mid-point (CMP) binning with 5 m bin spacing, normal move-out (NMO) correction and CMP stacking based on picked velocities. The stacked profiles were time-migrated with a finite difference method.

Our bathymetric data were collected with a Simrad EM120 multibeam system hull-mounted on R/V Meteor. For the data processing MBsystem software ([Caress and Chayes, 1996](#)) was used. Procedures include sound-velocity modelling, trace editing and gridding with a spacing of 50 m. The GMT software ([Wessel and Smith, 1991](#)) was used for bathymetry and seismic line location displaying.

## 6.4 Geological Setting

The Makran Prism marks an accretionary convergent margin, where oceanic crust in the Gulf of Oman is subducting under the continental Eurasian Plate. To its west and east, the prism is neighbored by the Zagros Range and the Himalayas, respectively. It trends largely west-east and is slightly curved at its both ends (Fig 6.1a). Currently, the convergence rate is 3 - 5 cm/yr (Quittmeyer and Kafka, 1984; DeMets et al. 1990), approximately normal to the strike of the prism, which grows 11 km/Ma into the Gulf of Oman (Platt et al. 1985). The Makran Prism is an extraordinarily wide accretionary prism, extending 150 km offshore and 200-300 km onshore (White and Klitgord, 1976). The accretion history dates back to the late Cretaceous (Arthurton et al. 1982; Harms et al., 1984), while substantial underplating since at least the late Miocene (Platt et al. 1985) uplifted a large portion of the prism above sea level. Turbiditic sediments in the Gulf of Oman and the Makran were first sourced from the Himalayas through the Indus River. At the late Tertiary, predominant supply shifted to the hinterland of Makran from the north (Gaedicke et al. 2002). Through both depositional episodes the Gulf of Oman has been maintained as a region of fast sediment accumulation since the Oligocene. Presently, the total sediments thickness immediately seaward of the Makran Prism amounts to 5 - 7 km (Fruehn et al. 1997; Schlüter et al. 2002).

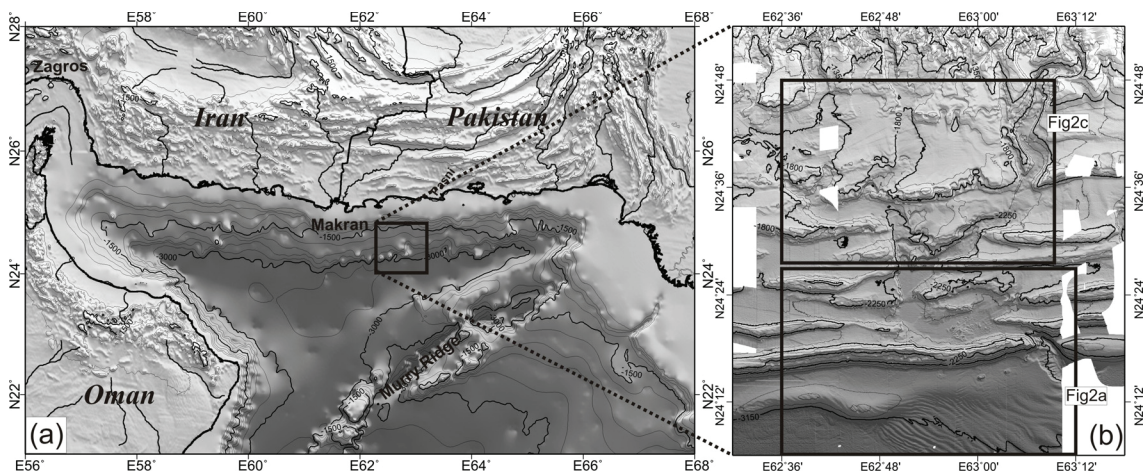


**Figure 6.1.** Makran Prism and the cruise M74/2 survey area. a) Location of Makran Prism, b) Bathymetry from M74/2, location of the study areas

Around our study area (E62°45' to E63°8', Fig 6.1a), the décollement at the deformation front is about 4 km beneath the seafloor (Fruehn et al. 1997; Kopp et al. 2000; Kukowski et al. 2001). Sediments above the décollement are being accreted by imbricate thrusting (Fruehn et al. 1997). The frontal Makran, designated as the portion of the prism immediately inboard of the deformation front, is comprised of lower slope ridges, and a mid slope terrace defined by Kukowski et al. (2001). The lower slope features many steep-sided sediment ridges, marking the surface expression of imbricate slices. These ridges can rise several hundred meters above the surrounding floor, but vary in elevation along-strike. The mid slope terrace is a relatively flat area, apparently as the result of ridges being buried by sediments from the north (Kukowski et al. 2001). Further landward, the frontal Makran is bounded by a steep upper slope.

The Makran Prism is segmented by a plate boundary fault, the Sonne Fault, which separates the underlying oceanic crust into two plates: the oceanic part of the Arabian Plate and the Ormara Plate (Kukowski et al. 2000). The fault causes a left-lateral offset to the sediment ridges

on the lower slope. In addition, several canyons run down-slope across the frontal Makran into the abyssal basin. They either zigzag cut through the ridges, or take the surface trace of Sonne Fault as their canyon floor (Kukowski et al. 2001).

### 6.5 Study area and its bathymetric features

Our study area is a section of the frontal Makran offshore western Pakistan, and we focus on two separate areas, one around the deformation front (Area DF) and the other around the mid slope terrace (Area MST) (Fig 6.1b). In the Area DF, First Ridge is elevated along most of its strike and locally rises more than 1000 m above the abyssal basin. However, its elevation drops down to ~ 800 m towards the east, where the ridge is cut by the Sonne Fault. The canyon (called Sonne Canyon hereafter), which takes the trace of Sonne Fault, incised a deep galley at its canyon mouth (Fig 6.2a). To the southwest of the galley, some sediment undulations strike largely parallel to the galley. Those closer to the galley have larger elevation and wavelength. Nascent Ridge is the seaward-most ridge of the entire Makran. Only in the western part of the Area DF (Fig 6.2a), it is elevated to ~400 m above the basin plain. Further to the east, its elevation drops to a few tens of meters.

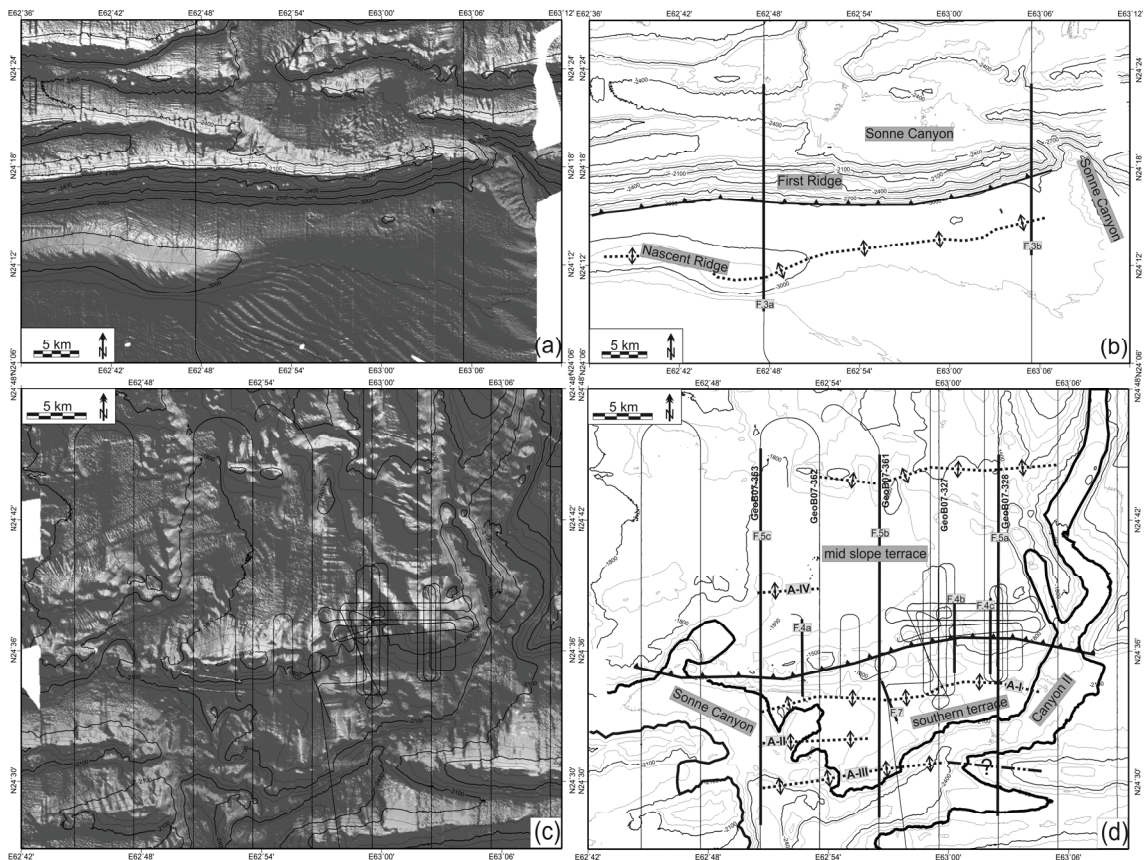


**Figure 6.2.** The study areas. a) Bathymetry of the deformation front and, b) Interpretation of major features; c) Bathymetry of the Fifth Ridge and its surrounding and, d) Interpretation of major features.

The mid slope terrace, its seaward bounding ridge (Fifth Ridge in Fig 6.2d) and another relatively flat area further south (the southern terrace in Fig 6.2d) are the major morphologic features in the Area MST. At the northern border of the mid slope terrace, another ridge (the sixth ridge) seems almost buried. The area is directly east to Sonne Fault and Canyon. To the

east, it is also intersected by another canyon (Canyon II in Fig 6.2c). Further down-slope, Canyon II kinks to the west, cutting out the southern boundary of the southern terrace. The Fifth Ridge shows an overall constant elevation, hundreds of meters higher than all the ridges further seaward. However, the ridge crest is cut by many small scale scarps at its western section, and a 1 km wide slump scarp sits in the central section. Because this ridge is bounded by the mid-slope terrace and the southern terrace, it appears to be isolated from other ridges in the frontal Makran. Although both terraces are flat in general, they are slightly tilted to the west, and grade into the floor of the Sonne Canyon or one of its tributaries (Fig 6.2c). In addition, some small undulations, only several meters in amplitude, are visible in the eastern part of both terraces.

## 6.6 Seismic Observations and Primary Interpretation

### 6.6.1 Nascent Ridge, First Ridge and their surroundings

The seismic profile in Fig 6.3a crosses the highest uplifted section of Nascent Ridge. It shows that the ridge is cored by a very broad and open anticline, much more open than e.g., the anticline land-ward to First Ridge (Arrow 4, Fig 6.3a). In addition, the anticline is highly asymmetrical, with a gently inclined backlimb (land-ward side) and a steeply dipping forelimb (up to 30°). Indeed, the forelimb dips so steeply as if it is faulted (Arrows 1, Fig 6.3a). Whether the forelimb is truly faulted will be discussed later.

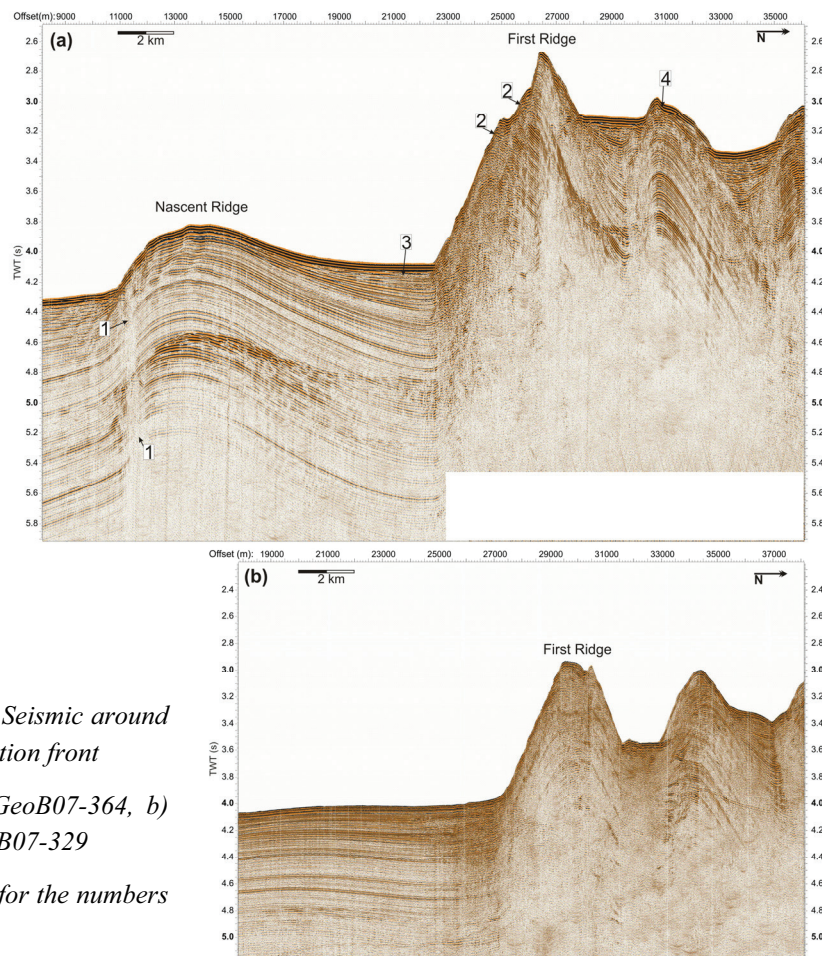


**Figure 6.3.** Seismic around the deformation front

a) Profile GeoB07-364, b) Profile GeoB07-329

see the text for the numbers and arrows

Shallowest sediments onlap the backlimb of the ridge (Arrow 3, Fig 6.3a), indicating they were deposited syn-kinematically to the folding of Nascent Ridge and accumulated to a recognizable thickness (up to 200 ms TWT, two-way traveltime). Because these sediments have higher reflectivity than the deeper sediments, they can also be recognized in the abyssal plain. For convenience, we name the sediments deposited before initiation of a folding or faulting as *imbricate slices*, while the sediments deposited thereafter and being incompatible to imbricate slices will be called *slope sediments*.

The First Ridge is much higher uplifted than the Nascent Ridge. The frontal side (basin-ward side) of the ridge seems to be piecewise normal-faulted or slided, with at least two steep and straight planes indicating scarps (Arrows 2, Fig 6.3a). Reflections in these slided sediments are very chaotic and structureless. Only 4 km further landward, another ridge rises as an asymmetrical anticline. East to Fig 6.3a, First Ridge drops in elevation and, instead of sliding at its frontal side, the ridge appears to be a complete anticline, which is much tighter than the one inside Nascent Ridge.

## 6.6.2. Fifth Ridge area

### 6.6.2.1 Sediment structural variation along the strike of Fifth Ridge

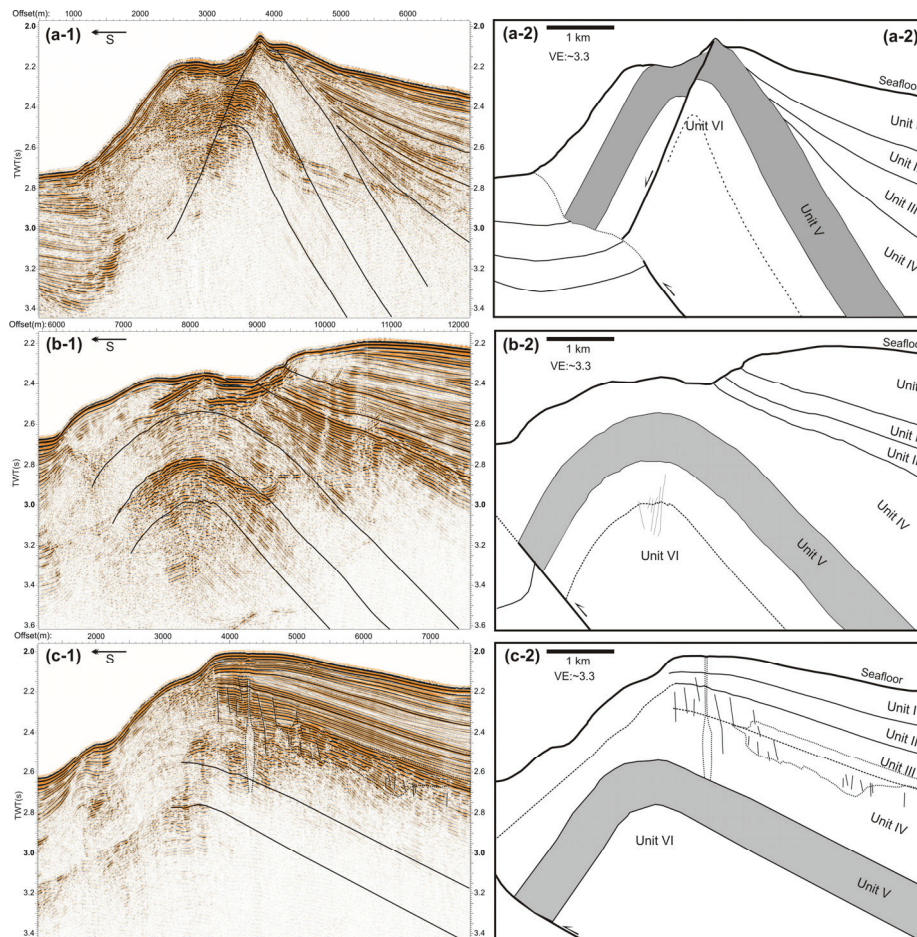


**Figure 6.4.** Fifth Ridge seismic profiles a-1) Profile GeoB07-413, a-2) Its structure interpretations, b-1) Profile GeoB07-343, b-2) Its structure interpretations, c-1) Profile GeoB07-354, c-2) Its structure interpretations. See Figure 2d for their locations

Sediment ridges in the frontal Makran rise and fall in elevation along strike, but the ~30 km long section of Fifth Ridge in Fig 6.2c seems to have a relatively constant elevation. Yet, our seismic data show that this section displays significant structural variation along-strike.

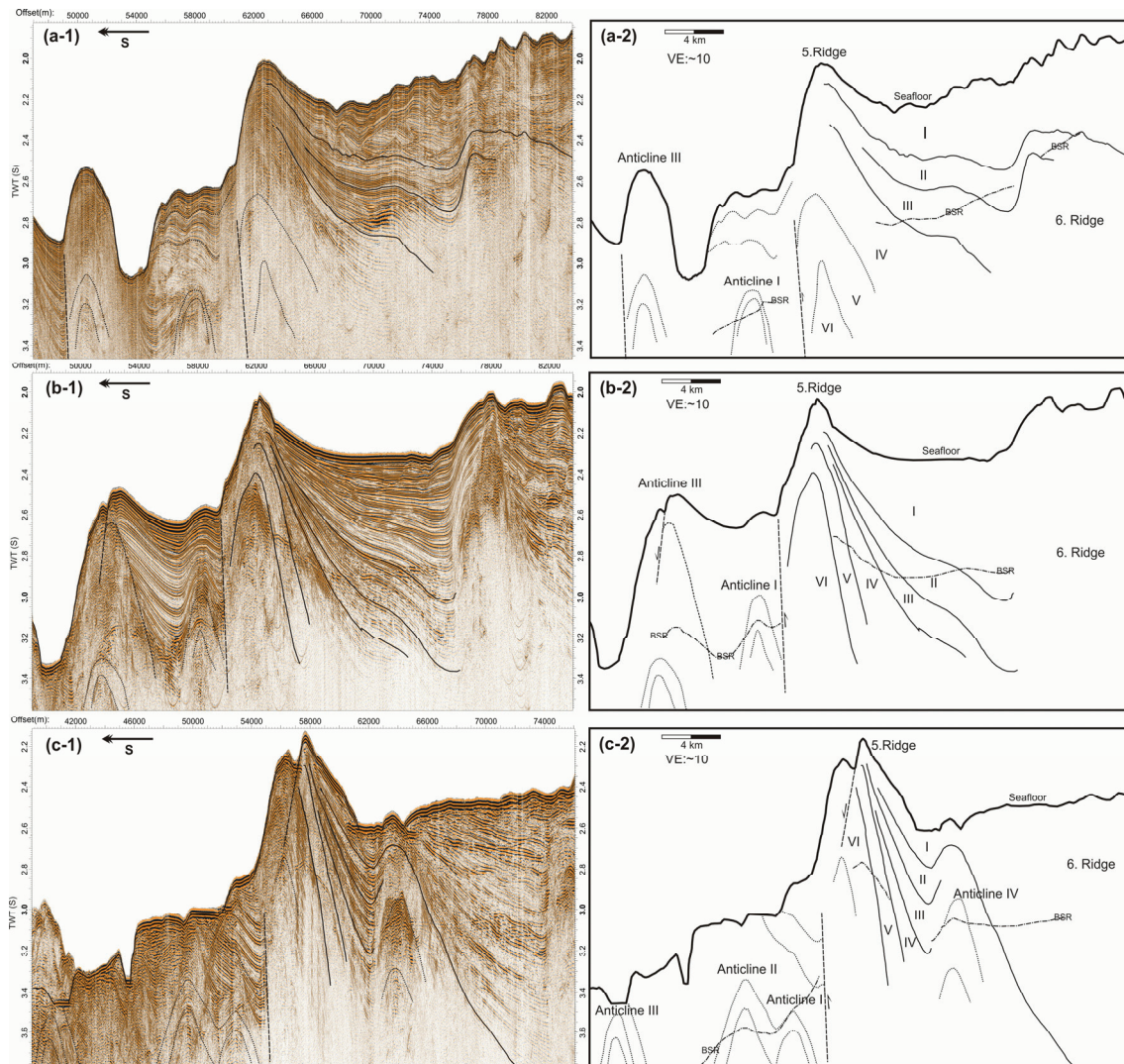


**Figure 6.5.** Seismic profiles on the mid slope and the southern terrace. a) Profile GeoB07-329, a-2) Its structure interpretations, b) Profile GeoB07-361, b-2) Its structure interpretations, c) Profile GeoB07-364, c-2) Its structure interpretations

See Figure 2d for their locations

In the westernmost part (Figs 6.4a and 6.5c), the sediments in the core of the ridge (Unit VI and V) have rather steep and constant dipping angles across the ridge, revealing also no thickness variation. They protrude to the surface at the apex of the ridge. At the frontal side of the ridge (basin-ward side), the two units seem to be normal-faulted and slided. At the backside, they are buried by sediments in the mid slope terrace (Units IV to I), which show clear thinning and onlaps towards the ridge, with gentler dipping angles in shallower units. These clear contrasting features between these shallower units and the units in the ridge core (Units VI to V) indicate that Units VI and V could be sediments of an imbricate slice, deposited before a thrust uplifted them, while Units IV to I are slope sediments, strata syn-kinematic with thrust faulting.

One step to the east (Fig 6.4b and 6.5b), the imbricate slice (Units VI and V) forms a tight anticline under the ridge crest. The four shallower units bury the imbricate slice even at the apex of the ridge. Note the small sediment undulations in the shallowest part of Unit I (Fig 6.5b), which are the subsurface continuation of the undulations seen in the bathymetry (Fig 6.2).

In the easternmost part (Fig 6.4c and 6.5a), Fifth Ridge is totally constructed from slope sediments (Unit IV to I). The sediment undulations in Unit I, barely visible in Fig 6.5b, become very pronounced in Fig 6.5a. The surface sediment undulations also have higher elevation and larger wavelength than those at Fig 6.5a (Fig 6.2). The imbricate slice (Units VI and V) is so deeply buried that it is almost out of the penetration limit of our seismic signal. However, these two units can be picked up in the more westerly profiles, where these two units are more uplifted, and in the easternmost profiles, where erosion by Canyon II brought these two units closer to the surface (Fig 6.2). Thus, depth and geometry of these two units can be interpolated in Fig 6.4c-2. This suggests the anticline of Units VI and V to become quite wide open, with quite gently dipping limbs.

Overall, to the west, the imbricate slice under the Fifth Ridge is significantly elevated, steeply dipping, forming a tight anticline inside Fifth Ridge. The frontal side of the ridge is often normal-faulted and reveals block sliding. To the east, the imbricate slice has a more gently dipping angle, with a wider anticline towards its upper end. The imbricate slice is also less elevated and deeply buried by slope sediments (Units IV to I), which also dip gentler than their counterparts in the west. With the lower elevated imbricate slice and higher seafloor to the east, the slope sediments also become thicker.

#### 6.6.2.2 Buried anticlines under slope sediments

In the bathymetry, Fifth Ridge seems to be an isolated high, bounded by the relative flat mid-slope terrace and southern terrace. However, these two terraces reveal fairly complicated subsurface features. In the eastern part (Fig 6.5a), a small anticline (Anticline I) seaward of the Fifth Ridge is buried by some 500 ms TWT of slope sediments. Without the knowledge about the deeper structure, we tentatively define it as an anticline. Only 10 km further to the west (Fig 6.5b), Anticline I becomes much shallower in depth. Furthermore, another anticline (Anticline III) shows up at the southern limit of the southern terrace. It appears very chaotic in its shallow part, but folded sediments are visible in greater depth. Further to the west (Fig 6.5c), erosion of the slope sediments by the Sonne Canyon exposes both Anticline I and III to the surface, and reveals one more anticline (Anticline II) between them. Furthermore, in the mid slope terrace, another anticline (Anticline IV) shows up ~5 km north to the Fifth Ridge.

In all, we count 4 anticlines in this study area, 3 in the southern terrace and one in the Mid-Slope Terrace. Mapping of their trends is shown in Fig 6.2, suggesting that Anticline III could be the continuation of a sediment ridge further to the east (Fig 6.2d). Except for this anticline, all the others drop in elevation and become more deeply buried by slope sediments from west to east, similar to the behaviour of the imbricate slice of the Fifth Ridge (Units VI and V).

#### 6.6.2.3 Seismic indications for fluids around Fifth Ridge

##### 1. BSR and its depth

A BSR occurs extensively around Fifth Ridge, with clear reversed polarity (Figs 6.4 and 6.5) and a relative stable depth of 500 - 600 ms TWT bsf (below seafloor) (Fig 6.6). Double or even triple BSRs are visible in several locations (Fig 6.4a), deeper than the most reflective BSR. These deeper BSRs are most clearly imaged in the imbricate slice (Unit VI and V) of the Fifth Ridge,

but occasionally extend into the two terraces. Because the shallowest BSR has more pervasive occurrence and similar depth to those BSRs in previous studies, only this BSR will be used for further discussion (implications of multi-fold BSRs are out of the scope of the study).

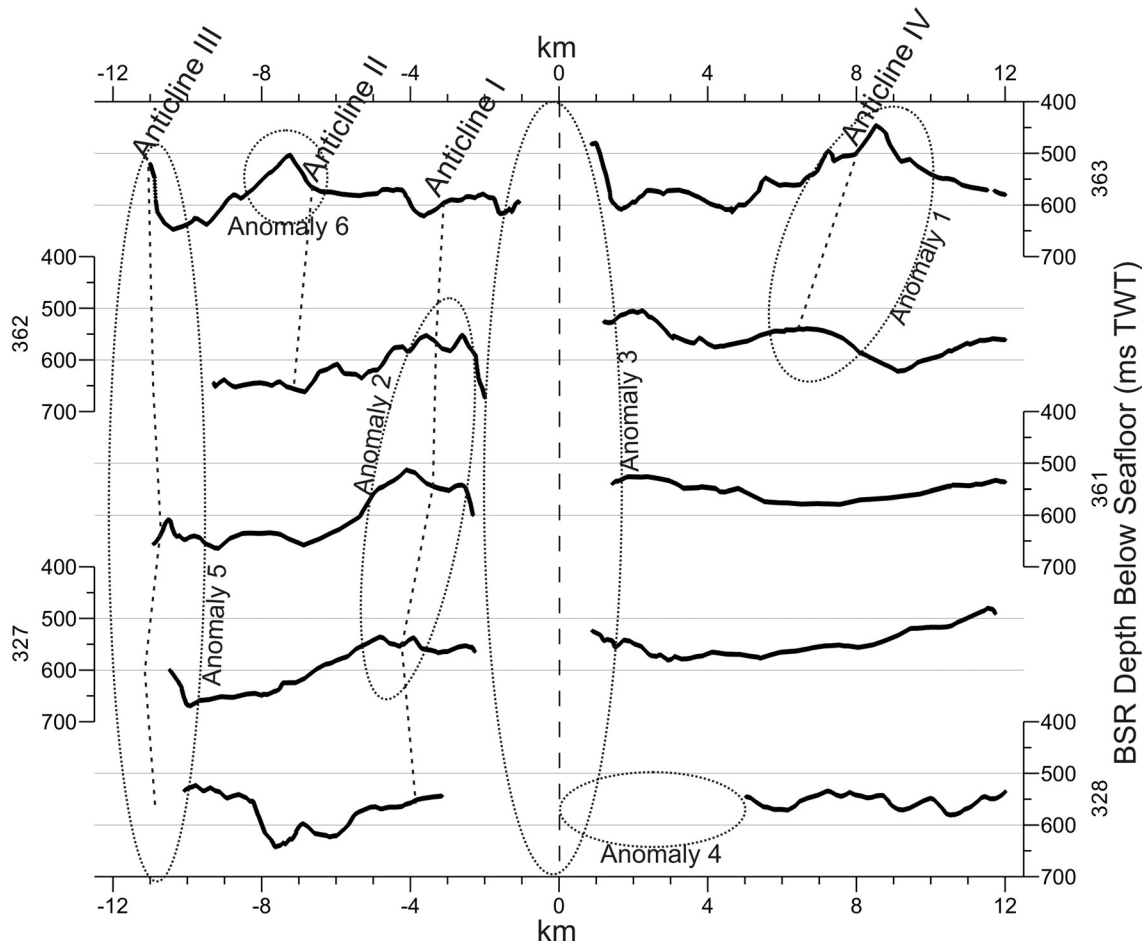


**Figure 6.6.** BSR depth picked in 5 profiles around Fifth Ridge.

X-axis is the offset from the peaks of Fifth Ridge. Profile numbers refer to Fig 2

Fig 6.6 shows the BSR depth along 5 long profiles around the Fifth Ridge area (Fig 6.2d). Despite of the sediment structure variations discussed above, the BSR depth varies little in the entire area, mostly 500 – 600 ms TWT bsf. Only at three spots the BSR slightly shoals by about 100 ms TWT relative to its surrounding: the western section of Anticline IV (Anomaly 1, Fig 6.6) and Anticline II (Anomaly 6, Fig 6.6), and the middle section of Anticline I (Anomaly 2, Fig 6.6). Furthermore, the BSR disappears at the frontal side of Fifth Ridge along the entire studied section (Anomaly 3, Fig 6.6), and also at the backside, eastern section of the ridge (Anomaly 4, Fig 6.6). A BSR is also absent or uplifts under parts of Anticline III (Anomaly 5, Fig 6.6). In a morphologically complicated area, a BSR may not be imaged when it is too steep, or it may shoal due to morphological effects related to the thermal field (Delisle and Berner, 2002; Gerevemeyer et al., 2004). So their implications might be ambiguous. However, Anomalies 1 – 4 do overlap with seismic high amplitude anomalies (Figs 6.4 and 6.5) discussed in detail below.

## 2. High reflectivity in Fifth Ridge

Along the entire studied section of Fifth Ridge, Unit VI shows strong reflectivity (at Anomaly 3), clearly distinguishing itself from the transparent Unit V (Figs 6.4 and 6.5). At the westernmost section, such high amplitudes further extend into the frontal, slided side of the ridge (Fig 6.4a). The polarity of the high amplitude reflection is ambiguous. In addition, if this unit is a coarse-grained sediment interval, its reflectivity would appear stronger at the top of an anticline, because the reflectors dip there is more gentle. Nevertheless, the high amplitude zone does show indications of reduced frequency (Fig 6.4b) suggesting the presence of free gas. Moreover, during the M74/2 Cruise, a 6 m long gravity coring in the central section of Fifth Ridge indicates a very shallow methane-sulphate transition (SMT) zone, thus pointing to higher methane flux above Unit VI (Spiess et al., M74/2 Cruise Report; in prep). These observations favour the interpretation that the high amplitude of Unit VI at the summit of the anticline is at least partially the result of gas accumulation.

At Anomaly 4, a section of high amplitude and low frequency reflectors appears to be strictly confined inside/under a weakly reflective interval of Unit III (Figs 6.4c and 6.5a), which is shallower than the expected BSR depth. The high amplitude zone extends along Unit III until under the crest of Fifth Ridge, where many small fault- or chimney-like features are present (Fig 6.4d and Fig 6.5a). Gas seeps were groundtruthed above these features during the Cruise M74/3 (Bohrmann et al., 2008).

### 3. High reflectivity at the anticlines under the two terraces

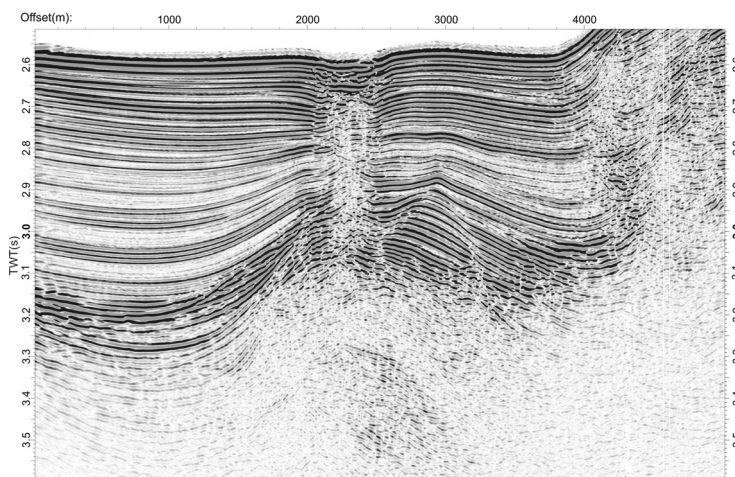


**Figure 6.7.** *Diatreme structure above Anticline I*

*See Figures 2c and 2d for its location*

Where the BSR slightly shoals at Anticline I (Anomaly 2), high amplitude reflections are observed at the anticline crest (Fig 6.5b). In the immediate vicinity of Fig 6.5b, a narrow seismic chaotic zone stretches straight and vertically from the top of the anticline to a depression on the seafloor (Fig 6.7). Such a feature extremely resembles the seismic appearance of a diatreme, indicating a previous fluid escaping event. This would justify interpreting the high amplitudes at the Anticline I to be the fingerprints of fluid accumulations. Similar high amplitude reflections also appear in Anticline IV (Fig 6.5c), where the BSR depth also slightly shoals (Anomaly, 1, Fig 6.6).

Note that all these high amplitude reflections under the two terraces are commonly buried by several hundred ms TWT of slope sediments. They are neither as deeply buried as the imbricate slice (Unit VI and V) in the eastern part of Fifth Ridge (Fig 6.5a) nor as exposed as Anticlines I to III at their westernmost part (Fig 6.5c). Moreover, the sixth ridge in Fig 6.5 shows

not only bright but also chaotic seismic features. These features are also buried by relatively thick slope sediments. All these high amplitude reflectors are inside the regional gas hydrate stability zone (GHSZ) (Fig 6.5), as they are shallower than the BSR or expected BSR depth.

## 6.7. Discussion

### 6.7.1 Imbricate folding and faulting at the deformation front

If we regard Nascent Ridge as an initial stage of ridge uplift, its structure shall eventually evolve similar to that of First Ridge. Accordingly, Nascent Ridge would be further uplifted and its open anticline shall be further tightened (Fig 6.3b). There are two different general scenarios for uplifting and folding of accreted sediments. Nascent Ridge could be continuously folding without any faulting. Only when the fold is rather tight, a thrust fault may develop as break-thrusts or faulted detachment folding etc. (Thorbjornsen and Dunne 1997; Mitra 2002). Alternatively, already at present-day, a thrust fault might have already developed below Nascent Ridge. Such a thrust might have branched from the décollement, offsetting deep strata, and would gradually propagate into shallower sediments: fault-propagating folds, tri-shear folds etc. (Suppe and Medwedeff 1990; Erslev and Mayborn 1997; Allendinger, 1998). Because deep strata are faulted, shallow strata would accommodate such offset by folding. With increasing fault offset of deeper strata, the fold at shallower strata also becomes tighter, until the thrust breaks through to the surface.

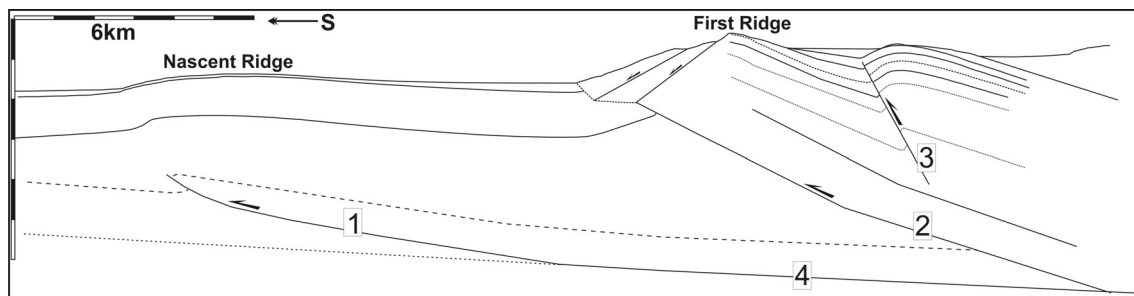


**Figure 6.8.** Interpretation and inference of structure under the Nascent and First Ridge down to décollement level

(1) Blind, upward propagating thrust fault under the Nascent Ridge; (2) The primary thrust of the First Ridge; (3) The secondary thrust of the First Ridge; (4) Décollement;

Geometric constraints are still insufficient to determine the exact fold evolution mode applicable for Nascent Ridge, but the second kind of scenario - synchronous development of faulting and folding - may more truly depict the deformation of Nascent Ridge, based on the following considerations. If the fold must be first tightened sufficiently to allow the development of thrusts, a relatively thick mobile or viscous layer above the décollement is required by geometric considerations (i.e. to infill the void in the core of tightening folds) (Stewart, 1999). However, it is very unlikely that a very thick mobile layer such as overpressured mud exists under Nascent Ridge. Although mud volcanoes occur in the interior Makran, at the deformation front most of the sediment above the décollement is normally compacted (Fruehn et al. 1997; Fowler et al. 1985). Furthermore, previous seismic surveys very close to our Fig 6.3a also indicate a blind thrust in deep. They the deep strata below the frontal limb of Nascent Ridge to be largely offset and thus faulted, while shallow sediments at the frontal limb seems to be only rotated but with no offset (Fruehn et al. 1997; Kopp et al. 2000), indicative of a (Fig 6.8). Furthermore, where Nascent Ridge is less elevated, it is also closer to First Ridge. This is also a typical feature for

an upward propagating fault, in which the fold of shallower strata is roughly above the tip of the fault. Where the thrust is yet small in offset, and its tip has just branched from the décollement and is closer to First Ridge, the surface fold would be also small and close to the ridge.

If such process continues, the frontal limb of Nascent Ridge would be steepened and even be overturned, and thus may fail by slumping or sliding. Alternatively, once the thrust reaches the seafloor and continues the activity, it may extrude the frontal limb into an open space - a sneak-headed forelimb, which would also cause it to fail. These two possibilities may explain the sliding at the frontal side of First Ridge at Fig 6.3a. Where First Ridge is relatively mildly deformed, the imbricate fold can be better preserved Fig 6.3b. Note that this scenario is based on the observations from both Nascent and First Ridge, and thus assumes the two ridges to follow a similar evolutionary path.

There are two important complications, however. One is that the frontal Makran and the abyssal basin are fast sedimentation regimes. Some 200 ms TWT of slope sediments already deposited on the back side of Nascent Ridge. If First Ridge is further thrust, it will move onto the slope sediments, instead of onto the imbricate slice of Nascent Ridge. The upper parts of foot-wall and hanging-wall of a thrust are thus “wedged apart” by these new sediments. Its implication will be explored in a later discussion.

The other complication is that during the propagation of an imbricate thrust, “secondary thrust faults” may develop. The previous seismic survey (Fruehn et al. 1997) reveals that First Ridge is separated from the overlying, land-ward imbricate slice by about 12 km (Fruehn et al. 1997; Kopp et al. 2000). The sediment ridge only 4 km further landward from First Ridge (Arrow 4, Fig 6.3a) is actually caused by such a secondary thrust inside the imbricate slice of First Ridge (Fig 6.8a). Similar secondary thrusts, although with much less offset, are also visible in a seismic profile in the east of the study area, collected during Sonne Cruise SO122-04a (Schlüter et al. 2002, their Fig 3).

The basinward vengeance of this thrust excludes it as a back-thrust. It is unclear when such a thrust starts to evolve, but absence of similar faults at Nascent Ridge (Fruehn et al. 1997, their Fig 2) indicates it should develop later than the primary thrust. We infer it may be the result of the movement of the imbricate slice from the flat (décollement) to ramp (primary thrust), i.e., evolved after the primary thrust incurred a large offset. If this would be true, the secondary thrusts may not only develop at the deformation front. New secondary thrusts may then also evolve in later stages. The secondary thrusts may also first develop at depth and propagate upward, resulting in the anticline in its hanging wall (Arrow 4, Fig 6.3a), which seems rather similar to those related to primary thrusts.

The upward propagation of primary thrusts argues against that the normal fault-like features at the surface of Nascent Ridge, seen previously in Parasound surveys (Kukowski et al. 2001), is the initial stage of thrusting. These “normal faults” dip to the south (Fig 6.3a), opposite to the dipping direction of the expected imbricate thrust. They also fade out around 200 - 300 m below seafloor, separated from the deep thrust under Nascent Ridge. In the bathymetry, these “normal faults” appear as sediment undulations, striking parallel to the gully of the Sonne Canyon and become larger and higher when closer to the gully (Fig 6.2a), where the elevation of Nascent Ridge is low. All these characteristics suggest that they are more likely to be sedimentary features: sediments deposited from or reworked by density out-spills from Sonne Canyon, instead of a result of accretion deformation.

## 6.7.2. Fate of imbricate and secondary thrust faulting in the Fifth Ridge area

### 6.7.2.1 Nature of the defined anticlines in the Fifth Ridge area

Fifth Ridge is ~37 km landward from First Ridge, which suggests their age difference to be ~2 Ma (Kukowski et al. 2000) considering the convergence rate, or ~3.4 Ma considering the prism progradation rate (Platt et al. 1985). About max. 1 km of sediments could have been deposited in the abyssal plain during this time. Thus, the imbricate slices of Fifth Ridge can be thinner than those of First Ridge, but should still amount to 3 km. The level of the décollement should be stable during this time, because it is believed to be a lithologically incompetent interval (Fruehn et al. 1997; Kukowski et al. 2001). Thus, Fifth Ridge and other ridges around may have deformed at the paleo-toe of the accretionary wedge with similar process of the present-day First Ridge, which would also explain the regularly shaped bathymetric ridges at the lower slope ridges (Fig 6.2a).

If so, we should observe similar tight anticlines resulting from primary and secondary thrusts around Fifth Ridge. Anticlines I to IV and the anticline in the core of Fifth Ridge are the only candidates for those expected thrust-induced anticlines. Furthermore, the 3 km thickness of imbricate slices at the Fifth Ridge area and their still gently dipping imbricate thrusts (Schlüter et al. 2002; Kopp et al. 2000) make it almost impossible to pack 4 original imbricate slices within a horizontal width of 13 km: the distance between Fifth Ridge and Anticline III. Fruehn et al. (1997) also suggested that every two neighbouring primary thrusts (and related folds) have a typical distance of 12 km in the frontal Makran. At least two of Anticlines I to III could be the result of secondary thrust-faulting in the imbricate slice basinward of Fifth Ridge, while Anticline IV could be a secondary thrust on the imbricate slice of Fifth Ridge. Strictly speaking, without a regional investigation, the Fifth Ridge could also be a secondary-thrusted block. Nevertheless, its pronounced elevation over all the anticlines in the study area suggests that it roots on an original imbricate slice.

### 6.7.2.2 Role of slope sediments

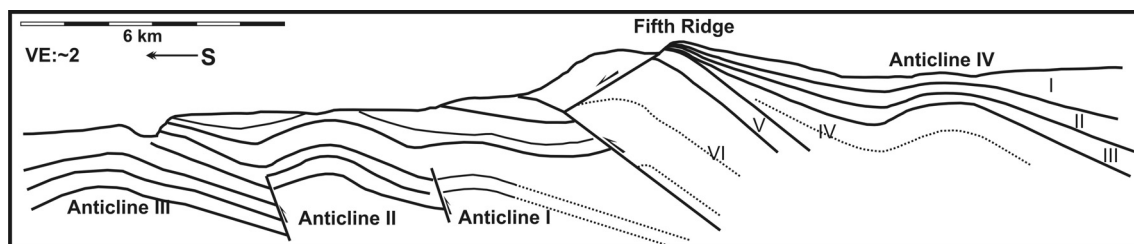


**Figure 6.9.** Complete structure interpretation of Profile GeoB07-364 around Fifth Ridge

Note the profile is partly presented in Fig 5c, but this figure shows features within the full depth penetration of this profile, with milder vertical exaggeration

Continuous thrusting can move the hanging-wall block into an unstable geometry, and thus the frontal part of the hanging-wall would fail (Similar to Fig 6.8). Immediately inboard of the deformation front, such a failure seems to be avoided by the secondary thrusting. As Fig 6.3a suggests, the secondary thrust behind First Ridge uplifts its hanging-wall, which then has close contact with the next landward imbricate slice, supporting it from collapse. However, the imbricate slice of Fifth Ridge is thrust at least 800 m higher above the foot-wall (Anticline I, Fig 6.5). In addition, the ~45° dipping of the thrust protrudes the imbricate slice basin-ward for 800 m (Fig 6.9). In this case, the thick slope sediments in the southern terrace seem to be the

only candidate to support the imbricate slice from collapse. It may be uncertain whether these newly deposited, mechanically weak materials underneath the imbricate slice can support the weight of Fifth Ridge. However, in the western section of Fifth Ridge, where slope sediments south to the Fifth Ridge are thin and the ridge is highly elevated, sliding occurs at the frontal part of Fifth Ridge (Fig 6.4a). This suggests that without the support of slope sediment or other materials, the protruded Fifth Ridge would fail.

If a secondary thrust causes significant offset to its corresponding imbricate slice, its hanging-wall will also be uplifted into an open space, and thus may collapse. However, the secondary thrusts, developing in the less elevated parts of the imbricate slices, may be quickly buried by slope sediments. If the faulting is always in subsurface, the hanging-wall cannot collapse. When so buried, thrusts would further propagate into the slope sediments or cause them to fold. Anticlines I, II and IV may well exemplify this: the slope sediments at these anticlines curve up and become part of the folding, instead of passively bury these folds and onlap to them (Fig 6.5b).

These observations suggest that slope sediments are actively involved in the activity of the primary and secondary faulting: they are folded by the shear strain of thrusts buried by them, and/or keep the hanging-walls of various thrusts from collapsing. Because thick slope sediments can wedge between the hanging-wall and footwall of a thrust, the upper section of the fault plane and the hanging-wall can dip much steeper than the footwall. Thus, the steepening of the thrust is not only controlled by rotation of imbricate slices.

#### 6.7.2.3. *Draping and burial of accretionary structures*

As the accretion and compression continues, the imbricate slices would move land-ward, down-slope of the décollement. Thus, if the imbricate slices are not thrust and uplifted fast enough and under-plating is still absent, they would subside. This may be the case for the eastern section of Fifth Ridge (Figs 6.4c and 6.5a). The gentler dip of the imbricate slice there indicates that it is less active than the same ridge further west. Thus, the slice drops in absolute elevation and is buried by the slope sediments. However, instead of simply smoothing out the seafloor, the slope sediments inherited the morphology of ridge. The entire studied section of Fifth Ridge seems to be equally elevated (Fig 6.2b), while the core of the ridge change from imbricate slices to slope sediments from west to east.

We suggest this could be explained by two considerations. First, the primary thrust of Fifth Ridge may be continuously active, uplifting the imbricate slice even when the slice is deeply buried. Slope sediments on the top of the imbricate slice are then also uplifted and keep the elevation of Fifth Ridge. The uplift caused the increasingly steeper dip of slope sediment units (Unit I to IV) from shallow to deep (Fig 6.5).

Secondly, the regional sediment source supplies from the north, the internal Makran wedge. Such a direction of sediment supply makes Fifth Ridge an effective sediment dam, prescribing faster sedimentation rates at the mid-slope terrace than at the southern terrace, keeping the former terrace higher than the latter one. With the formation of Canyon II, sediments are additionally supplied by spill-outs from it. Since this new sediment source enters from the east, Unit I shows clearer sediment waves closer to the canyon. The wavy sediments have similar thickness in the two terraces: the sediment-damming effect of Fifth ridge disappears. Because more sediments are deposited in the east, the seafloor and Fifth Ridge there become more elevated as a whole (Fig 6.2c). However, such waves are restricted to Unit I, which implies the

new sediment source and Canyon II itself are a very recent phenomena, and could not yet bury the positive part of Fifth Ridge.

### 6.7.3 Fluid accumulation and seepage

#### 6.7.3.1 Thermal field and water expulsion

Pronounced occurrences of BSRs and their nature as a of phase boundary of free gas to gas hydrate are suggested by many studies on the frontal Makran (e.g., White 1984; Minshull and White, 1989; Kaul et al. 2000; Schlüter et al. 2002). This BSR can thus be used to infer heat flow. Minshull and White (1989) calculated heat flow in the frontal Makran and found 20 – 25% of heat flow rise compared to that predicted by conductive heat dissipation model. These authors ascribed this anomaly to advective flow from depth, as a result of tectonic thickening and dewatering of the accreted sediments. Refraction seismic studies indicated a deep low acoustic velocity zone near Fifth Ridge, related to undercompaction and overpressure of deep sediments (Kopp et al. 2000). This would also support an elevated flow rate. Nevertheless, existence advective flow does not mean it is vigorous. Except for the above-mentioned spot, acoustic velocity analysis indicates undercompaction is largely absent in the accreted sediments inboard of Nascent Ridge (Fowler et al., 1985; Fruehn et al., 1997; Kopp et al., 2000). Accumulation of a thick free gas column below the BSR, suggested by previous studies (Grevemeyer et al., 2000; Sain et al., 2000), also counter-intuitively indicates slow water flow rate (Haacke et al. 2007).

Around Fifth Ridge, the BSR depth is relatively constant (Fig 6.6), mostly around 500 – 600 ms TWT bsf, without any systematic variation in the study area (Fig 6.6). With a calculation method similar to those of Minshull and White (1989) and Kaul et al. (2000), the BSR depth variation could imply only  $\sim 5$  mW/m<sup>2</sup> of heat flow variation in the area. This further implies that the advective flow rate varies little around Fifth Ridge, despite the significant west-east variations of the sediment structures and deposition/erosion patterns discussed above. Thus, we infer that a dispersive water flow may be present as the result of tectonic dewatering, but the flow rate is limited and does not rise where Fifth Ridge is more deformed. However, the shallow sediment structural variations do control the locations of the BSR Anomalies 1 – 4 (Fig 6.6).

#### 6.7.3.2 Structures trapping fluids

As discussed, Anomalies 1 – 4 are present where the BSR shows slight shoaling or disappears. They are located at anticlines that are related to the primary and secondary thrusts. Such thrust-related anticlines are typical petroleum structural traps at convergent belts. We have discussed that all of these anticlines are accompanied by high amplitude seismic reflections, and other anomalies indicating hydrocarbon or other fluid seepage on top of them. Thus, they may act as shallow reservoirs of fluids, supporting the surface seepage. When slope basin sediments are thin, the folded imbricate slice acts as a reservoir (at Anomaly 1, Fig 6.6), while when imbricate sediments are sufficiently buried, permeable intervals of slope sediments become shallow reservoir units (at Anomalies 2 – 4, Fig 6.6).

The fact that BSR anomalies are located on these reservoirs may indicate that these locations are thermally abnormal, implying they would be charged by warm fluids from greater depth. This is supported by low C1/C2 ratios of the sampled methane at the seeps indicating thermogenic, thus deep origin of the hydrocarbons fluids (Bohrmann et al., 2008). Fast deposited and TOC diluted slope sediments are also unlikely to produce significant amounts of biogenic gas to support the seeps.

The fluid charge may cause chaotic reflections and various fluid escaping features (diatremes and gas chimneys) in seismic profiles, but they are not seismically chaotic mud patches deposited by mud intrusion and volcanism. Such patches would be connected to deep overpressured mud sources by narrow feeder channels, totally independent of shallow sediment structures. Even at the landward edge of our study area, the Sixth ridge appears almost structureless (Fig 6.5), but its distance of 12 km away from Fifth Ridge strongly suggests it to be at the expected location for the anticline of another imbricate slice. In all, surface seeps observed around Fifth Ridge should be caused by leakage of hydrocarbons that are accumulated in thrust-related structural traps, instead of by intensive tectonic dewatering and mud volcanism.

## 6.8 Conclusion

At the deformation front, the sediments above the décollement are imbricated by upward-propagating thrust faulting from greater depth. Shallower sediments above the thrust are folded until the thrust reaches the seafloor. The thrust further induces secondary thrusts to the imbricate slices, with similar shallow sediment folding on their hanging-walls. The folding resulted from the primary and secondary thrusts can also be recognized around Fifth Ridge. The anticline in Fifth Ridge is caused by the primary thrust faulting, and Anticline III is on the hanging-wall of the next basinward primary thrust. Anticline I, II and IV are folded imbricate slices and slope sediments in response to secondary thrusts.

Slope sediments play an important role in shaping the current morphology of the frontal Makran. Without them to support thrust and uplifted imbricate slices by primary or secondary thrusts, the suspended hanging-walls would fail, and sediment ridges, many cored by anticlines, would not be preserved. Furthermore, because the slope sediments wedge apart imbricate slices at their upper ends, they cause thrusts and imbricate slices to have steeper dips than they otherwise would reveal. When slope sediments sufficiently bury imbricate slices, they are also deformed and folded by continuous thrusting. The upper part of Anticlines I, II and IV, as well as the eastern section of Fifth Ridge represents deformed slope sediments. These folded imbricate slices and slope sediments form near-surface structural traps for fluids escaping from the greater depth.

Vigorous dewatering is unlikely around Fifth Ridge. Instead, all the fluid indications (seismic anomalies and ground-truthed gas seeps) are hydrocarbon charged shallow structural traps discussed above. When these traps are sufficiently charged they can induce diatremes, gas chimneys on top of them, causing seepage. Thus, focused seepage around Fifth Ridge is supplied by hydrocarbons, possibly thermogenic and accumulated in shallow traps. The area lacks mud volcano-like features that are indicative of vigorous ascent of overpressured fluids and mud patches directly from the greater depth.

## 6.9 Acknowledgments

We thank the crew of the R/V Meteor during the cruise M74/2, for their excellent work for our onboard scientific survey and study. We are grateful to the Pakistani government for the permission to survey Pakistani national waters during the cruise. Special acknowledgements are given to Tim Minshull and Tim Le Bas of National Oceanography Centre, Southampton, for their discussions and shearing of data. F. D.'s research visits to NOC were supported by Bremen International Graduate School for Marine Sciences (GLOMAR). The M74/2 cruise and

this study are funded through DFG-Research/Exzellenz Cluster, “the ocean in the Earth system”.

## References

- Allmendinger, R. W.** 1998. Inverse and forward numerical modelling of trishear fault-propagation folds. *Tectonics*, 17(4), 640 – 656
- Arthurton R.S. Larah, A. and Ahmed, W.** 1982. The late Cretaceous-Cenozoic history of western Baluchistan, Pakistan – the northern margin of the Makran subduction complex. In: Leggett, J.K., (Ed.), *Trench and Fore-Arc Geology: Sedimentation and Tectonics on Modern and Ancient Active Plate Margins*, Special Publications of the Geological Society of London ; 10:373-385
- Bohrmann, G., Ohling, G., and other cruise participants.** 2008. Report and preliminary results of R/V Meteor Cruise M74/3, Fujairah - Male, 30 October – 28 November, 2007. Cold seeps of the Makran subduction zone (continental margin of Pakistan). *Berichte, Fachbereich Geowissenschaften*, Nr.266, Universität Bremen, Bremen, Germany
- Caress, D. W. and Chayes, D. N.** 1996. Improved processing of Hydrosweep DS Multibeam data on the R/V Maurice Ewing. *Marine Geophysical Researches*, 18, 631-650
- DeMets, C. Gordon, R.G., Argus, D.F., et al.** 1990. Current plate motions. *Geophysical Journal International*, 101, 425-478.
- Delisle, G. and Berner, U.** 2002. Gas hydrates acting as cap rock to fluid discharge in the Makran accretionary prism? In: Clift, P.D., Kroon, D., Gaedicke, C. & Graig, J. eds. *The tectonic and Climatic Evolution of the Arabian Sea Region*. Geological Society London, Special Publications, No. 195, 137 – 146
- Erslev, E. A. and Mayborn, K. R.** 1997. Multiple geometries and modes of fault-propagation folding in the Canadian thrust belt. *Journal of Structural Geology*, 19(3-4), 321 – 335
- Fowler, S. R., White, R. S. and Loudon, K. E.** 1985. Sediment dewatering in the Makran accretionary prism. *Earth and Planetary Science Letters*, 75, 427 – 438
- Fruehn, J., White, R.S. and Minshull, T.A.** 1997. Internal deformation and compaction of the Makran accretionary wedge. *Terra Nova*, Vol. 9, 101-104.
- Gaedicke, C., Prexl, A., Schlüter, H., et al.** 2002. Seismic stratigraphy and correlation of major regional unconformities in the northern Arabian Sea. In: Clift, P.D., Kroon, D., Gaedicke, C. & Graig, J. eds. *The tectonic and Climatic Evolution of the Arabian Sea Region*. Geological Society London, Special Publications, No. 195, 25-36.
- Grevemeyer, I., Rosenberger, A. and Villinger, H.** 2000. Natural gas hydrates on the continental slope off Pakistan: constraints from seismic techniques. *Geophysical Journal International*, 140(2), 295 – 310
- Grevemeyer, I., Kopf, A. J., Fekete, N., Kaul, N. Villinger, H. W., Heesemann, M. Wallmann, K., Spieß Volkhart et al.** 2004. Fluid flow through active mud dome Mound Culebra offshore Nicoya Peninsula, Costa Rica: evidence from heat flow surveying. *Marine Geology*, 207, 145 – 157

- Haacke, R. R., Westbrook, G. K. and Hyndman, R. D.** 2007. Gas hydrate, fluid flow and free gas: formation of the bottom-simulating reflector. *Earth and Planetary Science Letters*, 261, 407 – 420
- Harms, J.C., Cappel, H.N. and Francis, D.C.** 1984. The Makran coast of Pakistan: its stratigraphy and hydrocarbon potential. In: Haq, B.U. and Milliman, J.D. eds. *Marine geology and oceanography of Arabian Sea and coastal Pakistan*. VNR-SAE. 3-26.
- Kaul, N., Rosenberger, A. and Villinger, H.** 2000. Comparison of measured and BSR-derived heat flow values Makran accretionary prism, Pakistan. *Marine Geology*, Vol.164, 37-51.
- Kopp, C., Fruehn, J., Flueh, E. R., et al.** 2000. Structure of the Makran subduction zone from wide-angle and reflection seismic data. *Tectonophysics*, 329, 171 – 191
- Kukowski, N., Schillhorn, T., Flueh, E.R., et al.** 2000. Newly identified strike-slip plate boundary in the northeastern Arabian Sea. *Geology*, Vol.28(4), 355-358.
- Kukowski, N., Schillhorn, T., Huhn, K., et al.** 2001. Morphotectonics and mechanics of the central Makran accretionary wedge off Pakistan. *Marine Geology*, Vol.173, 1-19.
- Minshull, T. and White, R.** 1989. Sediment compaction and fluid migration in the Makran Accretionary Prism. *Journal of Geophysical Research*, Vol.94(B6), 7387-7402.
- Mitra, S.** 2002. Structural models of faulted detachment folds. *AAPG Bulletin*, 86(9), 1673 – 1694
- Platt, J.P., Leggett, J.K., Young, J., et al.** 1985. Large-scale sediment underplating in the Makran accretionary prism, southwest Pakistan. *Geology*, Vol.13, 507-511.
- Quittmeyer, R.C. and Kafka, A.L.** 1984. Constraints on plate motions in southern Pakistan and the northern Arabian Sea from the focal mechanisms of small earthquakes. *J. Geophysical Research*, Vol. 89(B4), 2444-2458.
- Sain, K., Minshull, T. A., Singh, S. C., Hobbs, R. W.** 2000. Evidence for a thick free gas layer beneath the bottom simulating felector in the Makran accretionary prism. *Marine Geology*, 164, 3 – 12
- Schlüter, H.U., Prexl, A., Gaedicke, C., et al.** 2002. The Makran accretionary wedge: sediment thickness and ages and the origin of mud volcanoes. *Marine Geology*, Vol.185, 219-232.
- Stewart, S. A.** 1999. Geometry of thin-skinned tectonic systems in relation to detachment layer thickness in sedimentary basins. *Tectonics*, 18(4), 719 – 732
- Suppe J. and Medwedeff, D.** 1990. Geometry and kinematics of fault-propagation folding. *Eclogae Geologicae Helvetiae*, 83(3), 409 – 454
- Thorbjornsen, K. L. and Dunne, W. M.** 1997. Origin of a thrust-related fold: geometric vs kinematic tests. *Journal of Structural Geology*, 19(3-4) 303 – 319
- von Rad, U., Berner, U., Delisle, G. et al.** 2000. Gas and fluid venting at the Makran accretionary wedge off Pakistan. *Geo-Marine Letters*, vol. 20, 10-19
- Wessel, P. and Smith, W. H. F.** 1991. Free software helps map and display data. *EOS* 72, 445-446.
- White, R.S. and Klitgord, K.** 1976. Sediment deformation and plate tectonics in the Gulf of Oman. *Earth and Planetary Science Letters*, Vol. 32, 199-209

**White, R.S.** 1984. Active and passive plate boundaries around the Gulf of Oman, north-west Indian Ocean. *Deep Sea Research*, Vol. 31(6-8), 731-745

**Yilmaz, Ö.** 1991. *Seismic data processing*. Society of Exploration Geophysics, Tulsa

## Chapter 7. Summary, Conclusion and Outlook

### 7.1 Summary and Conclusion

#### 7.1.1 Sediment Composition

In Campeche Knolls, our seismic dataset shows a relatively highly reflective thick sediment unit just above the signal penetration limit. It is called Unit VI in **Chapter 4** and corresponds to Unit C and the constant thickness unit in **Chapter 5**. Our age model suggests it to be of late Miocene age. Its coarse grain-size nature can be derived both by its high reflective seismic characteristics as well as its depositional age at an era of prevailing turbiditic sedimentation in the entire Gulf of Mexico (GoM). The overlying units (Units IV and V in **Chapter 4** and Unit B in **Chapter 5**) are an overall acoustically transparent interval, although they intercalate some high amplitude intervals in subsided mini-basins. Their age of late Miocene to early Pliocene corresponds to a period of high sea level, and the basin was dominated by hemipelagic sedimentation. Together with their low reflectivity, it suggests a fine-grained nature of these sediments. The uppermost sediments (Units I – III in **Chapter 4** and Unit A in **Chapter 5**) reveal strong reflectivity and clear onlaps at mini-basins, and thus have turbiditic origin and may reveal coarse grain size, despite the fact that the deep GoM basin is regarded as sediment-starved since Pliocene times. Nevertheless, at the top of knolls and ridges, these units are mostly transparent. The elevation of these bathymetric highs may have prevented turbidites to deposit and hemipelagic sediments were deposited instead.

The age of sediments in Makran is, however, much less easy to constrain than in the case of the Campeche Knolls. Absence of boreholes around our study area and uncertainties to trace reflectors through the accreted sediments in seismic profiles make age definition and correlation in the study area almost impossible. The bulk of the accreted sediments in the frontal Makran may date back to the Miocene, with constraints from the fast sedimentation rate in the Gulf of Oman and approximate outward growth rate of the accretionary prism. Pronounced sediment deformation hinders seismic profiles to reveal the sediments' lithology. However, the sediments are overall of turbiditic origin, relative coarse in grain size and permeable.

#### 7.1.2 Structure evolutions, deformation mechanisms, tectonics and general sediment structures

In the Campeche Knolls, our investigation on over 20 individual knolls and peaks along the ridges indicates three types of shallow subsurface structures: Chapopote Type, Passive Type and Asymmetric Flap Type. The first two types are distributed in the northern part of the study area and limited in numbers. The Asymmetric Flap Type is the dominant structural style in the entire study area: virtually all the peaks along the ridges and some knolls represent this structural style.

The Chapopote Type has a bathymetric appearance and internal structure similar to domes, with permeable sediments of late Miocene or older age (Unit VI in **Chapter 4**, Unit C in **Chapter 5**) composing the deep strata of the domes. These strata are highly uplifted above the present-day datum. The fine-grained overlying sediments thinly cover the top of the domes, while comprising stacked onlap events at the dome flanks. In contrast, the Passive Type may indicate typical passive salt diapirism, with a salt stock occupying the core of the structures while the sediments around are little deformed. An Asymmetric Flap Type structure is made up of an uplifted flap and a subsided chaotic flap. The deep sediments at the uplifted flap are synthetically upturned, and the younger sediments largely onlap at this flap. Although subsided,

the chaotic flaps are inferred to also be composed of upturned sediments, similar to the uplifted flaps. The salt may exist beneath both flaps, and at some bathymetric highs, it extruded to cover the chaotic flap and in turn buried by most recent deposited sediments.

The formation of the Passive Type would go through continuous down-building of depositing sediments, so the salt could always maintain a close distance to the seafloor. Such a process may have started immediately after the precipitation of the salt in the Late Jurassic and continued throughout the basin history, although there is currently no constraint. The Chapopote Type and the Asymmetrical Flap Type, however, would have started to evolve only in the Late Tertiary. This is suggested by the lack of onlaps in deeply buried sediments (Unit VI in **Chapter 4**, Unit C or the constant thickness unit in **Chapter 5**). The two structural types may have been similarly uplifted at the initial stage of the Late Tertiary.

For the Chapopote Type, the stacked onlap events at their flanks reveal that the structures were continuously uplifting until the present-day and had already gained high elevation at least before the deposition of the late Pliocene to Pleistocene sediments (Units I to III of **Chapter 4**). Thus, although nearly 1 km of sediments was deposited in nearby mini-basins since the uplift started, the structures still protrude above the modern regional datum. Furthermore, the symmetrical uplifting has led to their dome-like topography and internal structures. However, the symmetry is not everywhere strictly maintained. At the Chapopote Ridge (**Chapter 4**), a set of normal faults cut through the ridge's crest, downthrowing its SE flank. The amount of their total offsets appears to be controlled by the magnitude of the subsidence in the neighboring mini-basin. So, this mini-basin may have "pulled down" the SE flank of the ridge by its subsidence.

We speculate that when the mini-basin has a larger subsidence, it may give rise to an Asymmetrical Flap Type structure. The Asymmetrical Flap Type may have also initiated as symmetrical dome or ridge. The topography renders un-uplifted locations more sediments, and they subside due to the sediment load and salt withdraw, becoming mini-basins. The withdrawn salt is inflated into the uplifted structures, causing the structures to uplift further. Not surprisingly, the subsidence at two sides of an Asymmetrical Flap Type structure is not always exactly the same. The differential subsidence can cause breach of the structure and faulting at its crest, similar to the Chapopote Ridge. Afterwards, the two flaps of the structure would uplift at different rates, when salt further inflates into the core of the structure. The less uplifted flap is then the preferred side for possible salt extrusions. We suggest that this scenario has resulted in the present-day Asymmetrical Flap Type.

In all, we infer that both the Chapopote Type and the Asymmetric Flap Type (the majorities of bathymetric highs in the area) are resulted from tectonic activities and salt movements initiated in the late Miocene. However, the recent commence of salt tectonic activity apparently contradicts the latest understanding of salt tectonics. The salt of late Jurassic age had already been overlain by over 3 km of sediments in the Late Tertiary even in the deep gulf basin. Although the sediments provide a large density contrast between the sediments and underlying salt to drive upward salt movement, the thick sediments' mechanic strength also prohibits the salt to break through the cover. In turn, salt tectonic activity could not start at all with the thick sediment cover. We suggest two possible explanations. One is that the salt could have been continuously active throughout the basin history, keeping itself very close to the seafloor, by e.g., passive diapirism. Thus, it had been only buried by several hundred meters of sediments at the Late Tertiary, which is the deep sediment unit of our study (Unit VI in **Chapter 4**, Unit C and the constant thickness unit in **Chapter 5**). It is the last phase of salt tectonic activity that is

imaged in our seismic profiles. The other explanation involves a regional compressional event at the commencement of the salt deformation. This regional compression folded sediments to prototypes of the present-day Chapopote Type and Asymmetric Flap Type, which then allowed the differential sediment loading and other salt activities that shaped the two structural types. These two possibilities are not exclusive to each other and may have jointly provided an initial structural configuration for the tectonic activity under discussion.

In Comparison to Campeche Knolls, the importance of regional compression is self-evident for the formation of the Makran Accretionary Prism. The convergence between oceanic crust and continental Asia gave birth to this accretionary system as early as the Tethys Ocean time, while the frontal Makran marks the most recent accretion since ~5 Ma BP. The accretion at the deformation front (at Nascent Ridge in **Chapter 6**) occurs as development of blind thrust faults, bifurcating from the modern decollement, which is a lithologically thin and weak mud layer. The offset of the blind thrust faults caused the folding of the shallow sediments, similar to the model of fault-propagating folds. During this process, additional, secondary thrust faults may similarly develop, in board of the outermost thrust fault (the primary thrust), and cause similar sediment folding to the hanging-wall of the primary thrust. The simultaneous deep faulting and shallow folding caused pronounced development of anticlines in the shallow sediments, which appear as sediment ridges in the bathymetry of the prism.

When these the blind thrust faults reaches seafloor, it is inferred that new blind thrusts would develop further basinward, resulting in the outward growth of the accretionary prism. However, the thrusts that are already incorporated in the prism do not cease their activities. They continuously uplift their hanging-walls and/or rotate, causing ever steeper dipping angles of deeper slope sediments. Those slope sediments, deposited after the pre-kinematic sediments (imbricate slices) started to deform, are supplied from the hinterland of the Makran from the north. Thus, the slope sediments become thicker landwards. They first fill into morphological lows – the foot wall side of the thrusts, and can eventually bury the sediment ridges and thrust faults. Around the Sixth Ridge area (**Chapter 6**) many anticlines originated from thrust faulting are buried by the slope sediments, forming the relative flat area of the mid slope terrace and southern terrace.

Slope sediments do not only bury the deformed sediments, but also become deformed by the continuous activity of thrust faults. They are first tilted by the imbricate slices, and when they completely cover the imbricate slices, they are folded by the continuous uplifting. Around Sixth Ridge, the upper part of Anticlines I, II and IV (**Chapter 6**), as well as the eastern section of the Sixth Ridge are all deformed slope sediments. Moreover, because these sediments first fill on the foot wall of the primary or secondary thrusts, they mechanically support thrust and uplifted hanging-walls. Without the slope sediments the suspended hanging-walls would fail, and sediment ridges, many cored by anticlines, would not be preserved. Consequently, however, because the slope sediments wedge apart the upper ends of footwalls and hanging-walls of thrust faults, they cause the thrusts and imbricate slices to dip steeper than they otherwise would.

In all, despite the complex structures expected for accretionary prisms and strong lateral structure variations along-strike, the overall near-surface structural pattern of the frontal Makran can be outlined as regular occurrence of thrust-induced anticlines that incorporates both imbricate slices and slope sediments. Thrust faults are geometrically beside and under these anticlines. It is notable that although the development of primary and secondary thrusts, which

induce folding of shallow sediments were initiated at the deformation front (Nascent Ridge), it still seems to be the main theme in the Sixth Ridge area. Features signaling further stages of deformation, e.g., back thrusts and out of sequence thrusts, are not identified in the frontal Makran.

### 7.1.3 Formation of fluid focusing mechanisms and traps

In Campeche Knolls, the sediment sequence of coarse-grained late Miocene sediments overlain by fine-grained early Pliocene sediment forms a reservoir-seal sequence. This sequence is domed up by the Chapopote Type, and thus become a classical four-way hydrocarbon trap. Shallower Units I to III (**Chapter 4**) may also act as a seal on the top of the knoll, because they apparently have fine grain-size on morphological highs. The wide zone (over 15 km) of upturned coarse-grained sediments extends in the subsurface far beyond the extent of the bathymetrical highs. Such a configuration presents an ideal focusing mechanism to funnel ascending fluids into the core of Chapopote Type structures. However, the reservoir is extremely shallow below the seafloor and even above the regional datum, with the rather thin (magnitude of 200 m) seal atop. This does not only promote leakage of hydrocarbons possibly accumulated in the reservoir, but also facilitates infiltration of oxidants from seawater into the reservoir, and thus biodegradation of the hydrocarbons.

A fluid-focusing effect is promised for the Asymmetric Flap Type, with the upturned late Miocene or similar sediments in both chaotic and uplifted flaps being capable of guiding fluids into the centre of the structure. Thus, fluid accumulations, provided they occur, should be on the chaotic flaps of the structure. However, salt and other sealing materials in the upper parts of chaotic flaps tend to prevent accumulated fluids from escape. Unlike the Chapopote Type, the reservoirs and seals geometries of Asymmetrical Flap Types are more difficult to directly image, because the structurally most evolved parts are always blurred by extended occurrence of high amplitude, chaotic reflections, which are mostly signatures of extruded salt. However, our structural analysis suggests that the Asymmetric Flap Type is in principle an anticline or a dome that is cut in half by a normal fault, and thus the subsided half may truly outline the reservoir geometry. Even relatively subsided, the reservoirs are still rather close to seafloor and in many cases also above the regional datum. Thus similar to the Chapopote Type, biodegradation are very likely to occur to those accumulated hydrocarbons. Furthermore, the uplifted flaps, which are thinly covered at the peak of bathymetrical highs, present direct pathways for fluids from the deep.

Both the extended presence of salt stock and the featureless sediments on the flank of the salt underscore the Passive Type to be an efficient fluid-focusing structure. Within the available seismic data, there are no trap structures observed. Possible traps may be formed at the salt flank, due to the activity of passive diapirism. Because of seismic imaging difficulties at salt flanks, these traps may simply not be resolved on seismic profiles. However, compared to the Chapopote Type and the Asymmetrical Flap Type, even when some traps exist directly beside the salt flanks, their sizes of such traps are very likely to be much smaller. The absence of fluid-focusing geometry and the likely missing or small size of traps both disfavor large volume accumulation of hydrocarbons in the Passive Type structures. In turn, they are unlikely to support fluid seeps, unless the salt flank serves as a pathway for deep fluids to directly leak at the seafloor.

In the frontal Makran, a down to the decollement reaching fluid focusing geometry is produced by the primary and secondary thrust faulting that tilted accreted sediments into inclined

imbricate slices. At the top of these imbricate slices, the anticlines, resulted also from the development of primary and secondary thrusts, behave as near-surface structural traps for fluids migrating along the imbricate slices. As discussed, slope sediments filling morphological lows start to cover these anticlines at around the Sixth Ridge and were also folded by active thrusts. This further increases the size of the traps. However, when the slope sediments are deposited to certain thickness, or when their sedimentation rate is fast enough, they can totally bury the anticlines and the thrusts, as is the case of the southern terrace and the mid slope terrace. The thrust faults have been previously often suggested as fluid pathways. However, in this overall permeable sediment column it has to compete with sediment aquifers for fluids, and may not necessarily be the only escape route for ascending fluids.

Interestingly, the overall grain size of either imbricate slices or slope sediments is inferred to be relatively coarse. These sediments may be ideal to form reservoir units in these anticlines, but the sealing interval to close these structures is apparently missing. We suggest that the slope sediments cannot be uniformly coarse in grain size, and would usually also sandwich thin fine sediments, either through the shifting nature of turbiditic sediment supply or from intervals of hemipelagic sedimentation. Certainly, turbidites themselves can contain a decent amount of fine grain size as part of a typical Bouma sequence. When slope sediments sufficiently bury those anticlines, they as a whole can be impermeable enough to act as seals. Alternatively, imbricate slices themselves may contain relatively thick fine-grained intervals, such as Unit V in **Chapter 6**. These internal seals can also prevent any possible fluid accumulation from escaping.

#### **7.1.4 Fluid accumulation and seepage**

In Chapopote Knolls, the structural traps of Chapopote Type and Asymmetrical Flap Type formed during a time approximately overlapping the main petroleum generation window for the major source rocks of Jurassic, Cretaceous and Tertiary age. As long as there are pathways connecting the traps with the source rock or with deeper reservoirs, the traps under discussion are able to accumulate petroleum. Our seismic data have recorded extensive distribution of high amplitude patches under many bathymetric highs of all three structural types. As discussed, many of them are interpreted to be the upper surface of salt units, but some are more likely to be signatures of hydrocarbons accumulated in the reservoirs. The most confirmed example is Chapopote Knoll.

There, the high amplitude patches are confined inside the reservoir at most locations of Chapopote. This stratigraphic correlation between the reservoir and the high amplitude patches argues against these patches being salt units and favors them being hydrocarbon signatures. Furthermore, some of these patches show seismic features characteristic of gas accumulation. Only at the crest of Chapopote Knoll, high amplitude patches extend above the reservoir unit. This suggests hydrocarbons are invading into shallower seal sediment. This invasion is ubiquitous at the crest of the knoll, not just restricted to beneath the asphalt site. Fossil asphalt gravels and some gas seeps in other parts of the crest were also discovered during the M67/2 survey, but the asphalt site is currently the most active seep. The rest of the area might be temporarily sealed by solid phase hydrocarbons.

At most of the other bathymetric highs, the direct seismic evidence of fluid accumulation and leakage is rare. However, our structural analysis has located the positions of the near-surface traps and leakage pathways of all three structural types. This in turn enables us to infer the most seep-promising areas. If a seep is supported by hydrocarbons in these near-surface traps, it should be either above those traps or at the outer rings of seal units: extruded sealing salt

always has lateral limitations. Pathways that connect seafloor and greater depth may also lead to fluid seepage, such as the upper end of the uplifted flaps of Asymmetrical Flap Type structures and possibly the outer ring of Passive Type structures. These seepage promising areas are well consistent with seep sites identified from the analysis of satellite SAR images by NPA.

At Chapopote Knoll, Oil Ridge and some other locations in Campeche Knolls, their shallow reservoirs and thin seal covers may be one of the most important factors leading to natural asphalt deposition at the seafloor. Petroleum might have migrated into the reservoir as a mobile fluid. It was then reworked to lose its lighter components during the accumulation and seepage processes, and precipitate at the seafloor as solid phase. Petroleum exploration in Southern Gulf of Mexico shows the oil in this region is rather heavy even in deep accumulation, which further facilitates alternation of the oil into solid residues in near-surface processes. Because the near-surface fluids focusing and trapping structures have redirected deep fluids, the locations of the seeps are also aligned along the trends of these structures. Furthermore, the concentrated seepage occurrence in the three sub-study-areas: Area Chapopote, Area Oil Ridge and Area Middle Slope cannot be explained by shallow structure styles and trends alone. This might be the expression of petroleum generation and deep reservoir distribution in these areas.

For the Sixth Ridge in the frontal Makran, we have discussed that most of near-surface traps are anticlines related to the activity of primary and secondary thrust faults. These traps may lack effective seal intervals because of the overall coarse grain size and thus may be able to accumulate hydrocarbons only when they are sufficiently buried. Our seismic data suggest that fluid accumulation features: high amplitude, low frequency reflections, as well as fluid escaping features: chimneys and reflection chaotic zones are all located on the buried anticlines. These locations include the entire section of Sixth Ridge, the middle section of Anticline I and the western part of Anticline IV. Fluid seepage there is also confirmed by Parasound gas flare imaging, sidescan surveying and ROV dive ground-truthing. The more deeply buried traps are subject to the limitation of the seismic signal penetration, and not surprisingly the thick covering sediment may prohibit fluids from escaping from the traps. No fluid escaping features are observed in these covering sediments. The exposed traps also do not show fluid-indicating seismic features.

In addition, gas hydrates might also play an important role in the fluid focusing and accumulation at the frontal Makran. Extensive gas hydrate accumulation at the bottom of the gas hydrates stability zone (GHSZ) is indicated in the area as bottom simulating reflectors (BSR). The BSR shows this gas hydrate layer also slightly tilt upwards towards the structural traps. If the gas hydrate layer is sufficiently low permeable, they would provide an additional mechanism to focus fluids into the traps. Furthermore, similar to our inferences in Chapopote, if the accumulated gas in the traps, apparently within the GHSZ, is converted into gas hydrates, they could also behave as a sealing material, supporting fluid accumulation in the traps.

In all, our study shows that fluid seepage in both Campeche Knolls and the frontal Makran are focused upon near-surface traps that are large in volume and modestly sealed to allow both accumulation and subsequent leakage. We infer that such a mechanism would be most effective when the seeping fluids are dominantly hydrocarbons ascending by their own buoyancy. In contrast, typical focused overpressure-driven fluids migrate directly from deep reservoirs through either available pathways or vertical feeder channels cut by the fluids themselves. These overpressured fluids cannot be accumulated in rather shallow reservoirs,

because thin seal covers cannot sustain high overpressure, which can be readily produced by a small extra volume of fluids. Our results that fluid seeps are predominately located upon the near-surface traps, thus imply the nature of the fluids being hydrocarbons, which can accumulate large in volume before their column height pressure can breach the seal. In addition, large amounts of hydrocarbon gas supply has possibly led to accumulation of free gas in the GHSZ. This in turn, facilitates precipitation of massive gas hydrates in fluid pathways in original seals. Together with solid asphalts they may even temporarily clog the pathways. A mud volcano-like, pressure-driven seepage model is unlikely for both regions, even though their tectonic settings are fundamentally different. Many recent studies also suggest that the frontal Makran is normally compacted and overpressure occurs only in the hinterland of Makran. Furthermore, the structural evolution results enable us to argue that seepage patterns discovered in both areas are quite recent features. Because these seepage patterns are all based on near-surface structures, they cannot be older than those structures and hydrocarbon generation windows. For Campeche Knolls, it would be at the earliest Pliocene to Pleistocene, while for Sixth Ridge of Makran, in later Pleistocene.

## 7.2 Outlook

In **Chapter 3**, I have suggested a future approach of the cold seepage study by involving studies of deep fluid migration processes, basinal scale seepage investigation, historical reconstruction of seepage, physics-intensive seismic attribute studies. I also proposed available dataset from other study areas can also be applied with the current study approach, which has its own advantages. For these methodological outlooks, readers may refer to **Chapter 3, Section 3.4.4.2**. Here I present several envisages of the researches for the two study areas involved.

In the Chapopote, we have argued that the fluid seepage is not only restricted to the asphalt site, but in a larger extent across the crest. A detailed mapping and characterization of subsurface fluid distribution in this three dimensional, small lateral scale target, however, relies on 3D high resolution seismic data. For the southern Gulf of Mexico, we have now understood that asphalt occurrence is not only restricted to at Chapopote but in a larger extent of the Campeche Knolls. We have proposed a general structure and evolution model for these additional asphalt sites, using our available seismic data. However, further surveys as detailed as Chapopote should be justified by their intriguing structure and seismic features, extensive asphalt pavements and splendid chemosynthetic bio-communities. It would be extremely interesting to compare these knolls with Chapopote unbiased by data coverage.

In the Makran, we have proposed the dominant hydrocarbon fluid accumulation and seepage style for the internal ridge (Sixth Ridge). It was particularly interesting to see the fast deposition of the slope basin sediment that quickly infill the foot-walls of the thrusts. If a correlation between the sediments on these different foot-walls, there is a possibility to define their detailed age. This then would enable an age control on the seepage evolution. Furthermore, structure of the Nascent Ridge, despite of having several different settings from the Sixth Ridge (mildly folded, uncovered by slope sediments), still display very strong seismic anomaly. It is indeed a ground-truthed seep site. A detailed inspection to this structure is extremely worthwhile: possible fluid source might be different, due intensive dewatering at the deformation front.

## General Acknowledgements

*I would sincerely thank Prof. Dr. Volkhard Spieß for giving me this chance to work on my PhD study, for his great ideas and generous helps that made possible many critical progresses in the study. I am very thankful to my advisors in my thesis committee meeting: Volkhard Spieß, Gerhard Bohrmann and Sebastian Krastel. First to their in-depth education to me; second to their suggestions that made my PhD study progress under a consistent scientific topic; last but not the least to their helps during my manuscript writing and ship cruises. I had a smooth, pleasant and successful cooperation with the coworking students and researchers in my Marum project, including Markus Brüning, Florence Schubotz, Andre Gaßner, Gerhard Bohrmann, Matthias Zabel, Heiko Sahling, Thomas Pape, Katrin Huhn, Achim Kopf, Kai-Uwe Hinrichs etc. Their sharing of data and ideas has been immensely valuable.*

*I appreciate the helps from the secretary (Angelika Rinkel), researchers (Tillmann Schwenk, Noemi Fekete and Hanno Keil) and my fellow students (Luisa Palamenghi, Anna Trampe, Jacob Geersen, Jan Metzen and Benedict Preu) in my working group (AG Spieß). They are always lending me a friendly hand in setting up administrative documents, in seismic data processing and interpretation. Thanks are given to those other researchers and students in Marum and the University of Bremen who have helped me in various ways.*

*I am especially grateful for the lectures, seminars and travelling funds provided by Glomar organized by Dierk Hebblen. They had brought me to a much broader scientific circle in my study fields and made possible my more frequent presence to the circle.*

*The detailed administrative documentation and arrangements of funding applications in Glomar are carried out by Uta Brathauer, Carmen Murken and Gabi Ratmeyer. The administrative documents for my study, thesis submission and doctoral title application were arranged by Anja Stöckl. Silke Bertram has helped me with miscellaneous administrative issues during the study. Many warm thanks to them.*

*Special thanks are given to those researchers from Texas A&M University and National Oceanography Centre Southampton, such as Ian MacDonald, Bramley Murton, Tim Minshull etc. for their support of my visiting, sharing of data and modifications of my manuscripts.*

*Particularly acknowledged are the crew of R/V Meteor during the Meteor Cruises M67/2 and M74/3 for their excellent cooperation with the onboard scientific works.*

*This PhD study is funded by DFG (Deutsche Forschungsgemeinschaft) as an integrated part of the research in Marum Project “Seepage of Fluid and Gas”.*